

## Particle separation and sorting in microfluidic devices: a review

P. Sajeesh · Ashis Kumar Sen

Received: 18 April 2013 / Accepted: 11 November 2013 / Published online: 29 November 2013  
© Springer-Verlag Berlin Heidelberg 2013

**Abstract** Separation and sorting of micron-sized particles has great importance in diagnostics, chemical and biological analyses, food and chemical processing and environmental assessment. By employing the unique characteristics of microscale flow phenomena, various techniques have been established for fast and accurate separation and sorting of microparticles in a continuous manner. The advancements in microfluidics enable sorting technologies that combine the benefits of continuous operation with small-sized scale suitable for manipulation and probing of individual particles or cells. Microfluidic sorting platforms require smaller sample volume, which has several benefits in terms of reduced cost of reagents, analysis time and less invasiveness to patients for sample extraction. Additionally, smaller size of device together with lower fabrication cost allows massive parallelization, which makes high-throughput sorting possible. Both passive and active separation and sorting techniques have been reported in literature. Passive techniques utilize the interaction between particles, flow field and the channel structure and do not require external fields. On the other hand, active techniques make use of external fields in various forms but offer better performance. This paper provides an extensive review of various passive and active separation techniques including basic theories and experimental details. The working principles are explained in detail, and performances of the devices are discussed.

### 1 Introduction

Microfluidics concerns design, fabrication and experiments of miniaturized fluidic systems, which has undergone rapid developments during the last decade (Whitesides 2006). As an interdisciplinary area, this rapidly growing field of technology has found numerous applications in biomedical, diagnostics, chemical analysis, automotive and electronics industries. One of the pivotal applications of microfluidics is the development of Lab-on-Chip (LOC) devices as point-of-care diagnostic tools. A typical Lab-on-Chip device includes various functional modules: sample transportation and preparation module, separation module and detection and analysis module. The separation module has importance in preparative applications where a sample is purified through separation of biological objects as well as in analytical applications where these separated objects are carefully studied. Besides this, size-based sorting of objects in a sample is one of the important technologies in the fields of industrial production, food and chemical industry, environmental assessment and chemical or biological research. The sorting of micron-sized objects in a continuous flow is required for a wide variety of applications, including chemical syntheses, mineral processing and biological analyses (Manz et al. 1992; Reyes et al. 2002; Toner and Irimia 2005). For example, in food industry, harmful bacterial activity is carefully monitored and can be prevented with the help of separation techniques. In defense sector, separation is required to detect threatening agents such as Anthrax. In diagnostics, the separation techniques can be utilized to separate living cells from dead cells, cancer cells from normal cells and malaria-infected cells from healthy cells (Suresh et al. 2005; Alshareef et al. 2011).

P. Sajeesh · A. K. Sen (✉)  
Department of Mechanical Engineering, Indian Institute  
of Technology Madras, Chennai 600036, India  
e-mail: ashis@iitm.ac.in

The ability to sort cells into distinct populations based on physical properties is an important tool in a wide range of applications including healthcare, research and industrial applications. It has been found that several diseases alter physical properties of cells and therefore, sorting of cells has great significance in health care (Suresh et al. 2005; Vaziri and Gopinath 2008). For example, healthy red blood cells are deformable enough for which they can easily circulate in blood vessels. The cells infected with malarial parasites are rigid (~50-times) and unable to pass through the capillaries, leading to blockage of capillaries (Cranston et al. 1984). Similarly, epithelial cancer cells are found to be larger in size as compared to healthy cells (Suresh et al. 2005). Thus, the ability to sort cells based on physical properties can provide a powerful diagnostic tools. Sorting of cells is also important in biological and biomedical research in which a heterogeneous mixture of cells can be sorted into specific populations. Also, developments in digital microfluidics, where droplets are used as micro-reactors or for encapsulation, have led to the need of droplet sorting for various applications, including pharmaceutical, cosmetic, food and material industries (Link et al. 2006). In such applications, sorting of droplets based on physical properties is crucial to ensure that the droplets contain precise volume and composition, or to remove specific droplets of interest, or to ensure uniformity of emulsions for consistent product quality.

Bhagat et al. (2010) presented various separation and sorting methods for the separation of cells. Label-free cell separation and sorting techniques were reported by Gosset et al. (2010). Although most of the active and passive separation and sorting methods are described in these papers, extensive discussion on the devices invoking the operational principles is limited. Additionally, effect of the separation and sorting techniques on the cell viability is not addressed. Doddabasavana et al. (2012) described various methods used for the separation of whole blood into its components. Pamme et al. (2007) reported various continuous separation and sorting techniques used in microfluidics. However, some of the passive separation techniques including the inertial and dean flow fractionation and micro-hydrocyclone are not discussed. In another review paper by Lenshof and Laurell (2010), some of the passive microfluidic separation and sorting techniques were discussed, but few other techniques including cross-flow filtration and Zweifach–Fung effect were not presented. Most of the above review papers do not address separation and sorting of particles and cells based on deformability, which is discussed in this review paper. Also, the above papers do not discuss regarding methods or devices that employ a combination of two or more principles for increasing separation and sorting throughput, which is included in the current review paper. Additionally,

discussions on different possible design variants employing a particular principle have not been reported in the literature, which is covered in this paper.

The current review is mainly focused on separation and sorting of micron-sized neutral particles (e.g., cells). The separation and sorting of submicron-sized particles including ions and molecules (e.g., DNA, etc.) is beyond the scope of this review; however, these have been covered elsewhere in detail (Heller 2001; Morgan et al. 1999). Here, a detailed review of the theoretical and experimental aspects of various active and passive separation and sorting techniques is reported. The separation and sorting of micron-sized particles, cells, droplets, parasites and biological entities based on size, deformability and intrinsic properties is presented. The performance of the devices is discussed based on the separation time, particle separation efficiency, throughput and applicability. The separation and sorting techniques are broadly classified as (i) passive, (ii) active and (iii) combined techniques. A broad classification of various particle separation and sorting techniques is presented in Fig. 1. Active sorting techniques involve an external field for sorting of particles, and passive sorting techniques make use of interaction between the particles, microchannel structure and the flow field (Doddabasavana et al. 2012; Kersaudy-Kerhoas et al. 2008). The passive sorting techniques have advantages over the active techniques that no external field is required for the sorting process. In active sorting techniques, the particle sorting efficiency and throughput are relatively higher. Thus, passive separation techniques can be

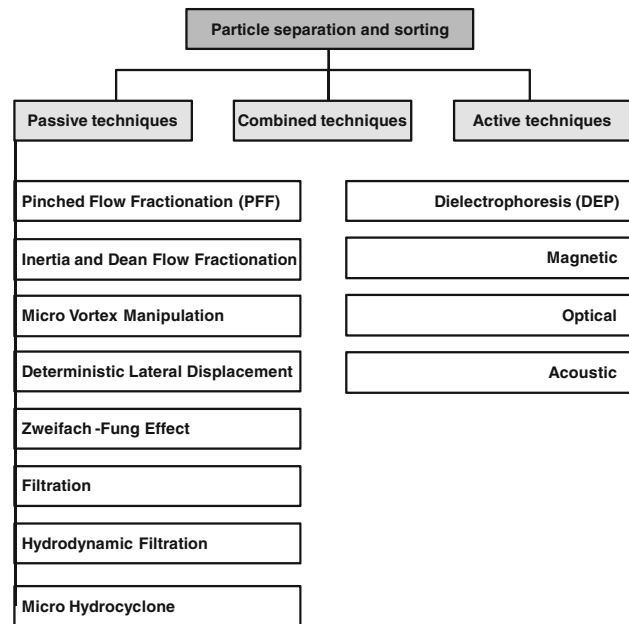


**Fig. 1** A broad classification of various microfluidic separation and sorting techniques

preferred in applications where energy input is of critical concern, whereas active separation techniques can be used where higher particle sorting efficiency is required. In combined techniques, some of the passive techniques employing external fields are used to further improve the separation and sorting performance. The passive and active separation techniques are categorized into different methods based on the operating principles. In each method, first, the underlying operating principle is thoroughly discussed, and then different design variants employing the same principle are presented and discussed. The different design variants have distinctive advantages over a basic design employing only the basic principle. Here, we have tried to include the different separation and sorting techniques (operating principles) and various design variants employing each of these techniques reported in literature. Although it is difficult to claim that the current review is exhaustive, it extensively covers the different methods and principles used in the area of particle separation and sorting. Additionally, the current review addresses some of the operating principles and important design aspects that are not covered in the existing review papers.

## 2 Passive techniques

### 2.1 Pinched flow fractionation (PFF)

Pinched flow fractionation (PFF) is a passive sorting technique that can be used for continuous sizing of particles in a microchannel by employing the characteristics of laminar flow (Oakey et al. 2002). The fluid containing the particles to be sorted is focused by a particle-free fluid, as depicted in Fig. 2. The microchannel includes a ‘pinched segment’ where particles are aligned to one of the sidewalls by controlling the flow rates of both fluids. In laminar flow, a particle has a tendency to flow along the streamline passing through its center of mass. For smaller and larger particles, the streamlines passing through their center of mass are closer toward the channel wall and center of the channel, respectively. The mixture of fluid and particles coming out of the pinched segment is separated by the spreading streamlines according to their sizes (Yamada et al. 2004).

The PFF technique assumes that the fluid is incompressible, and no-slip condition, low Reynolds number and steady-state conditions are satisfied. Also, it is assumed that the particles do not perturb the fluid flow or interact with the channel walls. This technique can be applied to separate various kinds of particles, and the number of particles present in the fluid does not affect separation efficiency. The size limit of the sorted particles mainly depends on precise distribution of flow rates at the inlet

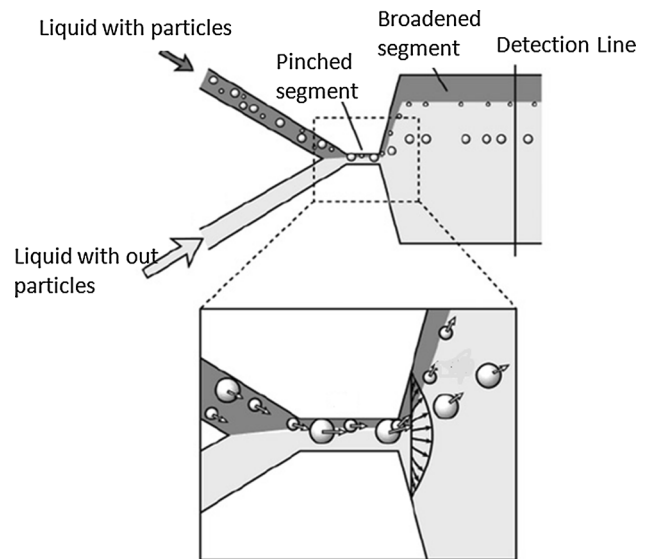


**Fig. 2** Schematic illustration of pinched flow fractionation (PFF) (Yamada et al. 2004)

branches, and fractionation quality is highly depended on the shape of the pinch and pinch-to-broad transition. If the width of pinched segment is high, the flow profile at the boundary between pinched and broadened segment becomes gentle, resulting in lower efficiency. The width of the pinched segment depends on the size of particles in the flow, as observed in the empirical model (Yamada et al. 2004).

$$Y_0 = \left( w_p - \frac{D}{2} \right) \frac{w_0}{w_p} \quad (1)$$

In Eq. 1,  $w_0$  is the width of the outlet,  $w_p$  is the width of the pinched segment,  $Y_0$  is the effluent position of the particle center at the outlet, and  $D$  is the diameter of the particle. The resolution of separation is a function of aspect ratio of microchannel, particle size difference and the microchannel sidewall roughness. Particles with diameters on the order of the sidewall roughness or less cannot be separated using pinched flow fractionation method (Jain and Posner 2008). In PFF methods, the outlet branches are placed symmetrically about the pinched segment as shown in Fig. 3a. So, the fluidic resistances in all the branch channels are equal, and liquid is uniformly distributed to all branches. Here, the particles having diameter equal to the pinched segment directly migrate into the center branch channel, and most of the branch channels below the central channel are inoperative. Separation can be amplified by keeping width of pinched segment much narrower, but particles whose diameter is less than the width of the pinched segment cannot be separated by this method. In asymmetric PFF (AsPFF), branched channels are arranged asymmetrically over the pinched segment by making one

**Fig. 3** Schematic of **a** PFF and **b** asymmetric pinched flow fractionation (AsPFF) (Takagi et al. 2005)

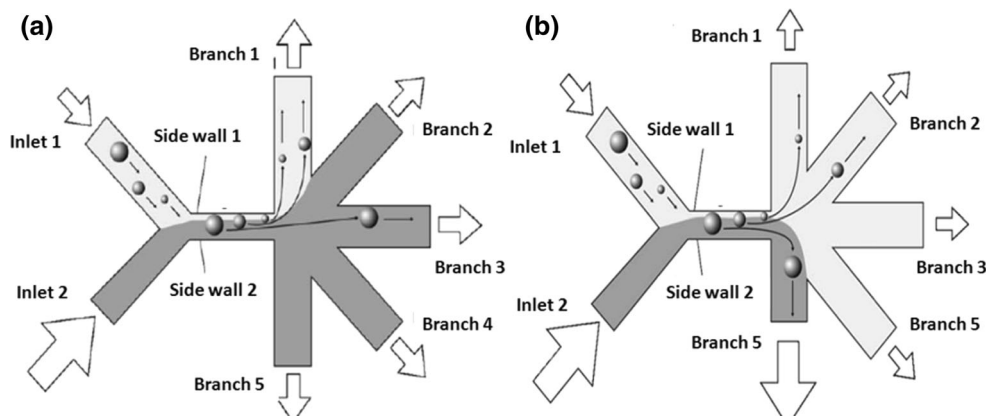
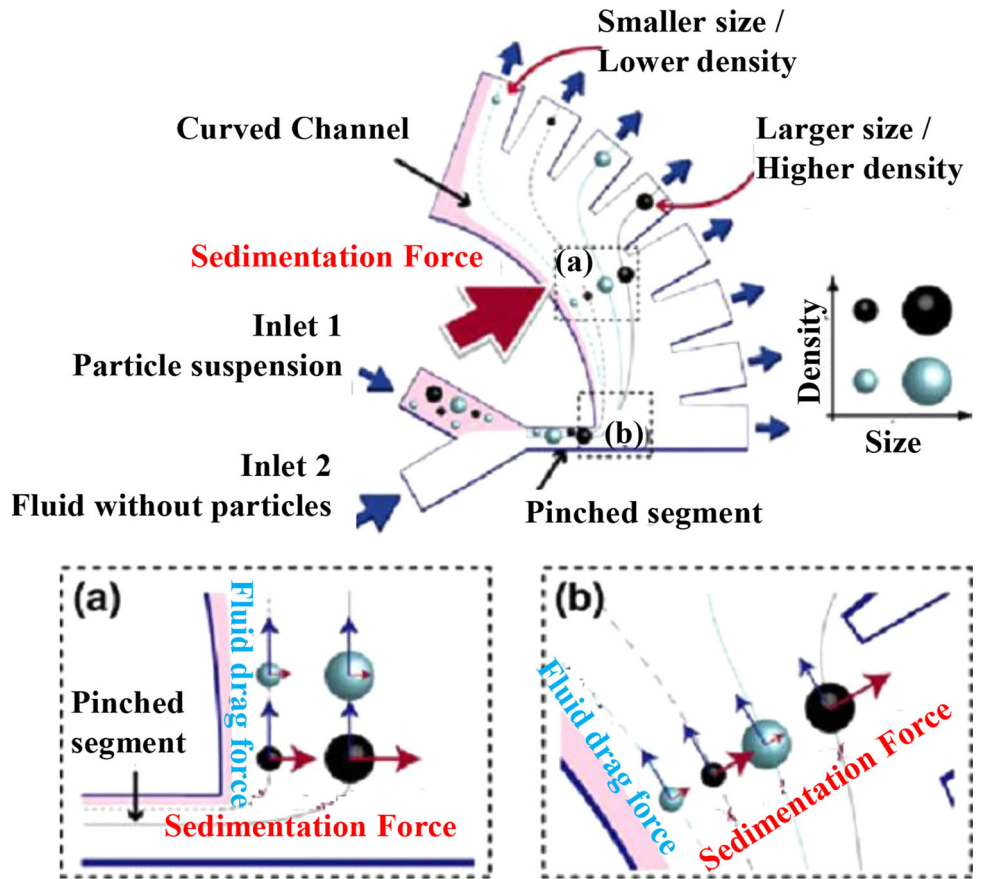


**Fig. 4** Separation mechanism using sedimentation pinched flow: **a** enhanced view of forces acting immediately after pinched segment; **b** sedimentation force acting in the curved section (Morijiri et al. 2011)



branch shorter and/or broader than others, as shown in Fig. 3b, to reduce the resistance in that channel (Takagi et al. 2005). So, most liquids flow into that channel, which is called ‘drain channel.’ By this arrangement, flow can be asymmetrically distributed to different branches, and the position of a particle that is aligned in the ‘sidewall 1’ of the pinched segment is amplified. Particles aligned at the pinched segment are distributed to all branches, and thus, all branch channels are effectively used by this method. Sorting of small-sized particles as well as the particles having small size difference can be achieved by AsPFF

(Takagi et al. 2005). PFF can be extended for sorting of droplets based on their size, which is difficult to be achieved using other methods such as centrifugation and filtration (Maenaka et al. 2008).

Sedimentation effect can be added with PFF method to enhance sorting based on size and density, as shown in Fig. 4. There are two methods: One is based on the inertial force acting on the particle due to momentum change in the curved channel, and second is based on the centrifugal force on the particle by rotation of the device (Morijiri et al. 2011). In the first method, the outlet of the pinched

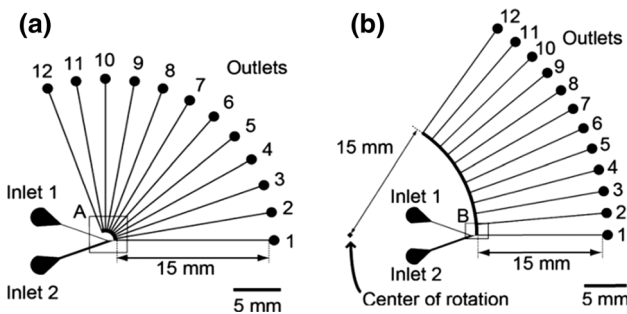


**Fig. 5** Schematic drawing of microchannel designs **a** for particle inertia and **b** device rotation scheme (Morijiri et al. 2011)

segment is connected to a curved channel having small radius (1 mm) with twelve branched outlets, as shown in Fig. 5a. Pressure-driven flow is employed to transport fluids and particles. As the flow coming out of the pinched section enters the broadened curve section, the sedimentation force due to inertia acts perpendicular to the primary flow in order to move the particles outward. Therefore, particles of same size but different densities can be separated with particles of higher density moving outward than particles of lower density. The sedimentation velocity of particles in the curved channel  $U_s$  is given by Eq. 2 (Morijiri et al. 2011) as:

$$U_s = \frac{\rho_p}{18\mu r_c} D_p^2 U^2 \quad (2)$$

In Eq. 2,  $\rho_p$  is particle density,  $D_p$  is particle diameter,  $r_c$  is curvature radius of the flow,  $\mu$  is fluid viscosity, and  $U$  is average flow velocity. In the above equation,  $U_s$  is proportional to the square of flow rate ( $U^2$ ). Since retention time  $t$  is inversely proportional to flow rate and particle migration distance is given by product of particle velocity and time, the particle migration distance is proportional to the flow rate, and hence, higher the flow rate, higher is the particle migration distance. At lower flow rate, sorting is purely based on size similar to conventional PFF where effect of sedimentation is negligible. In the second method (centrifugal pinched flow fractionation) (Sunahiro et al. 2008), the radius of curvature of the curved channel is higher (15 mm) in order to have a strong centrifugal force and to achieve a long retention time (refer Fig. 5b). Initially, each inlet and outlets are partially covered by a lid in order to avoid spilling of the solution during the rotation of the device. The device is rotated on a spinning device with a time period between 30 and 300 s with rotational speed between 3,000 and 750 rpm, respectively. The device is rotated to generate centrifugal force to improve the resolution of particle separation based on density. In this method, the sedimentation velocity  $U_s^1$  is a function of both inertial and centrifugal forces and can be expressed by Eq. 3 (Morijiri et al. 2011):

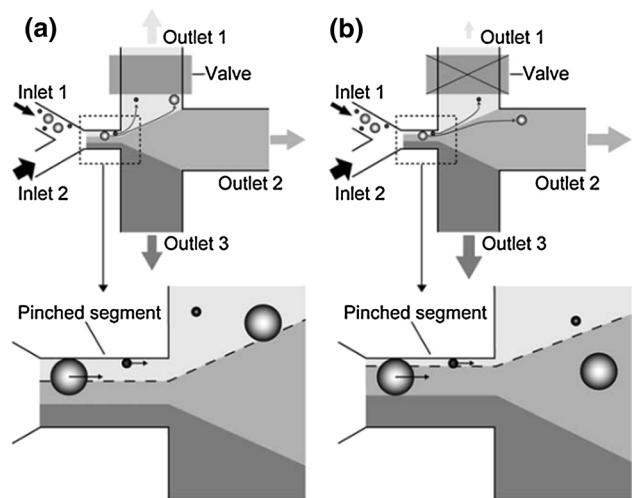


**Fig. 6** Tunable PFF with **a** microvalve at outlet 1 is fully open and **b** microvalve at outlet 1 is partially closed. Effluent position of particle at pinched segment is also shown in both cases (Sai et al. 2006)

$$U_s^1 = U_s + U_c = \frac{\rho_p}{18\mu r_c} D_p^2 U^2 + \left( \frac{\rho_p}{18\mu} - \frac{\rho_f}{18\mu} \right) D_p^2 r_d \omega^2 \quad (3)$$

In Eq. 3,  $U_c$  is migration velocity caused by the centrifugal force,  $r_d$  is distance between the particle and the center of rotation,  $\rho_f$  is fluid density, and  $\omega$  is angular velocity of device rotation. The above equation suggests that sedimentation velocity  $U_s^1$  is proportional to the square of angular velocity  $\omega$ . The retention time is inversely proportional to square of  $\omega$ , so the expected particle migration is given by the product of  $U_s^1$  and retention time  $t$  is independent of angular velocity. Using the three different rotational speeds as mentioned above, it was observed that the ratio of particle recovery at each outlet is nearly the same, which shows that rotational speed does not have much influence on particle separation efficiency. Inertial-based PFF offers higher throughput than centrifugal PFF, but the later does not require external pumps and has high sorting efficiency.

A modification of PFF is tunable PFF (Sai et al. 2006). PDMS membrane valve is connected on the outlet channels to independently control the flow rate through the outlets. Initially, when the valve is fully open, all the liquids that flow in the pinched segment are equally distributed to all outlets. Here, the effluent position of particles is insufficient for the sorting of micron- and submicron-sized particles. So, both large and small particles leave the outlet channel 1 as shown in Fig. 6a. When the microvalve is partially closed, flow rate through outlet 2 is decreased and the effluent position of large-sized particle is shifted to outlet 2 and smaller particle remains in the outlet 1, as

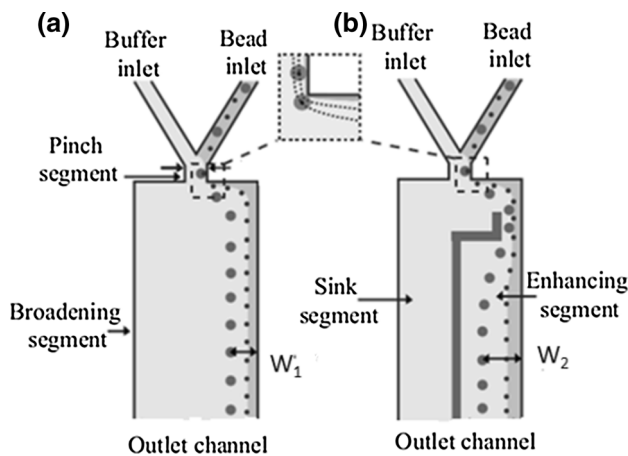


**Fig. 7** Illustration of **a** conventional pinched flow fractionation and **b** enhanced pinched flow fractionation (Vig and Kristensen 2008)

shown in Fig. 6b. Thus, by tuning the flow rates at the outlets, target particles can be collected from the desired outlet. In tunable PFF, separation accuracy is improved compared to conventional PFF and AsPFF. Enhanced pinched flow fractionation (Vig and Kristensen 2008) involves introduction of serpentine structures in the broadened segment, as shown in Fig. 7. The part of the channel in the RHS of the serpentine structure is called ‘enhanced segment,’ and the part in the LHS is called ‘sink segment.’ The difference in the hydraulics resistances between both segments ensures that particle fluid mixture is flown in the enhanced segment. Since the fluid containing the particles moves from narrow ‘pinched segment’ to wide ‘enhanced segment,’ the distance between the streamlines increases. This expansion of streamlines happens only in ‘enhanced segment,’ resulting in the enlargement of the particle trajectories from the wall (from  $W_1$  to  $W_2$  as shown in Fig. 7), which leads to enhanced fractionation.

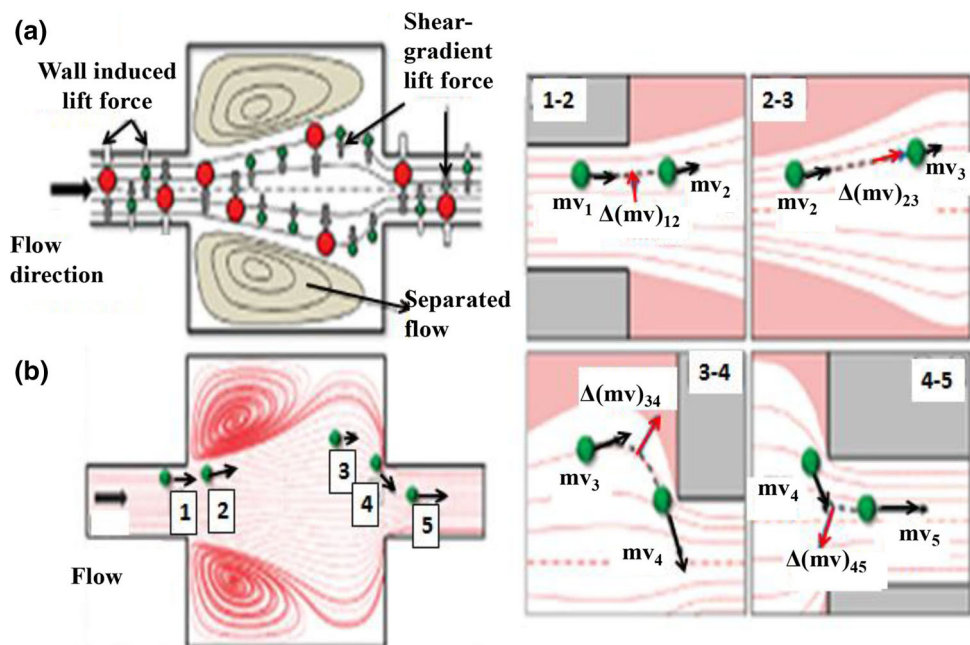
## 2.2 Inertia and dean flow fractionation

When a particle moves along a straight microchannel, there are two inertial lift forces acting on the particle (Park and Jung 2009): (i) shear-gradient-induced lift force and (ii) wall-effect-induced lift force. The ‘shear-gradient-induced lift force’ is a result of the parabolic nature of the velocity profile inside the channel. For a spherical particle present close to the centerline of the channel, the gradient of velocity is higher on the wall side of the particle as compared to the centerline side (Asmolov 1999; Bhagat et al. 2008). So, the spherical particles roll from the center down toward the microchannel walls. The ‘wall-effect-induced lift force’ can be explained by considering the flow field around a spherical particle in the presence of a wall that

gets disturbed leading to the formation of an asymmetric wake around the particle. This asymmetric wake leads to a lift force that directs the particles away from the wall (Zeng et al. 2005). Both of these lift forces will be acting in opposite directions. Lateral migration of particles in microchannels occurs due to the superposition of the two inertial lift forces. Particles are positioned within the microchannel cross section depending upon their size relative to the microchannel dimensions, and thus, sorting of different-sized particle becomes possible. Segre and Silberberg (1961) first demonstrated the existence of lateral forces on rigid spherical particle and the migration of particle to a position distant 0.6 tube radii from the axis.

When arbitrarily positioned particles move along a number of contraction and expansion structures in a straight microchannel, all particles will be concentrated at the wall, which is the principle of inertial focusing (Park and Jung 2009). In this device, the particle focusing is based on the vortex flow (or separated flow), which is created at the expansion region. In the expansion chamber, the wall-effect-induced lift forces by the sidewalls are weakened as compared to the shear-gradient-induced lift force due to long distance from the mainstream to the sidewalls. The particles moving close to the centerline are drifted to the sidewalls due to the dominance of the shear-gradient-induced lift force. Majority of the particles are focused close to the sidewalls while passing through a series of contraction and expansion channels. The inertial separation of the particles based on size is demonstrated by the effect of inertial lift forces and induced inertial lift force due to the momentum change. When the particles move from one contraction to another contraction through the expansion chamber (multi-orifice microchannel) as shown in Fig. 8a (Park and Jung 2009), there is momentum exchange between the particle and fluid. In the first transition between 1 and 2 and 2 and 3, there is no considerable mismatch between the particle and fluid path. Thus, momentum change and induced inertial force are less. When the particle moves from region 3 to 4, due to the mismatch in the path of fluid and particle, the momentum change is considerable and the direction of the induced lift force is acting in a direction toward the wall. Due to the presence of the wall, the particle will align in the direction of the wall irrespective of the size of the particle. The movement of particle from 4 to 5 is crucial. Here, the mismatch in the path and the resulting change in momentum are high, and the induced lift force is acting in a direction away from the wall. This induced lift force is  $F_L = \rho_p \pi d^3 U^2 / 6D_h$ , where  $\rho_p$  is the density of particle,  $d$  is the diameter of particle,  $U$  is the average velocity of flow, and  $D_h$  is the hydraulic diameter of channel. The equilibrium position of the particle is achieved by the

**Fig. 8** **a** Flow between a pair of contraction-expansion in an array in a straight channel. **b** Path of particles with momentum exchanges between particle and fluid (Park and Jung 2009)



balance between this inertial force and the drag force. The lateral migration velocity of the particle is given by the expression  $U_d = \rho_p d^2 U^2 / 18\mu D_h$ , where  $\mu$  is the viscosity of the fluid in which the particle is moving. As observed, the lateral migration of particles is proportional to the square of the diameter of the particle and the flow rate of the fluid. Thus, the larger particles are subjected to larger lateral shift than the smaller particles and thus separated.

Screening of cells is important in the detection of cancer cells (Rivet et al. 2011; Situma et al. 2006; Dong et al. 2013). Cancer cells are found to be larger in size and have higher deformability as compared to healthy cells (Cranston

et al. 1984; Suresh 2007). Current technologies are inefficient for the measurement of cell deformability. Label-free cell enrichment and separation technique with size and deformability as suitable markers have been investigated (Hur et al. 2011), as shown in Fig. 9. The chip comprises an inlet with a flow filter and a straight channel for focusing a gradually expanding chamber and five outlets (B and C for blood cell and cancer cell collection, respectively) with high fluidic resistance. The solid particles migrate toward the center of the channel due to the inertial lift force. If the particle is deformable, in addition to this inertia force, nonlinear lateral migration of the particles occurs. Theoretical investigations have shown that elastic solid particles in Poiseuille flow experience a force away from the wall and get laterally migrated toward the centerline, even in the low  $Re$  limit (Tam and Hyman 1973). Followed by this, several studies were carried out to investigate motion of bubbles, liquid drops, vesicles and viscous capsules surrounded by elastic membranes under wall-bounded flows (Tam and Hyman 1973; Leal 1980; Doddi and Bagchi 2008; Chan and Leal 1979; Abkarian and Viallat 2005; Magnaudet et al. 2003). Lateral migration of deformable particles was observed due to the nonlinearity caused by matching of velocities and stresses at the particle-droplet interface (Magnaudet et al. 2003). It was also observed that the magnitude of the lateral drift velocity and lift force is related to the deformed shape of the object. The shape of the droplet is determined by the Webber number, capillary number and the ratio of internal to external viscosity ( $\lambda$ ). As the deformability of the droplet increases, the drift force tries to push the droplet toward the center of the channel and occupies an equilibrium position ( $X_{eq}$ ) due to the balance of

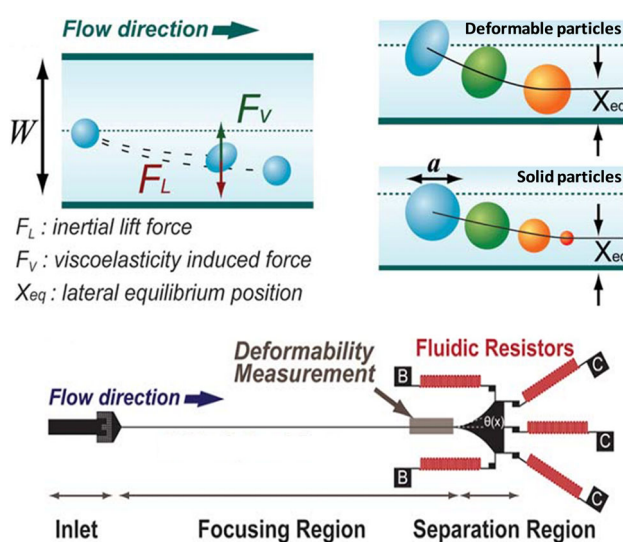


**Fig. 9** Microfluidic device used for cancer cell enrichment based on size and deformability (Hur et al. 2011)

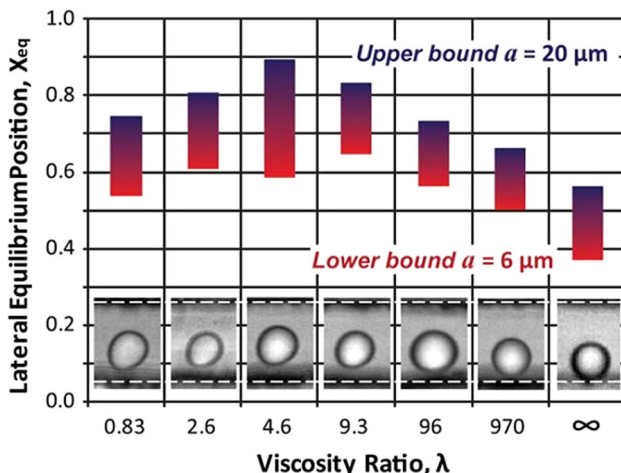


**Fig. 10** Equilibrium positions of particles/droplets of different deformability (Hur et al. 2011)

inertial lift force and deformability induced lift force, as shown in Fig. 9. This equilibrium position is the measure of deformability of a droplet or cell. Nondeformable cells of very large viscosity and elastic solid particles of the same size can be separated due to the large value of  $X_{\text{eq}}$  for the cells. Even if the cell is nondeformable, the nonsolid boundary will produce the dynamics of internal fluid circulation and tank-treading motion of the surfactant molecules at the interface. The equilibrium positions of cells having different viscosity ratios are shown in Fig. 10.

The effect of ‘dean flow’ on the manipulation of the equilibrium position of particles is demonstrated in Fig. 11. In case of flow through a curved microchannel, a secondary flow is established due to centrifugal effects, which is called ‘dean flow’ (Yoon et al. 2009). In fluid flow through a curved channel, the fluid pressure at the inner wall is slightly higher than that at the outer wall. So, the fluid from the center of the channel is pushed outward as a result of this pressure gradient, and fluid near the top and bottom walls moves inward to satisfy conservation of mass. This is responsible for a symmetrically swirling secondary flow (two counterrotating vortices) on the cross-sectional plane of the microchannel. This secondary flow will affect equilibrium position of particles in the flow apart from the inertial lift forces explained previously. As discussed earlier, in case of parabolic flow, lateral migration of particles

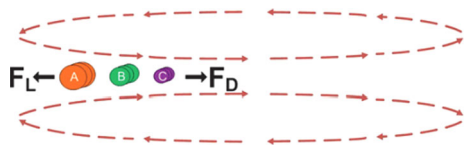


**Fig. 11** Schematic representation of dean flow with  $R_{fA} > R_{fB} > R_{fc}$ , lift force and dean drag acting on the particle are also shown (Carlo et al. 2008)

happens by the dominant inertial lift forces due to the presence of shear-gradient-induced inertia toward the channel wall and wall-induced inertia acting toward the center of the channel away from the wall. The transverse dean flow induces drag force ( $F_D$ ) that moves particles located at the top and bottom toward the inner wall. However, the particles located near the midplane (between top and bottom walls) are pushed toward the outer wall and recirculated following the top or bottom streamlines (in the rotating vortices) to find their equilibrium positions. Here, the equilibrium position depends on the Reynolds number and ratio of inertial lift force to dean drag force (Russom et al. 2009).

The lift force ( $F_L$ ) and dean drag force ( $F_D$ ) vary in magnitude across the cross section of the channel, and the exact nature of this variation is not clearly understood. However, two nondimensional parameters, dean number ( $De$ ) and curvature ratio, can be used to explain how the above two forces scale in flows through curved channels. Those two important nondimensional parameters are dean number  $De = R_c \sqrt{D_h/2r}$  and curvature ratio  $\delta = D_h/2r$ , where  $D_h$  is the hydraulic diameter of the channel,  $R_c$  is the Reynolds number of the channel, and  $r$  is the radius of the curvature of the channel. Drag force acting on the particle due to the dean flow can be scaled as  $F_D = \rho_m D_h^2 U_m^2 a/r$ , where  $U_m$  is the maximum channel velocity,  $\mu$  is the viscosity,  $\rho$  is the density of the fluid, and  $a$  is the particle diameter. The ratio of lift force to drag force is given by  $R_f = \frac{1}{\delta} (a/D_h)^3$ . Separation of particle is possible if the value of  $R_f \geq 1$  for one size of particle and  $R_f < 1$  for another size of particle. Flow velocity in the channel should be selected by considering three cases: (i) When the flow velocity is small, then  $R_f \gg 1$ , in that case there is no flow focusing in the entire channel length; (ii) when flow velocity is moderate, then  $R_f \geq 1$ , there are one or more flow-focusing streams; and (iii) if flow velocity is large, then  $R_f < 1$ , this leads to mixing of particles inside the channel (Carlo et al. 2008). To avoid entrainment of particles in the dean vortices, the dimension of the microchannel should be such that  $(\frac{a}{D_h}) \leq 0.07$ . Similarly, if the dean number increases, the particles reach an equilibrium position quickly, but  $De$  should be maintained less than 20 to avoid entrainment of the particles in the dean vortices (Chatterjee 2011). While the channel Reynolds number ( $R_c$ ) is used to describe the inertial effect of fluid flow, particle Reynolds number ( $R_p$ ) represents the inertial effect from a fluid on a particle and the Stokes number ( $S_t$ ) is used to study trajectory mismatch between the fluid and particle and the size separation effect under the same flow condition (i.e., same  $R_c$ ). In case of a particle in accelerating flow, the Stokes number ( $S_t$ ) represents how quickly the

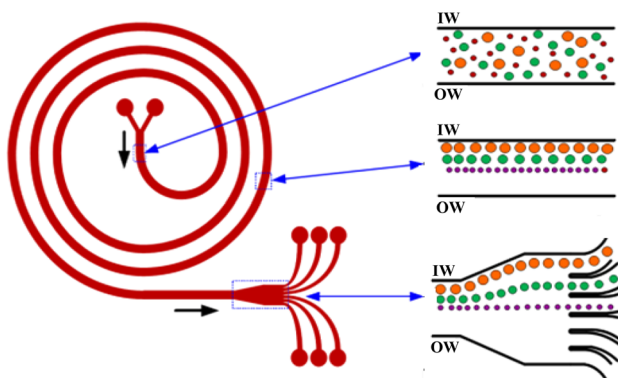


**Fig. 12** Separation of particles in a spiral-shaped microchannel (Kuntaegowdanahalli et al. 2009)

particle responds to the modifications in the surrounding flow. To achieve the equilibrium position stability, which is required for the separation of particles, the channel Reynolds number ( $R_c$ ) in the range 10–270 (Pamme 2007; Carlo et al. 2009; Gossett and Carlo 2009a), particle Reynolds number ( $R_p$ ) in the range 0.05–5.0 (Russom et al. 2009; Wu et al. 2009) and the Stokes number ( $S_t$ ) in the range 9–64 (Wu et al. 2009) have been used.

Use of curved channels requires shorter distance for flow focusing, thus providing reduced hydrodynamic resistance, which is promising for low power inertial focusing or separation (Gossett and Carlo 2009b). A spiral microchannel has been used for the sorting of particles of different sizes into six different outlets, as depicted in Fig. 12 (Kuntaegowdanahalli et al. 2009). In Fig. 12, IW is the inner wall and OW is the outer wall. The sorting efficiency can be improved by keeping the opening of the spiral channel into a wider straight channel. Spiral microchannel can also be used for the synchronization and

selection of cancer cells at different phases of cell cycle from blood in order to predict the condition of disease (Lee et al. 2011a). Different stages of cancer cells have different sizes. Particles of different sizes achieve different lateral location inside the spiral channel due to the balance of inertial lift force and dean drag force (Gossett and Carlo 2009a). The use of dean force to focus large particles to the inner wall of the spiral channel and transport of smaller particles from the inner half of the channel to the outer half of the channel has been demonstrated (Bhagat et al. 2008). Separation of particles and exchange of medium can be achieved using a contraction–expansion array (CEA) (Lee et al. 2011b, c) with sheath flow for flow focusing, as shown in Fig. 13a. The principle of separation is based on the force balance between the inertial lift force and dean drag force acting on the particles. The sample stream is supplied through an inlet, and the buffer solution is supplied through the other inlet to keep the particles close to the wall. Each  $y-z$  plane shows the cross section of three contraction regions in the microchannel. The inertial lift force ( $F_L$ ) is less than the dean drag force ( $F_{DD}$ ) if the aspect ratio of the channel is equal to one. Then, the red particle and green dye both are influenced by the dean flow and move to the sidewall  $S_2$ . This method can be explained for sorting of two different-sized particle. If the size of the particle is more than the critical cutoff value determined by the balance between  $F_L$  and  $F_{DD}$ , then the particle will move to  $S_1$  since  $F_L > F_{DD}$ , but particles smaller than the critical cutoff radius still move to  $S_2$ , as shown in Fig. 13b.

In a single-stage multi-orifice flow fractionation (SS-MOFF) device shown in Fig. 14a, the separation efficiency of larger particle is low. So, the recovery of larger particles at the center of the channel is required to be improved, which can be achieved by keeping a number of SS-MOFF

**Fig. 13** **a** Schematic of a multi-orifice flow fractionation device. **b** Movement of particle under  $F_L$  and  $F_D$  for aspect ratio  $AR = 1$  and  $AR < 1$  channel geometry (Lee et al. 2011b)

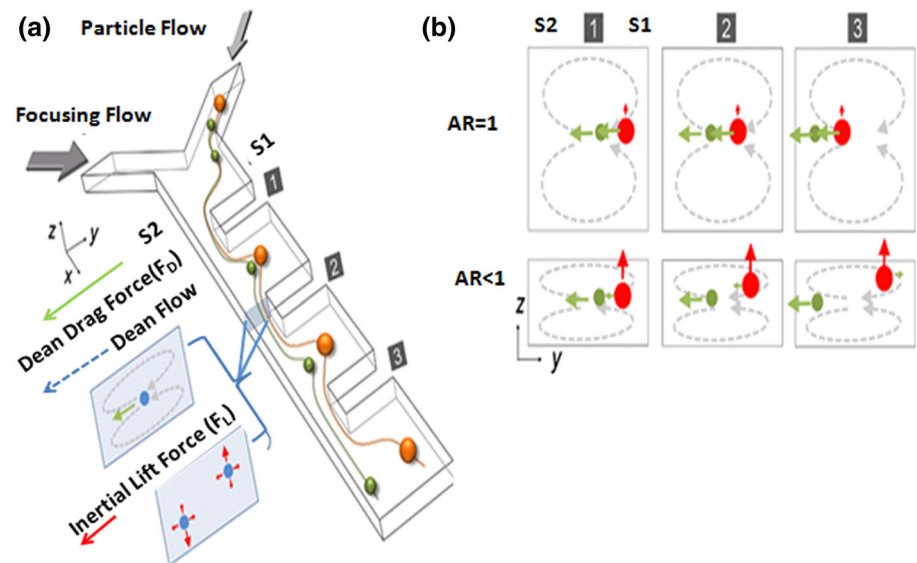
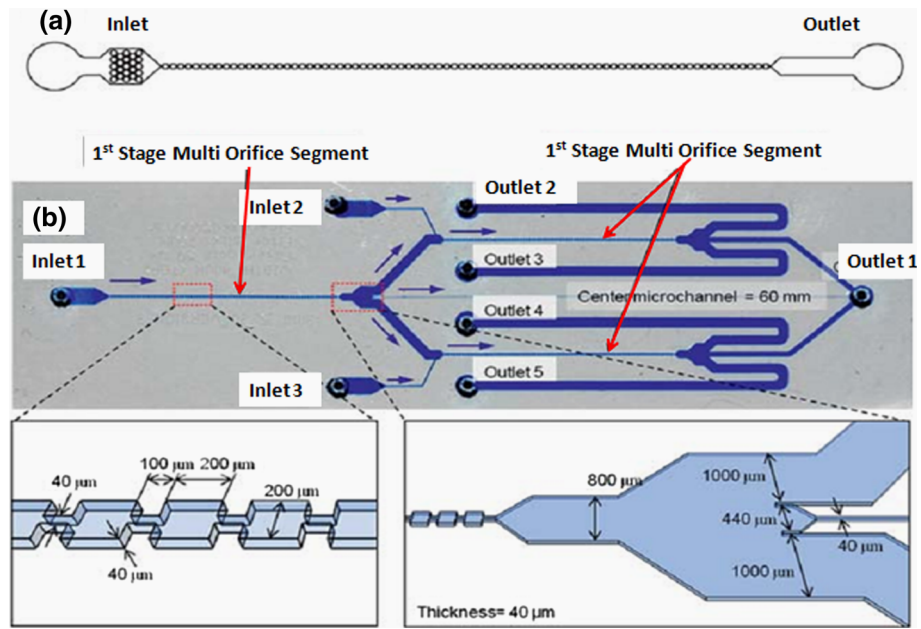


**Fig. 14** **a** Single-stage multi-orifice flow fractionation (SS-MOFF). **b** Multistage multi-orifice flow fractionation (MS-MOFF) (Sim et al. 2011)



in series called multistage MOFF (MS-MOFO) (Sim et al. 2011; Lee et al. 2011d; Kwon et al. 2010), as shown in Fig. 14b. In this case, reseparation of the unselected particles in the first stage is done in the subsequent steps. Another modification to the SS-MOFO is the parallel MOFO (p-MOFO) (Hyun et al. 2012) device in which four SS-MOFO channels are connected in parallel, which has been demonstrated for the separation of circulating tumor cells from blood of metastatic breast cancer patients. When a scattered particle distribution is supplied to the inlet of a rectangular microchannel, the particles would align in four equilibrium positions, which are the center of the four sides of the channel. These four streams of focused particles can

be reduced to two streams using symmetrically curved channel and can be further reduced to one stream for asymmetrically curved channels (Seo et al. 2007; Carlo et al. 2007), as shown in Fig. 15a. In both symmetric and asymmetric cases, the dean number should be less than 20. Figure 15b shows flow focusing at the outlet of a straight rectangular channel with a number of streams. Figure 15c shows flow focusing at the outlet of a symmetrical curved channel with two focusing streams, and Fig. 15d shows flow focusing at the outlet of an asymmetrical micro-channel into a single stream. The nature of particle focusing with increase in the particle Reynolds number ( $R_p$ ) is also shown in Fig. 15b–d.

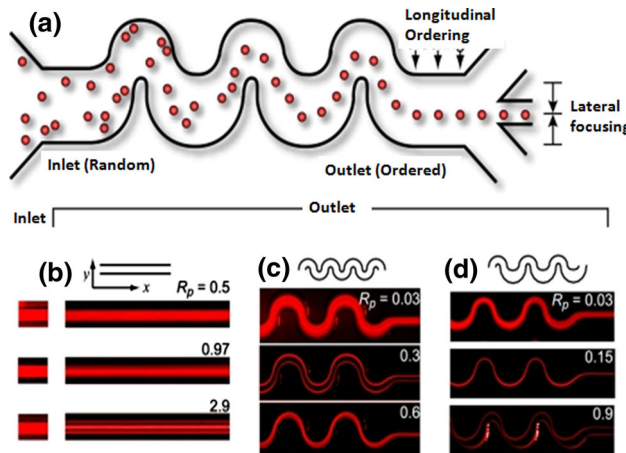


**Fig. 15** **a** Particle focusing in asymmetrically curved channel; **b** particle focusing in rectangular channel; **c** particle focusing in symmetric curved channel; and **d** particle focusing in asymmetric curved channel (Carlo et al. 2007)

### 2.3 Microvortex manipulation

Microvortex manipulation (MVM) (Hsu et al. 2008) is used for the focusing of particles into multiple streams and separating the particles, as shown in Fig. 16. Here, a number of herringbone grooves are constructed on the bottom of a channel. Equilibrium positions are achieved by the particles based on the balance between the gravitational force, buoyancy force and hydrodynamic drag force. When flow is generated over the grooves, vortices are created in the direction of the streams and a helical flow pattern is created. Each set of grooves produces symmetric microvortices of alternating directions. Microvortices exert drag forces on the particles both in the vertical and in the lateral directions, and particles are focused on the interface of the vortices. When the particle is lighter than the medium, particle moves to the top of the channel and occupies a position due to the balance between upward buoyancy

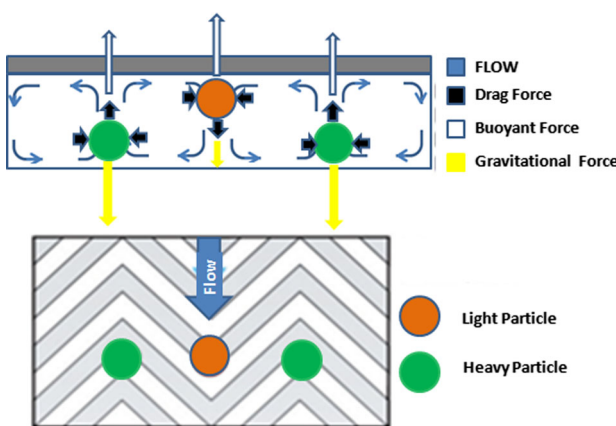


**Fig. 16** Position of the particles in micro-vortices manipulation (MVM) (Hsu et al. 2008)

force and downward drag and gravitational forces and the heavier particles stay at the bottom of the channel.

#### 2.4 Deterministic lateral displacement (DLD)

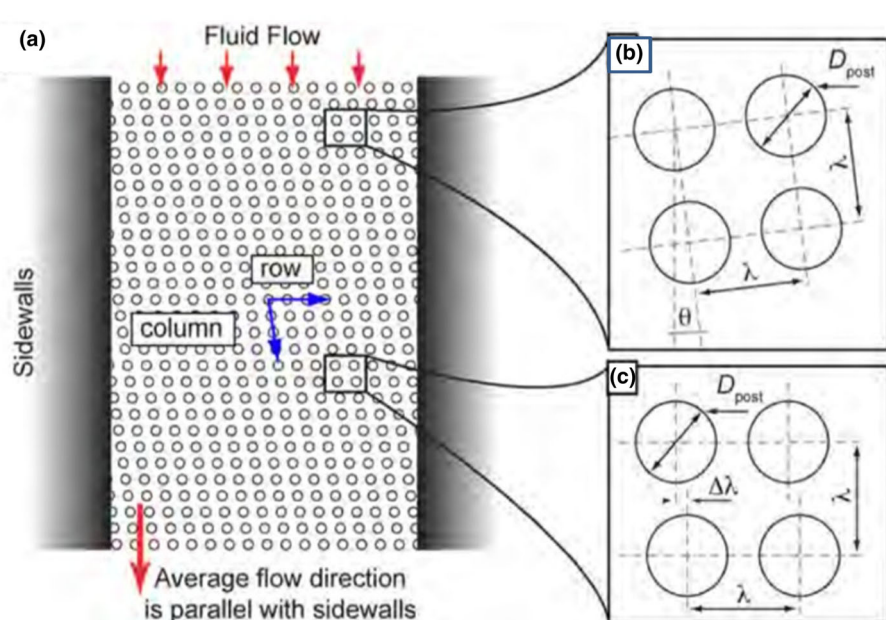
Deterministic lateral displacement (DLD) is a steric method of continuous separation that makes use of asymmetric bifurcation of laminar flow around obstacles (Huang et al. 2004). Particles moving through an array of obstacles with gaps larger than the particle size select their path deterministically on the basis of their size and deformability. Particles of given size and deformability follow equivalent migration path leading to an efficient separation method (Huang et al. 2004). In this case, the periodic arrays of posts of cylindrical shape are placed in the flow direction (Huang et al. 2004). The center-to-center distance between the adjacent posts is  $\lambda$ ,  $D_{\text{post}}$  is the diameter of the

post, and the array posts are set at angle  $\theta$  with respect to the flow direction (called migration angle), as shown in Fig. 17a. Successive rows in the flow direction are placed with a lateral shift of  $\Delta\lambda$  in a direction perpendicular to the flow direction. So,  $\Delta\lambda = \lambda \tan \theta$ . There are two methods used to arrange the post structures. In the first method (Fig. 17b), a square array is rotated with respect to any post, and in the second method (Fig. 17c), a rhombic structure is used (Beech 2011; Long et al. 2008).

The motion of a sphere in a DLD ratchets was studied to understand the directional locking of particle. This shows that the presence of irreversible interactions between the moving particle and the obstacles breaks the symmetry of the particle trajectory and a lateral displacement is induced to the particle. Although this lateral displacement is small, periodic nature of the DLD system makes the lateral displacement to accumulate and leads to a macroscopic change in migration angle (Balvin et al. 2009). The movement of particle in the periodic array is also studied by means of Stokesian dynamics simulations. Due to nonhydrodynamic and short-range interactions between the particle and the obstacles, the moving particle becomes locked in a certain periodic trajectories with an orientation along one of the lattice directions (Frechette and Drazer 2009).

The periodicity of the array of posts is maintained by ensuring that the posts in the first row and ‘ $N + 1$ ’ row are in-line, in which case the period of DLD structure is ‘ $N$ .’ If a flow is maintained through the structure, the direction of the flow is determined by the sidewall. Flow between two adjacent posts  $\phi$  is split into ‘ $N$ ’ streams (namely  $\phi_1, \phi_2, \phi_3, \dots, \phi_N$ ) separated by streamlines whose positions are denoted by  $P_1$  to  $P_N$ . The width of fluid stream ( $\beta$ ) at

**Fig. 17** a Schematic of DLD chip with post placed at an angle to the flow direction; b rotated square array posts; c rhombus array posts (Beech 2011; Long et al. 2008)



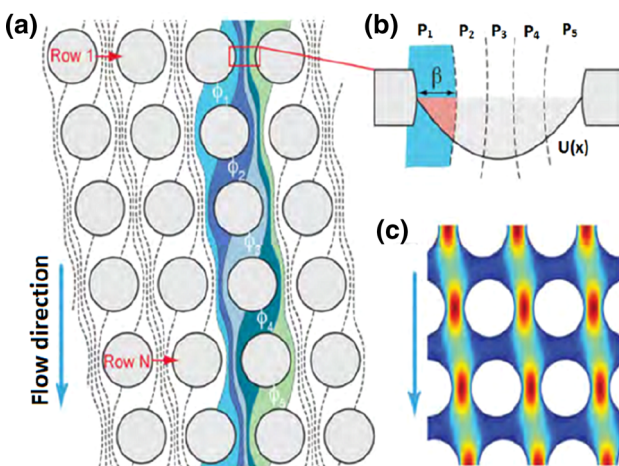


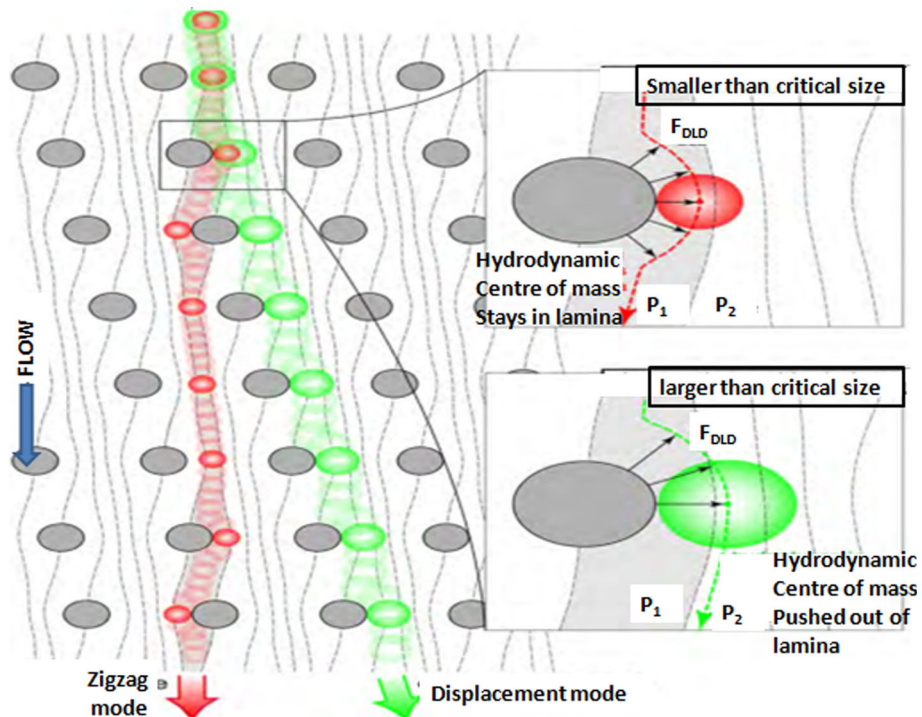
**Fig. 18** **a** DLD structure; **b** splitting of fluid stream between the posts; **c** velocity profile between the posts (Beech 2011)

position  $P_1$  is critical for a post which determines the size of particle that can be sorted using the DLD structure. The movement of the fluid streams in the direction of flow past the successive rows is presented in Fig. 18a–c. The approximate value of  $\beta = \sqrt{(N/3)}(d/N)$  where  $N$  is the period of the array and  $d$  is the diameter of the posts (Inglis et al. 2006). The critical diameter of the particle that can be sorted using DLD is  $D_c = 2\beta$ . If the diameter of a particle is less than this critical diameter, its center of gravity will be inside the first stream  $\phi_1$  and the particle will flow along that streamline only in a zigzag path, as shown in Fig. 19. But, if the diameter of a particle is more than this critical

diameter, then the center of the particle lies in the next stream (i.e.,  $\phi_2$ ). Due to the presence of ‘steric force,’ the particle is shifted to the next stream. In the next row, this stream ( $\phi_2$ ) occupies the position  $P_1$ . The lateral shifting happens again and continues at each post on the successive rows. In this way, the larger particles move away in a displacement mode, thus leading to sorting of particles. Arrays of triangular posts can be used instead of cylindrical post (Loutherback et al. 2010), which reduces clogging, lowers the pressure requirement at inlet to drive the fluid and increases the range of displacement characteristics.

The DLD method can be extended for sorting of particles of different sizes in a mixture (Davis et al. 2006; Davis 2008). This can be achieved by placing different arrays of posts in series in the direction of flow, where each array is intended to sort one type of particle from the mixture. Here, the critical diameter for each array will be manipulated depending on the diameter of the particle to be sorted in that array. This modified DLD structure having thirteen different arrays of posts was successfully used for the fractionation of blood components, as shown in Fig. 20. DLD has also been used for sorting of nonspherical particles (Beech et al. 2012). Here, the effective radius of the particle is the critical parameter for sorting. The critical radius ( $R_c$ ) of a particle is defined as the distance from the post to the center of the gravity of a nonspherical particle along the line joining the center of the two nearest posts, as shown in Fig. 21a, b. By comparing the critical radius of the DLD array and effective radius, particles can be moved in displacement or zigzag mode. Usually, particles have a

**Fig. 19** Sorting of particle using DLD principle into zigzag and displacement mode (Beech 2011)



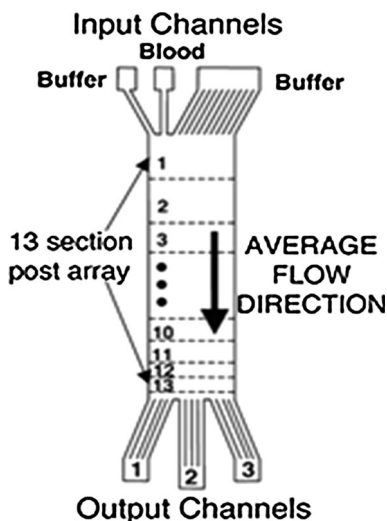


**Fig. 20** Fractionation of blood into RBC, WBC and platelets (Davis et al. 2006)

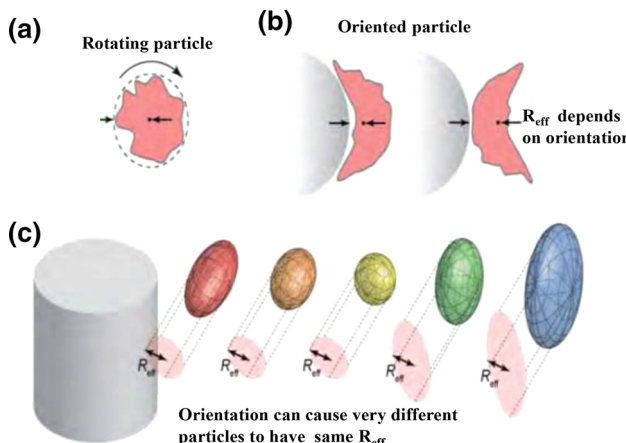


**Fig. 21** **a** Effective radius of rotating nonspherical particle; **b** effective radius of deformable particle; **c** different-sized particle shows same effective radius (Beech 2011)

tendency to rotate in the DLD structure. This rotating mode has no effect on sorting of spherical particles, but for nonspherical particle, this rotation becomes critical. The particles with different sizes can rotate and align as shown in Fig. 21c to produce same critical radius in which case sorting of particles will be difficult. To overcome this problem, the depth of the device is kept equal to the smallest dimension of all the particles (Beech et al. 2012) to prevent the rotation of particles. So, different non-spherical particles will show different effective radii ( $R_{\text{eff}}$ ) for which sorting is possible, as mentioned above. Sorting of deformable objects can also be achieved using DLD by applying different pressures to the flowing fluid (Quck et al. 2011; Ghasemi et al. 2012). A clear picture of the rate of deformation of objects at different pressures is required for sorting. At a particular pressure, more deformable

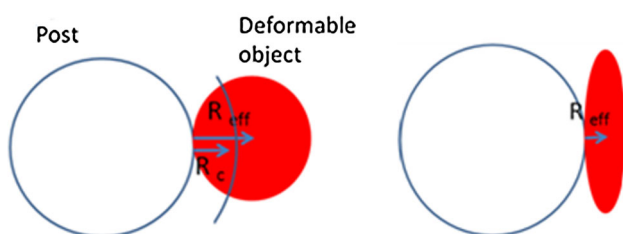


**Fig. 22** Deformation of object under pressure and change in effective radius ( $R_{\text{eff}}$ )

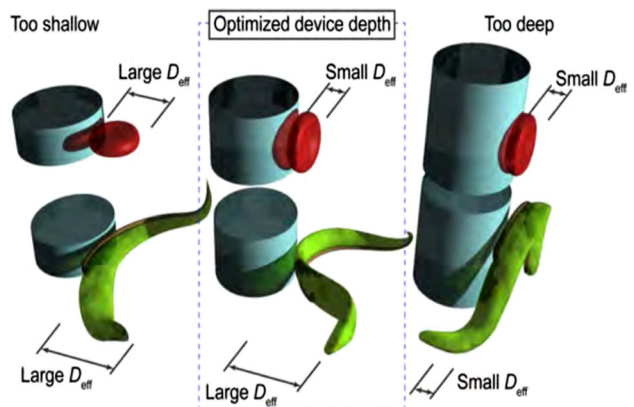


**Fig. 23** Use of DLD for the separation of parasites from RBCs (Holm et al. 2011)

objects produce smaller critical radius compared to objects that are less deformable. So, at the same pressure, the objects can be sorted based on different effective radii due to difference in deformability. As pressure is increased, the objects are deformed more, as shown in Fig. 22. A disposable device having parallel DLD structure was used for the fractionation of blood into its components. This parallel DLD structure will give high flow rate and high throughput (Inglis et al. 2011).

The DLD method has been used for the sorting of circulating tumor cells (CTCs) from normal cells (Loutherback et al. 2012). Usually, CTCs have the size of 15–30  $\mu\text{m}$  and are larger than the normal blood cells. Conventionally, active method has been used for this purpose, but the operating flow rate in such devices has been quite low ( $\sim 1 \text{ mL/h}$ ) for achieving high efficiency. A DLD device used for sorting of CTC and normal cells has 58- $\mu\text{m}$  triangular posts with 42- $\mu\text{m}$  gaps between them, and a 1/20 array tilt is given to each mirrored array with respect to the flow direction. The larger CTC cells are deflected away from the flow direction to the center of the channel, and smaller normal blood cells follow the streamlines of the flow defined by the walls of the device to the waste outlet. The DLD method can handle large flow rate of  $\sim 10 \text{ mL/min}$ , which is higher than the flow rates used in any other sorting methods.

The DLD method has also been used for the separation of sleeping parasites from blood (Holm et al. 2011), as shown in Fig. 23. The RBCs have a dumbbell shape where the parasites are long. Here, the height of the post is a critical design parameter. If the height of the post is very high or too low, both parasite and RBC produce almost the same effective diameter ( $D_{\text{eff}}$ ) and sorting becomes difficult. There is an optimum height for which the parasite and RBC show different effective radii; thus, sorting is possible.

As a modification to DLD technique, tunable DLD (Beech and Tegenfeldt 2008) device has been reported, which employs the elastic property of PDMS that is used as the substrate for fabricating the microfluidic device. The entire DLD structure is placed on a movable chuck connected to a micrometer, as shown in Fig. 24. The DLD structure made of PDMS has the distance of 10  $\mu\text{m}$  between the posts, which is 0.1 % of the overall length of the device. By adjusting the micrometer, the device is pulled by the chuck to control the distance between the posts. If the length of the device is changed by 10  $\mu\text{m}$ , the local strain changes the dimension between the posts by 0.1 % of the 10  $\mu\text{m}$ , i.e., 10 nm. So, the critical radius is changed by a very small value of the order of 0.1  $\mu\text{m}$ . So, by tuning the DLD structure, sorting of particles can be achieved to the precision of 0.1  $\mu\text{m}$ .

The DLD method can be extended to the separation and sorting of droplets of different diameters (Joensson et al. 2010). Droplets of two different sizes with oil as continuous phase and water (with and without yeast cells) as discrete phase were generated. The encapsulated droplets shrink due to the presence of yeast inside them, and droplets having no yeast cell retain their size. The droplets with and without encapsulated yeast inside were sorted using DLD (Joensson et al. 2010). In another work, droplets having *Saccharomyces cerevisiae* inside them reduce their size during the incubation, whereas the droplets having only yeast cell inside them retain or slightly increase their size (Joensson et al. 2011). DLD device is

used for the separation of both of these droplets. These experiments prove the ability of DLD method to separate the droplet based on the biological content.

As another modification of DLD, a constant force is applied to drive the particles, which is called ‘force-driven deterministic lateral displacement (f-DLD).’ If gravity is used as the external force field, then it is called ‘gravity-driven DLD (g-DLD).’ In this method (Devendra and Drazer 2012), the DLD chip is placed at an angle called ‘forcing angle.’ The arrays are placed at an angle to the flow called ‘migration angle.’ Experiments have been conducted on different-sized particles independently and at different forcing angles to determine an optimum forcing angle for each size of particles, which leads to directional locking to increase the separation efficiency. Droplets of various sizes including droplets having size larger than the gap between the obstructions in the DLD are also reported. In this case, drops will undergo large deformation. In all the forcing directions and for the entire range of sizes of drops, migration angles can be found out by collision model. The difference between the critical angles at which the largest and smallest drops move across the line of obstacles in this array is approximately 20° (Bowman et al. 2012). The DLD technique can also be used for the purification of spores (Inglis et al. 2010). Aspergillus spores are spherical in nature with narrow size distribution, which makes sorting difficult. The DLD structure used for this purpose had different array configurations with two different angles of tilt that sort the spores into different groups (small 0–3.5  $\mu\text{m}$ , medium 3.5–5  $\mu\text{m}$  and large 5–10  $\mu\text{m}$ ) (Inglis et al. 2010). Separation of suspended particles under the action of a uniform external force in a two-dimensional periodic energy landscape can also be done. The migration angle of particles is analyzed as a Poincare map, showing that it corresponds to a tangent bifurcation (Herrmann et al. 2009).

In an upscaled DLD device, instead of micrometer-sized gaps between the posts, larger gaps are utilized (Lubbersen et al. 2012). In that case, the Reynolds number of the flow

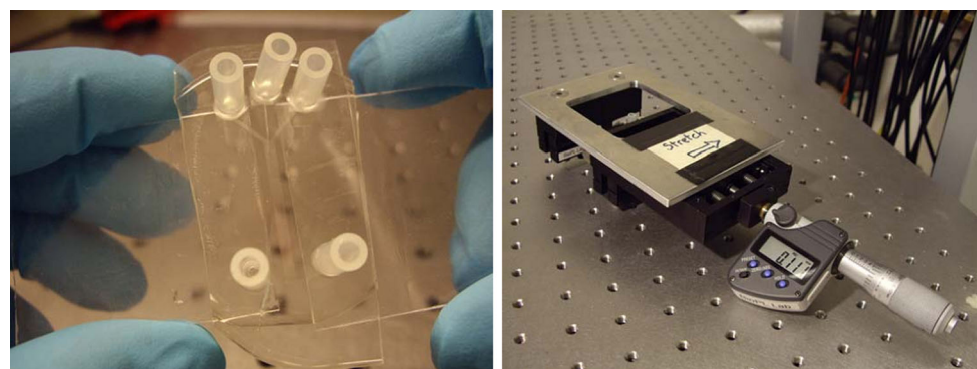


**Fig. 24** Tunable DLD for sorting of particles [82 (Electronic supplementary information)]

and the separation efficiency increase. This is mainly due to the additional deflection of particle in the ratchet array by the inertial lift force acting on the particle and the pair of vortices produced behind the obstacles at high Reynolds number. From the experimental and numerical studies, vortex formed at a  $Re = 9$  in a cylindrical ratchets grew to a size of 70 % of the gap size between the nearest posts at  $Re = 30$ . For quadrilateral-shaped obstacles, vortices developed at  $Re = 2$  and grew to 75 % at  $Re = 26$ . This vortex formation avoids the usage of narrow gap between the posts to create a zigzag motion for the particle. It also increases the number of flow lanes in the DLD ratchets. This reduces the critical size of particle required for the displacement (Lubbersen et al. 2013). Since the gaps between the posts are high, blockage of the device due to high particle concentration of the sample can be eliminated. This also helps to reduce the pressure drop (Lubbersen et al. 2012).

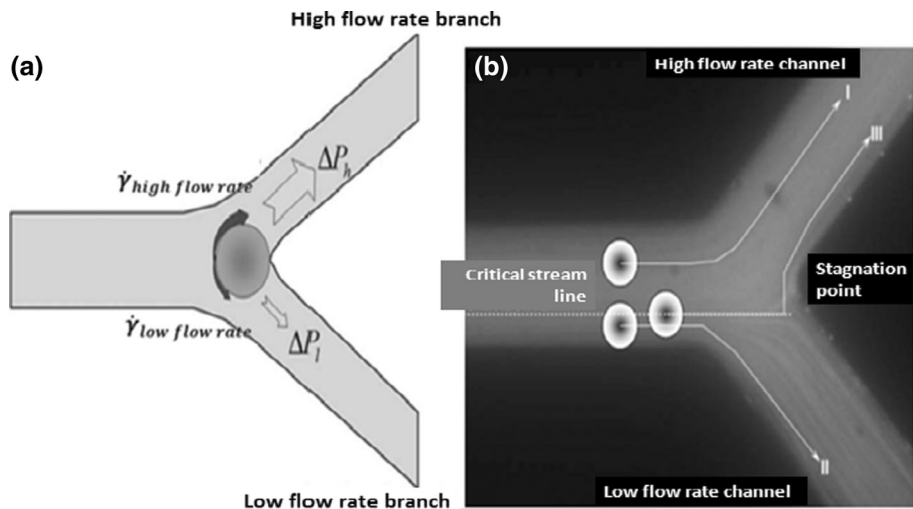
## 2.5 Zweifach–Fung effect

‘Zweifach–Fung effect’ states that when a particle reaches a bifurcation region, the particle has a tendency to follow the high flow rate channel (Yang et al. 2006). As shown in Fig. 25, a channel ( $35 \mu\text{m} \times 35 \mu\text{m}$ ) bifurcates into two daughter channels having different flow rates (Yang et al. 2006). It has been observed that a particle (I) whose centroid is located beyond the critical streamline (i.e., a streamline separating the flow streams into the daughter channels) flows into the high flow rate channel. A particle (II) whose centroid is within the critical streamline will flow into the low flow rate channel, and a particle (III) whose centroid is on the critical streamline will flow into the high flow rate channel because of the Zweifach–Fung effect. The differential pressure drops and shear forces acting on the particles are the primary reasons behind such

effect. The pressure gradient in the high flow rate channel ( $\Delta P_h$ ) is more compared with pressure gradient ( $\Delta P_l$ ) in the low flow rate channel. In addition, shear force acting on the particle along the high flow rate direction ( $\dot{\gamma}_{\text{highflowrate}}$ ) is more than shear force in the low flow rate direction ( $\dot{\gamma}_{\text{lowflowrate}}$ ) and that generates a torque on the particle. As a result, the particle rolls into the higher flow rate channel when it reaches the bifurcation point. For a design, the minimum flow rate at which all the particles escape into the high flow rate branch is called ‘critical flow rate.’ The critical flow rate ratio between the daughter channels is approximately 2.5:1, for a particle-to-channel diameter ratio of 1.0.

When blood flows through a microchannel, RBCs migrate toward the center of the channel due to Poiseuille flow and RBC-rich inner core and cell-free outer core (near the wall) are formed. Thus, RBCs at the center of the channel have higher velocity than the other blood components close to the wall. This leads to a reduction in transit time of RBCs through a given microchannel segment and therefore to a reduction in concentration of RBCs in that segment as compared to the concentration of RBCs entering or leaving it. This dynamic reduction in the concentration of RBCs is called ‘Fahraeus effect’ (Pries et al. 1996). The cell-free layer also serves as a lubrication layer and helps to reduce the blood viscosity. This phenomenon is called ‘Fahraeus–Lindqvist’ effect. When RBCs migrate to the center, interactions between the RBCs and leukocytes lead to the displacement of leukocytes toward the wall, which is called ‘leukocyte margination’ (Pries et al. 1996). Sometimes, these RBCs adhere to each other to form rouleaux at low shear rate, which increases the viscosity of the blood and helps to marginate the stiffer leukocytes from the inner core of RBCs. The ‘margination effect’ is also observed for platelets in concentrated blood flow. This margination principle is also used to separate the

**Fig. 25** **a** Pressure gradient and shear stress distribution on the particle at the bifurcation; **b** three possibilities of particle tracks (Yang et al. 2006)



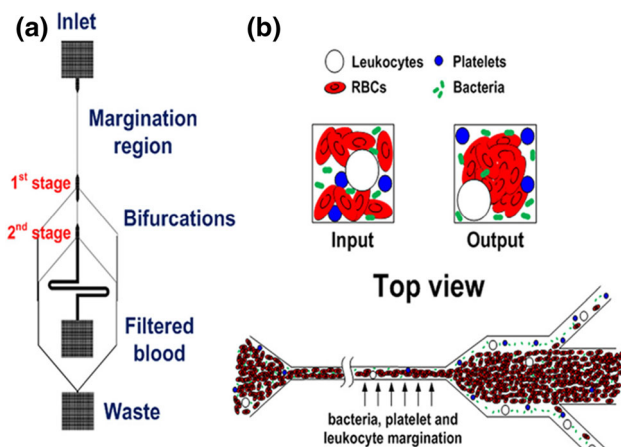


**Fig. 26** **a** Margination chip for the removal of pathogen from blood. **b** Cross-sectional view at inlet and outlet of microchannel (Hou et al. 2012)

bacteria from blood (Hou et al. 2012), as shown in Fig. 26. Due to ‘Fahraeus effect’ and hydrodynamic forces arising from intercellular microbe–RBC interaction, the margination of microbe occurs. There are differences between microbes and RBCs in terms of size and stiffness of the surface of the cells. The nonspherical rod-shaped bacteria have tumbling and rotational motion unlike spherical cells. Due to this, the bacteria have got higher lateral drift velocity and can be easily separated from blood cells.

In another design, two cascaded straight microchannels with two bifurcations in series are used as shown in Fig. 26. When blood flows through the channel, deformable RBCs migrate axially to the center of the channel, whereas bacteria, platelets and leukocytes are migrated to the channel wall. These blood components can be removed through the channel sidewalls, and the bacteria-removed blood can be taken out through the center. Another device (Rainer et al. 2007) that is used for the plasma skimming with bifurcation law is shown in Fig. 27. Inverted-T bifurcations with one inlet and two outlets are used. The device has high aspect ratio resulting in cell screening and high fluid throughput. It was observed that the flow rate and channel dimensions affect the red blood cell density across

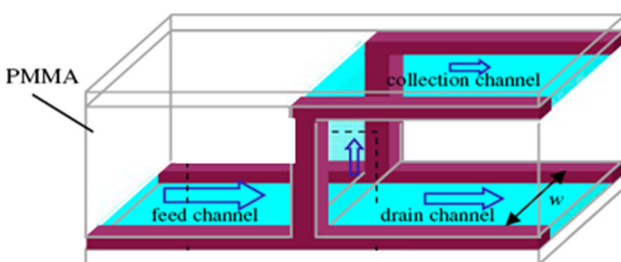


**Fig. 27** Schematic representation of the separation device with an inverted-T bifurcation (Rainer et al. 2007)

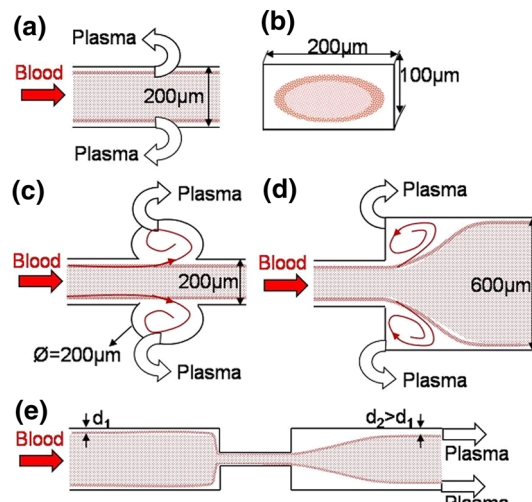


**Fig. 28** **a** Plasma separation in a straight channel; **b** cells inside annular cell-free plasma; **c–e** plasma skimming in microchannel with cavity, expansion and constriction–enlargement structures, respectively (Sollier et al. 2009)

the channel. Red blood cell depletion efficiency also improves with decrease in the channel depth. To increase the throughput, single bifurcation layout can be expanded to series of bifurcations with more number of collecting channels. In that case, the flow resistance in the collecting channels can be maintained such that only plasma enters the collecting channels.

For given flow rate and geometry, inclusion of a geometrical constriction in the flow channel can enhance the cell-free layer adjacent to the wall (Faivre et al. 2005, 2006). It was observed that a reduction in the constriction width leads to increased width of the cell-free layer. A constriction helps in focusing the particles/cells in a sample toward the center of a microchannel where particles will get influenced by higher pressure gradient. Constriction also accelerates the flow and increases velocity difference between particles and fluid (Xue et al. 2012). By using cavity, expansion and constriction–enlargement features in the channel, cell-free plasma regions can be created due to the ‘margination process,’ as shown in Fig. 28a–e (Sollier et al. 2009). The plasma can be taken out through the side channels. The recirculation of flow will happen in the expansion regions and cavities, which produce the centrifugal effect to enhance separation. Constrictions placed in a microchannel also increase the cell-free layer downstream the channel and improve the plasma extraction (Sollier et al. 2009). A series of constrictions and expansion regions can be arranged in series to further enhance the extraction process.

In the microseparator (Xue et al. 2012) shown in Fig. 29, the main channel comprises one constriction, series of branched channels and T-bifurcations. The constriction focuses particles to the center and increases the

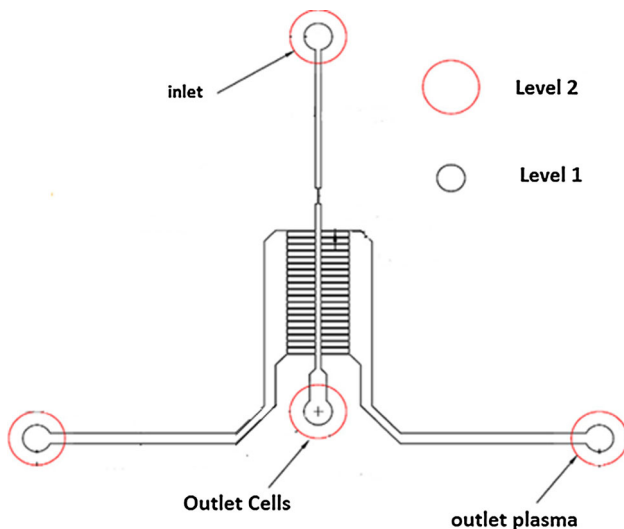


**Fig. 29** Multiple bifurcation channel along with a constriction to increase the throughput (Xue et al. 2012)

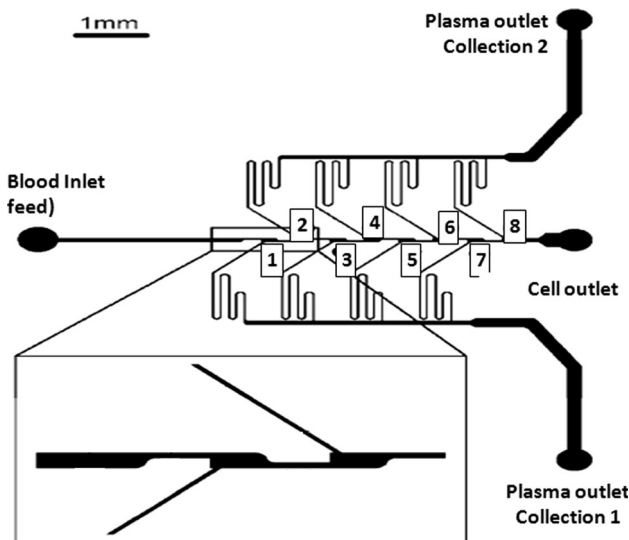


**Fig. 30** Blood plasma separation device design with alternate constrictions and bifurcations (Kersaudy-Kerhoas et al. 2010a)

cell-free layer downstream. When blood flows through each junction, plasma is extracted to the side daughter channels. At a single bifurcation, only small amount of plasma is removed. But, applying a number of bifurcations as shown in Fig. 30, throughput of the collected plasma is improved. To further increase the throughput, the effect of bifurcation and constriction can be together exploited as shown in Fig. 30 (Kersaudy-Kerhoas et al. 2010a). Here, alternate constriction and bifurcations are provided to ensure that plasma channel has higher fluid resistance than blood cell channel. The design offers higher throughput and prevents clogging of the main channel with blood cells. In another recent work (Tripathi et al. 2013), plasma skimming in a device with a T-junction that has dimensions more than the suspended blood cells was studied. The device offered good plasma separation efficiency with width of main channel, feed hematocrit and flow rate distribution as critical parameters that determine the separation efficiency. This method enabled plasma skimming from dense hematocrit blood content, whereas most of the existing methods require dilute blood for high-throughput separation. At high concentration of blood, formation of aggregates occurs under the influence of gravity and surface charge (Fahraeus 1929), and the rate of aggregation would be higher at increased Pe number (Brunet et al. 2005). At the T-junction, the moving cell aggregates have lower chance to escape into the plasma channel due to higher momentum while the free aggregates have a higher chance to get into the plasma channel because of lower momentum.

Separation of plasma from whole blood is also done in a microfluidic chip using a combination of Zweifach–Fung bifurcation law, centrifugation and diffuser–nozzle effect (Geng et al. 2011). Here, two Archimedean spiral microchannels of different width and length are connected to diffuser–nozzle channels. Angle between the microchannel and diffuser channel is 45°, whereas angle of the diffuser–nozzle is 30° as shown in Fig. 31a. Due to centrifugal effects, the cells migrated toward the outer side of the main

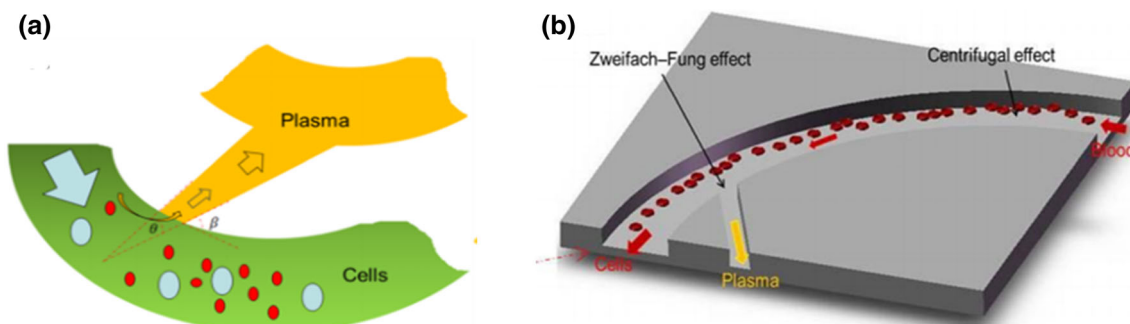


**Fig. 31** **a** Nozzle diffuser structure connection to the spiral channel; **b** principle of combined Zweifach–Fung effect and centrifugal effect (Geng et al. 2011)

microchannel as shown in Fig. 31b. At the branching point, cells continue in the high flow rate channel due to the bifurcation law, but plasma flows from the inner side of the microchannel to the side channel. The diffuser–nozzle structure further improves the throughput by giving a differential pressure distribution between the main channel and plasma channel.

## 2.6 Filtration

Filtration is a method that can be used for size-based separation of particles. Microfabricated filters are also used for fractionating blood into its components. Mainly, four different types of microfilters are used: membrane, weir, pillar and cross-flow, as shown in Fig. 32 (Gossett et al. 2010a). Membrane-based separation methods have been used for the separation of particles from sample (Crowley and Pizziconi 2005). In plasmaphoresis using membrane filtration, plasma flux depends on the concentration of hematocrit, transmembrane pressure and wall shear rate. If the concentration of hematocrit is large, the filter fouling is more and flux is reduced. Initially, flux increases with transmembrane pressure and then reaches a pressure-independent equilibrium due to the deposition of RBCs at filter face, as shown in Fig. 33. In this range of operation, wall shear rate determines the plasma flux. As shear rate increases, fouling layer of RBC at the filter face is modulated by the shear-enhanced diffusion.

The major problem with membrane filtration method is the accumulation of particles on the filter faces, which reduces the separation efficiency. To reduce fouling of cross-flow membrane, periodic reverse flow has been utilized for cleaning the membrane (Redkar and Davis 1995). Experiments were performed with reverse-filtration time ranging from 0.5 to 4 s and forward-filtration time ranging from 1 to 40 s. It was found that for a given back-filtration

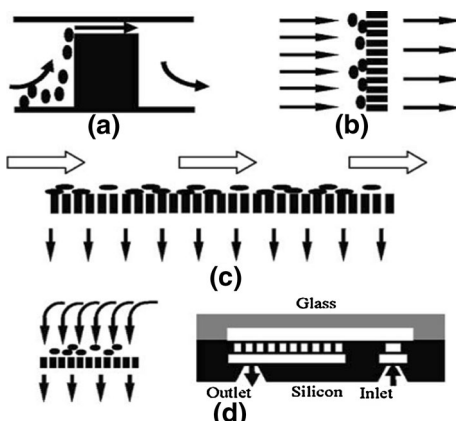


**Fig. 32** Schematic diagrams of microfilter designs: **a** side view of weir filter; **b** top view of pillar filter; **c** top view of cross-flow filter; **d** side view of membrane filter (Gossett et al. 2010b)

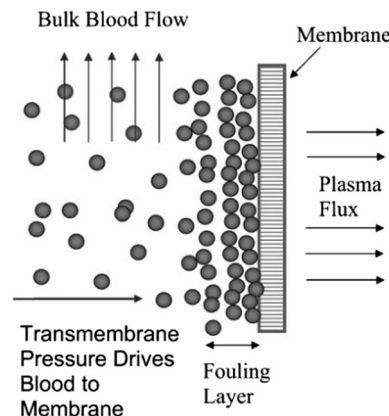


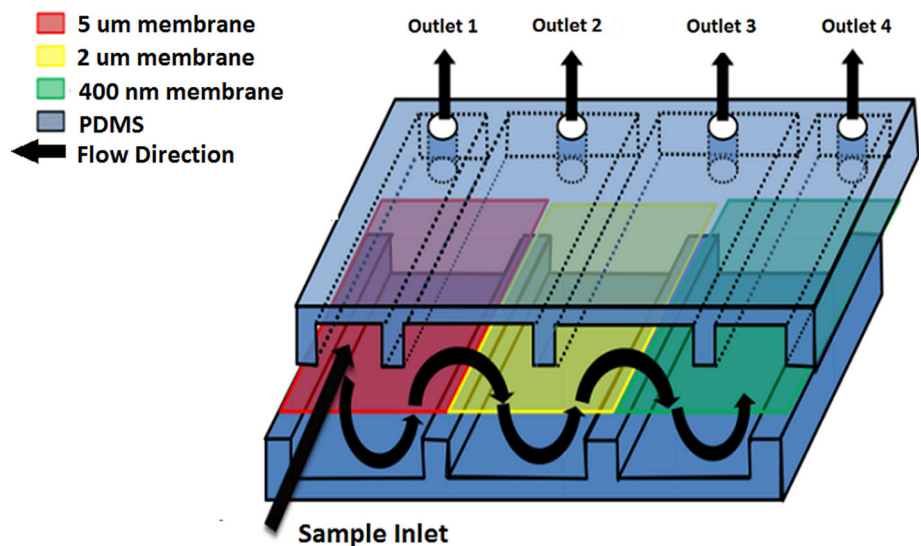
**Fig. 33** Membrane filtration using microporous membrane (Crowley and Pizziconi 2005)

time, an optimum forward-filtration time exists that provides maximum separation efficiency. The average flux increases with decrease in back-filtration time and feed concentrations. Cross-flow velocity and reverse-filtration transmembrane pressure have little effect on the average flux. The average flux obtained with back-flushing is 20–30 times higher than the filter without back-flushing. From an economic point of view, microfiltration with back-pulsing has lower costs than centrifugation, rotary vacuum filtration and cross-flow microfiltration without back-pulsing (Kuberka et al. 1998). A microfiltration device was fabricated in PDMS in which microchannels were bonded to semipermeable polycarbonate membranes coated with a solution of 3-amino propyl triethoxysilane (APTES) (Aran et al. 2011). This device with a single membrane was used for the separation of plasma from whole blood.

In order to separate and sort multicomponents from the sample, different-pore-sized membranes were placed inside the microchannel structure (Lo and Zahn 2012). The device consists of three membranes with pore size 5, 2 and 400 nm, as shown in Fig. 34. The membrane with smallest pore size is used on the left compartment and membrane with largest pore size on the right compartment. A sample containing 15-μm, 3-μm and 710-nm polymer fluorescent beads was infused into the left inlet reservoir. At outlet 1, only 15-μm beads were collected; at outlet 2, only 3-μm and 710-nm beads were recovered due to filtration across 5-μm membrane; and at outlet 3, only 710-nm particles were collected due to filtration across 2-μm membrane. Finally, at outlet 4, only fluid was recovered by filtration across the 400-nm membrane. The device was also demonstrated for the separation of sheep blood into its components.

Pillar-type and weir-type filtration chips are well reported in the literature. This is mainly used for the separation of RBC and WBC. The device consists of an inlet for blood sample, filtration barriers within a tortuous channel, one outlet for collecting the WBC and one more

**Fig. 34** Schematic diagram of a multicompartiment microfiltration device (Lo and Zahn 2012)



outlet for collecting RBC. The tortuous channel has three subchannels spaced in which two-row filtration barriers are placed in parallel. In pillar-type filtration barrier, 20- $\mu\text{m}$ -diameter pillars spaced by 6.5  $\mu\text{m}$  are arranged in two rows, whereas in weir-type filtration barrier, two integral weirs of 26.5  $\mu\text{m}$  height and 20  $\mu\text{m}$  width are used. Both of these filtration barriers provide obstruction to the larger WBC and allow the passage of biconcave RBC. The separation efficiency can be further improved by increasing the separation length. Due to smaller pillar gap, the separation efficiency of weir type is more than the pillar type (Murthy et al. 2006). Cross-flow filtration is similar in operation of weir type and pillar type, but only difference is that flow is perpendicular to the micropost array or weir. The major hydrodynamic forces on the particle during the deposition of the particle on the membrane are drag force due to the filtered flow and lift force due to the shear flow. All the hydrodynamic forces in the vicinity of the membrane surface are shown in Fig. 35 (VanDelinder and Groisman 2007).

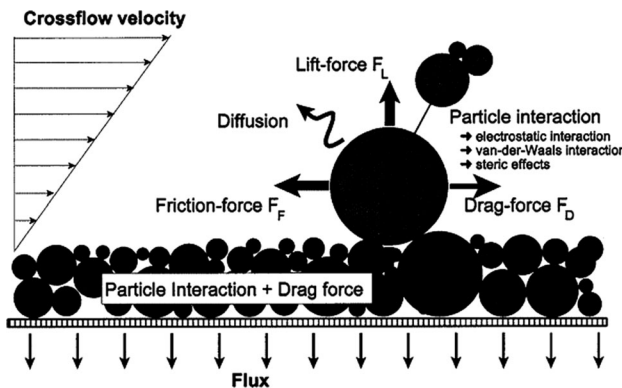


**Fig. 35** Various forces acting on the deposited particle in cross-flow microfiltration (VanDelinder and Groisman 2007)

Microfabricated filter devices have been developed for the plasmaphoresis process (Brody et al. 1996). Optimum filter design is possible in micromachining by the precise dimensional and geometric control which cannot be performed by traditional membrane filtration methods. Porous filters that were fabricated inside microchannels using photopolymerization technique, were used to separate blood sample into its components based on size (Moorthy and Beebe 2003). RBCs, WBCs and platelets have sizes of 8, 8–12 and 1–3  $\mu\text{m}$ , respectively. A cross-flow filtration device used for the separation of plasma from blood based on size (VanDelinder and Groisman 2006) is illustrated in Fig. 36. In this device, blood was infused from the inlet (port 1) to the outlet through channel A, which is permeable. A filter region was placed on the first part of the main

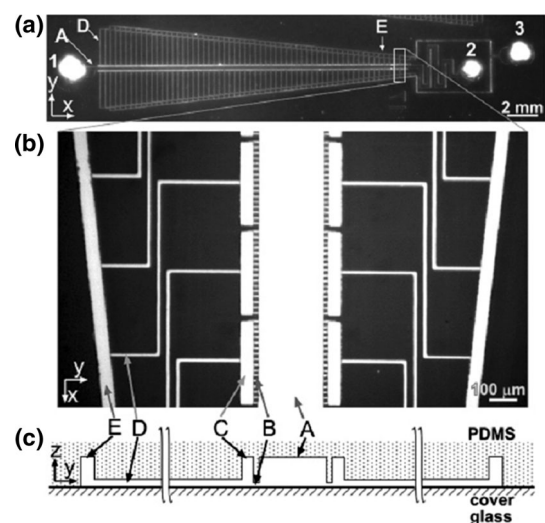


**Fig. 36** **a** Schematic diagram of cross-flow filter for plasmaphoresis; **b** magnified view of the filter region; **c** cross-sectional view of the device (VanDelinder and Groisman 2006)

channel. There were large numbers of B channels placed perpendicular to both sides of the channel A. These channels are small enough such that the channel B is permeable to plasma but not blood cells. From a cluster of parallel B channels, plasma is collected to E channels through C and D channels, which is connected to the plasma outlet (port 3). B, C, D and E channel network is symmetric about the channel A. The blood cells can be removed through port 2 as shown in Fig. 36.

A plasma separation device (Xing et al. 2009) was fabricated in silicon substrate, as shown in Fig. 37. The device consists of microchannels, square microposts array and input and output ports. There are parallel feed and side channels, which are connected by a number of square microposts. Apart from these channels, assistant microchannels are provided to get high tangential rate, and a cell microchannel is included to increase the resistance to the flow of blood cells. As blood is supplied to the feed channel via inlet port, plasma enters the side channels through

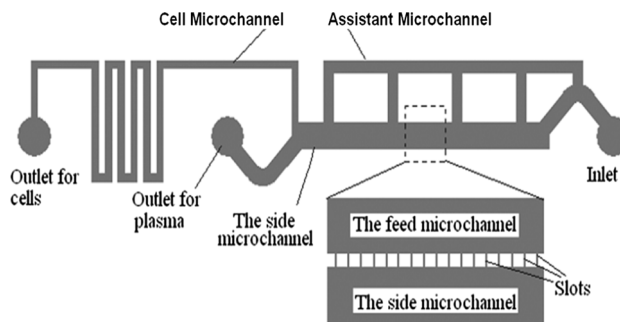
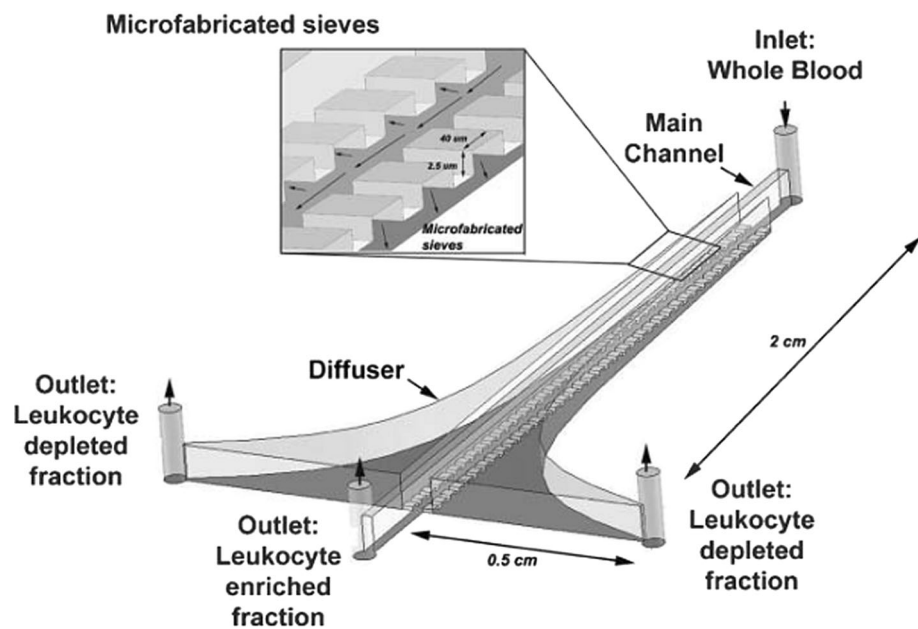


**Fig. 37** Schematic of continuous flow filtration chip for plasmapheresis (Xing et al. 2009)

**Fig. 38** Microfluidic diffusive filter for apheresis (Sethu et al. 2006)



narrow slits between the square microposts due to tangential force. The blood cells that could not pass through the slit remain in the feed channel and finally move to the cell microchannel. The plasma and cells can be collected at separate outlets without clogging. The performance of the filter relies on the shear focusing at the walls. Usage of corrugated channels instead of straight channels improves the shear focusing with reduced clogging and cell cake formation (fouling of filter faces) as compared to conventional cross-flow filtration devices (Mielnik et al. 2005). Cross-flow filtration method has also been used for the leukapheresis (Sethu et al. 2006), which is the process of removal of donor leukocytes from blood before transferred to the recipients during blood transfusion. As shown in Fig. 38, the device is a continuous flow diffusive filter which has microsieves to deplete leukocytes from blood. The sieves were designed to allow erythrocytes to pass through but to act as a barrier to leukocytes. Sieves were placed on the sides of the main channel and connect to the diffuser to prevent the clogging of the filter as shown. The shape of the diffuser was modified to have a flared geometry to ensure equal flow rate through all the sieves. This device was used for the separation of leukocytes based on the size and shape difference. Size-based separation of myocytes from nonmyocytes from the neonatal rat myocardium is also reported by the same method (Chen et al. 2007).

A cross-flow filter was developed (Crowley and Pizziconi 2005), which utilizes capillary action alone for the isolation of plasma from the whole blood. The average flow velocity due to capillary action is given by the Washburn equation (Crowley and Pizziconi 2005),

$$U_{ave} = \sqrt{\frac{h^2 \Delta P}{6\mu t}} \quad (4)$$

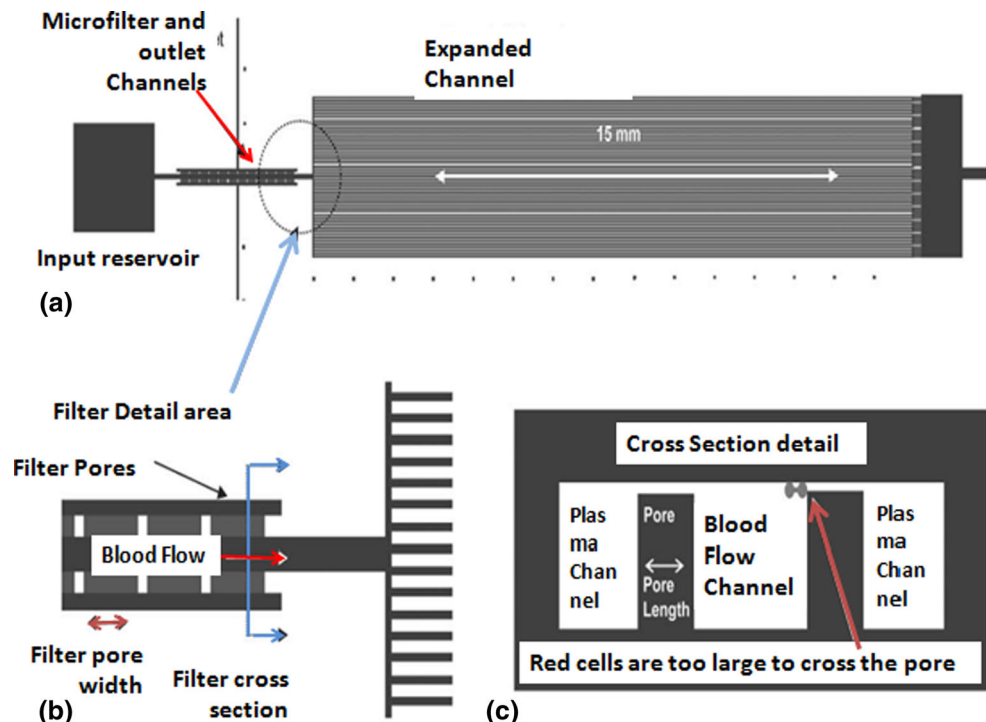
In Eq. 4,  $h$  is half the channel height,  $\Delta P$  is the driving pressure defined by the Young–Laplace equation,  $\mu$  is the viscosity of the fluid, and  $t$  is the time at which capillary-driven flow is established. From Eq. 4, it is observed that the average flow velocity decays with square root of time. With straight channels, the time for which the capillary action is effective to drive the fluid is very low (~seconds). To increase the passive flow time and to get a steady-state average velocity, narrow channels are connected in series to the expanded channels, as shown in Fig. 39. The wide channels provide large surface area for capillary wetting, and narrow channels decrease the overall flow rate. By providing a number of parallel expanded channels in series to the filtration channels, capillary action time can be increased from seconds to minutes. A number of planar microfilters are used in this device for the fractionation of blood. Series of rectangular openings called pores are placed on both sides of the filtration channel, which does not allow the passage of blood cells through it but only permits the plasma to flow through it. Thus, plasma can be collected from the side outlet placed on the filtration region. Efficiency of this device was found to be three times higher than that of microporous membrane under similar condition.

Another novel microfluidic device consisting of microfilter, micromixer, micropillar array, microweir,

microchannel and microchamber was used for the sample pretreatment of whole blood. Continuous separation of cell, cell lysis and DNA purification were performed in this single device. Cross-flow filtration was used here for the separation of blood into its components. Blood cell lysing was performed in a guanidine buffer, and the porous matrix, made by anodizing silicon in HF/ethanol electrolyte release, absorbs the genomic DNA in WBC. Using this integrated device, genomic DNA was purified from 1  $\mu$ L rat blood (Ji et al. 2008). The cross-flow microfilter was found superior for the separation of WBC from RBC in a given blood sample, in comparison with four microfilters made of silicon, viz., weir, pillar, cross-flow and membrane type on the basis of their blood handling capacity, trapping efficiency of WBC and passing efficiency of RBC (Chen et al. 2008).

Perfusion is another technique used to separate the WBCs from whole blood (Ripperger and Altmann 2002). It has deep main channel and large number of shallow side channels orthogonal to the main channel. The separation is performed in cross-flow direction to the main channel. As the particle suspension flows through the main channel, perfusion flow through the side channel exchanges the suspension fluid and washes the smaller particle that cannot enter into the shallow side channel. The technique of perfusion is used to enrich the rare cells based on the difference in size, shape and deformability.

**Fig. 39** **a** Top view of narrow and expanded channel; **b** detailed view of filter pore and expanded channel layout; **c** cross-sectional view of microfilter (Crowley and Pizziconi 2005)

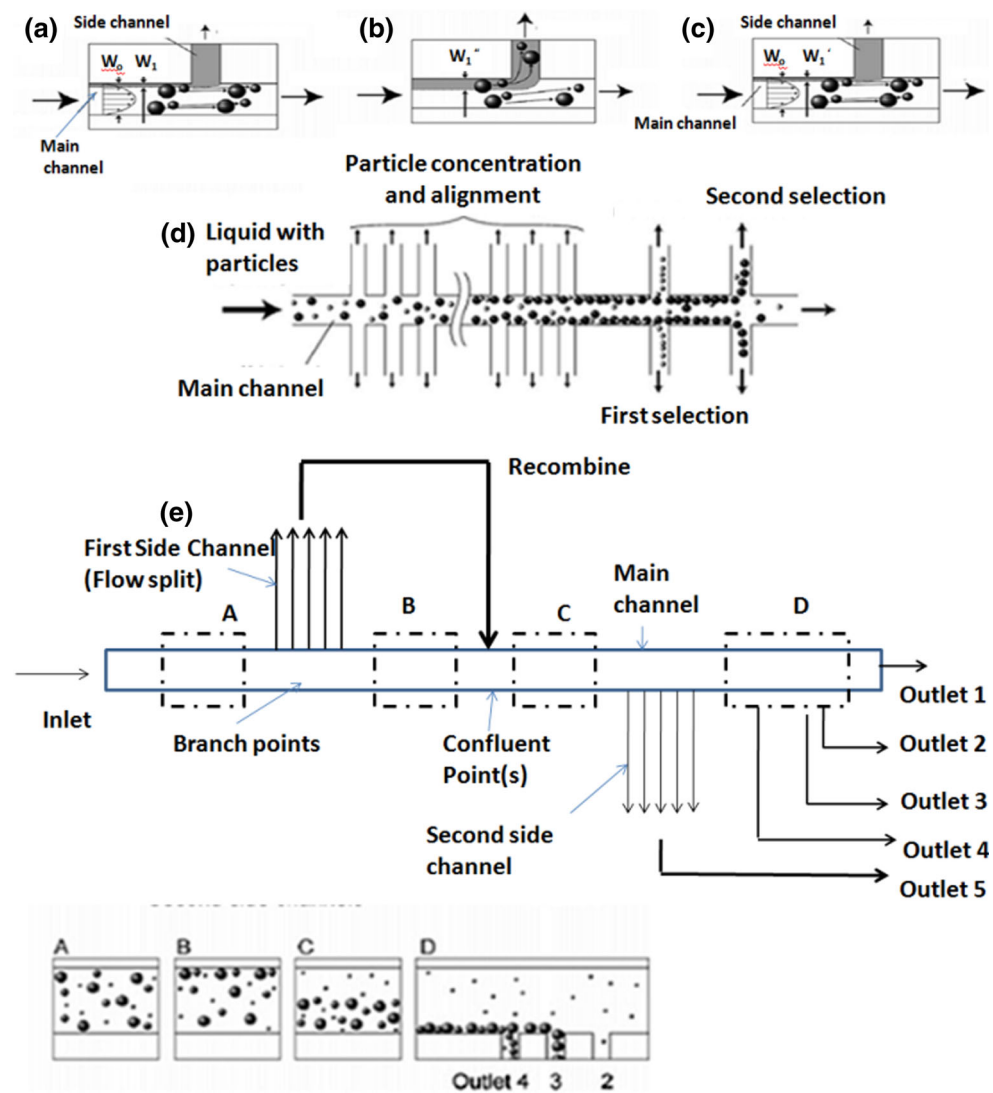


## 2.7 Hydrodynamic filtration

Hydrodynamic filtration is similar to cross-flow filtration, but they are based on different principles. In cross-flow filtration, only carrier fluid is collected through the side channels, but in hydrodynamic filtration, the particles are also collected through the side channels. When a side channel is placed along a microchannel carrying the sample, some amount of carrier fluid transfers to the side channel. If the volume flow rate of the side channel is very small compared with the main channel, the particles of diameter larger than a particular value will not flow into the side channel. This critical diameter is determined by the virtual width ( $w$ ) (shown in Fig. 40) of the side channel stream split from the main channel. As shown in Fig. 40a (Yamadaa and Seki 2005), initially none of the particles move to the side channel since virtual width  $w'_1$  is very small as compared to the diameter of the smallest particle.

If the flow rate of the side channel increases, then the width also increases to  $w'_1$  and  $w''_1$ , as shown in Fig. 40b, c. The particles having diameter less than this width move to the side channel. The initial branched points are created to concentrate the sample by removing some portions of the carrier fluid and to focus the particles to the channel walls. Then, particles of different diameters migrate to the side channels depending on their size and flow rates. Finally, high concentration of target particles of large diameter can be collected at the exit of the main channel. This work was extended to design a hydrodynamic filtration device by employing a flow splitting and recombination scheme (Yamadaa and Seki 2006), as shown in Fig. 40e. When the fluid stream in the main channel is split into an array of side channels and recombined into the main channel after a short distance, the large target particles are focused onto the wall opposite to these side channels. The smallest particles that can follow the side channels will disperse in

**Fig. 40** a–c Particle behavior for various flow rates in the side channels; d target particle sorting at side channel; e particle sorting by flow splitting and recombining (Yamadaa and Seki 2005, 2006)



the main channel fluid without getting aligned to the wall. Then, using the method described above, these focused particles can be sorted. In a similar work, channels having one inlet and five outlets were fabricated, and the method was used for the separation of RBCs from plasma (Kersaudy-Kerhoas et al. 2010b).

## 2.8 Micro-hydrocyclone

A micro-hydrocyclone device for particle–liquid separation (Bhardwaj et al. 2011) employs a cylindrical chamber with a frusto-conical bottom and an inlet channel tangential to this cylindrical chamber to separate particles from liquids based on centrifugal force. The design of the micro-hydrocyclone device showing the flow inside the device and a photograph of the structure are depicted in Fig. 41a. The structure of the device includes an inlet microchannel, a cylindrical chamber with a frusto-conical bottom as the main functional element, bottom outlet (underflow) leading to a microchannel and top outlet (overflow) leading to a microcapillary. An important element in the hydrocyclone is the ‘vortex finder’ which is essentially the top outlet capillary, which is extended up to a certain distance within the main body of hydrocyclone to aid the formation of a vortex from the inlet flow. The inlet microchannel is tangential to the cylindrical chamber. The tangential flow into the cyclone generates a spiral flow pattern enabling particle–liquid separation due to a net outward radial velocity experienced by the solid particles. The fluidic interface between the microfluidic chip and the external capillaries is established using 1/4–28 UNF threaded fittings as the interconnection mechanism. The microfluidic chip is fabricated in three different layers that are thermally bonded together. Given the spiral motion of the fluid, the velocity can be divided into two components: a tangential

component,  $v_t$ , and a radial velocity component,  $v_r$ . If an isolated particle of diameter  $D_p$  and volume  $v_p$  circles in the upper cylindrical component of the cyclone of diameter  $D_c$  at a rotational radius of  $r$  from the cyclone’s central axis, the particle will be subjected to centrifugal ( $F_c$ ), drag force ( $F_d$ ) and buoyant forces ( $F_b$ ), as shown in Fig. 41b. In equilibrium, the summation of these three forces will be zero from which an expression for the radial velocity  $V_r$  can be obtained,

$$v_r = \frac{v_t^2(\rho_p - \rho_f)D_p^2}{9\mu D_c} \quad (5)$$

Here, if the density of the fluid  $\rho_f$  is greater than the density of the particle  $\rho_p$ , the motion is toward the center of rotation, and if the particle is denser than the fluid, the motion is away from the center. Typically, the values of the density of particles encountered in chemical and biological analysis are greater than that of the suspending medium. Hence, the microparticles migrate outward toward the wall and are separated. The selected micro-hydrocyclone was simulated to predict the flow and particle dynamics by solving the NS equations for the flow and using a Lagrangian approach for particles. The influence of inlet velocity, vortex finder diameter, particle size and density on separation efficiency was investigated. The device was fabricated using a combination of photolithography and micromilling, and experiments were performed using polystyrene microbeads suspended in PBS as the feed sample. Separation of particles was clearly demonstrated using microscopic counting as well as absorbance measurements. The influence of inlet velocity and particle size on separation efficiency was experimentally studied, and the results were compared with that predicted from simulations, and good agreement between the two was found. The proposed device can be easily integrated with

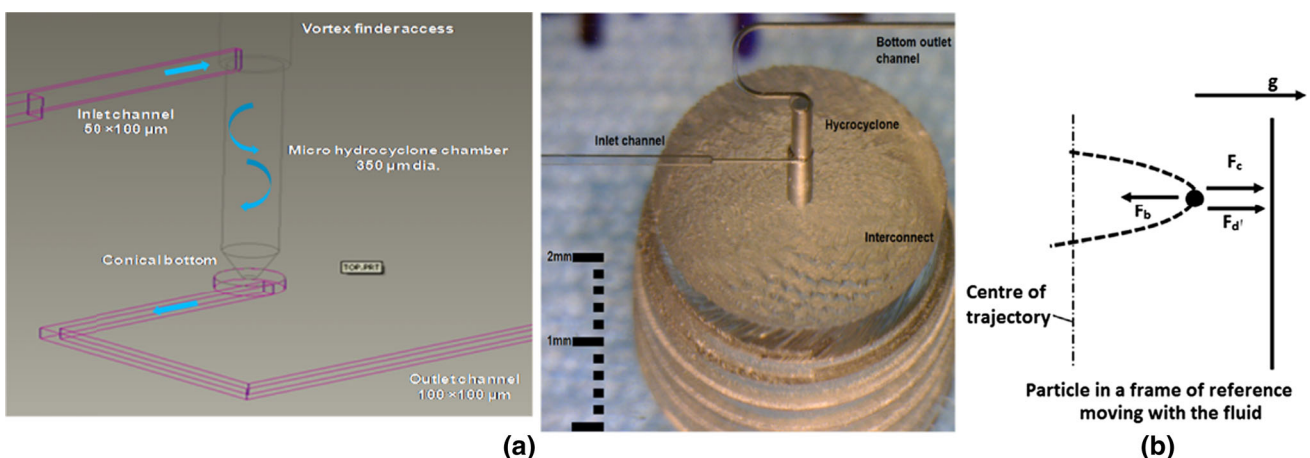


**Fig. 41** a Flow inside micro-hydrocyclone (left) and image of the micro-hydrocyclone (right); b different forces acting on the particle (Bhardwaj et al. 2011)

microenvironments; thus, it is suitable for Lab-on-Chip and microsystems development. Also, the device is compatible with microfabrication approach which could be easily mass produced and thus could be economical. The device may have potential applications in many areas including chemical analysis, materials research, point-of-care, PCR, blood-sample preparation and other biomedical applications.

### 3 Active techniques

#### 3.1 Dielectrophoresis (DEP)

If a neutral particle is placed in a nonuniform electric field, the particle gets polarized and subjected to a force called ‘dielectrophoresis (DEP).’ If the field is homogeneous, the DEP force acting on the neutral particle is zero. DEP has been widely used for electrically controlled trapping, focusing, translation, fractionation and characterization of particles, chemical and biological analytics that are suspended in a fluid. The expression for the time-averaged DEP force (Gascoyne and Vykovakal 2002; Gagnon 2011) is given by,

$$F(t) = 2\pi\epsilon_m r^3 \left\{ \text{Re}(f_{CM}(\omega)) \nabla E_{rms}^2 + \text{Im}(f_{CM}(\omega)) \times (E_x^2 \nabla \varphi_x + E_y \nabla \varphi_y + E_z \nabla \varphi_z) \right\} \quad (6)$$

In Eq. 6,  $r$  is the particle radius,  $\omega$  is the angular frequency,  $E_{rms}$  is the root-mean-square value of the applied electric field, and  $E_i$  and  $\varphi_i$  ( $i = x, y, z$ ) are the magnitudes and phases of the electric field components in the principal axis directions.  $\text{Re}(f_{CM}(\omega))$  and  $\text{Im}(f_{CM}(\omega))$  are real and imaginary parts of dipolar Clausius–Mossotti factor (CM), respectively. CM is a measure of the frequency dependence of the particle and its surrounding that produces the induced dipole moment. The expression for the DEP force has two parts (Gascoyne and Vykovakal 2002): The first part of the RHS of Eq. 6 is the DEP force produced due to the real part of the CM of the induced dipole moment of the particle and  $E_{rms}^2$  of the field. This part of DEP force will produce the attraction and repulsion of the particle to and from the electrodes depending on whether the value of real part of CM is positive or negative. The CM is given by the following expression,

$$f_{CM}\left(\epsilon_p^*, \epsilon_m^*, \omega\right) = \frac{\epsilon_p^*(\omega) - \epsilon_m^*(\omega)}{\epsilon_p^*(\omega) + 2\epsilon_m^*(\omega)} \quad (7)$$

In Eq. 7,  $\epsilon_p^*$  and  $\epsilon_m^*$  are the frequency-dependant complex permittivity of the particle and medium, respectively. Here,  $\epsilon^*$  depends on the electronic, permanent dipolar and interfacial mechanisms of polarization and electrical conductivity. If  $\epsilon_p^* > \epsilon_m^*$ , the CM is positive and the DEP force

( $F_{DEP}$ ) is in the same direction as the gradient of the electric field. This is called positive DEP in which particles are pulled toward strong electric field. If  $\epsilon_p^* < \epsilon_m^*$ , CM is negative and the DEP force is in the opposite direction as the gradient of electric field. This is called negative DEP in which the particle is pulled toward the weaker electric field. The positive and negative DEP forces acting on a dielectric particle present in a nonuniform electric field are depicted in Fig. 42. The directions of the polarization vector  $\mathbf{P}$  are also shown.

The second part of the RHS of Eq. 6 is the traveling field component, which depends on the imaginary part of CM and the spatial nonuniformity  $\Delta\varphi_i$  of the field. It describes how the electric field distribution moves with time. This force will try to push the particle in the same or opposite direction as the electric field depending on the sign of the imaginary part of CM. It helps to move the trapped particle along an electrode array in the presence of the inhomogeneous electric field. DEP is most versatile while operating in alternating (AC) fields. Using the frequency-dependent behavior of the dielectric property of the particle, DEP can be used for a wide variety of sorting and separation of particles from a mixture (Gascoyne and Vykovakal 2002). When a particle reaches the electrode, steric force prevents further movement of that particle, and it is trapped by positive DEP. This method can be used to separate a single particle from a suspension (Pohl 1977; Nascimento et al. 2008). From Eq. 6, it can be observed that DEP force acting on a particle is proportional to the third power of radius, square of the gradient of electric field and dielectric properties of the particle. So, the DEP force acting on the particle will be different based on the size and intrinsic property of the particle. This can be employed to separate particles and cells of different sizes and intrinsic properties (Holmes and Morgan 2002).

In AC DEP, by manipulating the frequency of the applied field, sorting of different particles having different dielectric properties can be achieved (Becker et al. 1995;

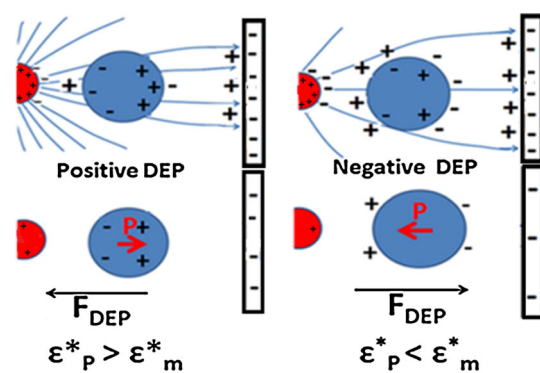


**Fig. 42** Positive DEP and negative DEP forces acting on a neutral particle

Gascoyne et al. 1997). If the frequency of the field is in between the crossover frequency of two dissimilar particles in a mixture, one fraction of the particles experiences negative DEP and moves toward the weak field region and another fraction experiences the positive DEP and moves toward the strong field region. This is called ‘differential DEP affinity’ which can be used for separation and sorting of particles. This method is only applicable when the crossover frequencies of the particles are much different.

The schematic diagram of a dielectric-affinity separation chamber is depicted in Fig. 43a. In this method, the cell sample is loaded into the chamber through the cell sample port. Electrical voltage is applied to the DEP electrodes. Eluate is pumped into the eluate inlet port, and then fluid flow is started. Elute cells are collected from outlet port on the other end of the chamber. The process inside the chamber is explained in Fig. 43b–e. A mixture of blood cells and cancer cells is taken into the microfluidic channel as shown in Fig. 43b. By the application of DEP, all the cells are collected on the electrodes, as shown in Fig. 43c. Then, the flow rate of the surrounding medium was adjusted to 5  $\mu\text{l}/\text{min}$ , and electrical signals were controlled so that frequency reduces from 200 kHz to 80 kHz to increase the retention time of cancer cells inside the channel. In this case, all the tumor cells stick to the electrode, and blood cells are focused into the bands that flow between the electrode tips as shown in Fig. 43d. But, some blood cells were also trapped with tumor cell. For the purification of tumor cells, again frequency is reduced from 80 to 20 kHz. Finally, toward the chamber outlet, only blood cells moved (Fig. 43e) while tumor cells still trapped. By applying the swept signal for 20 min, 99 % of the tumor cells could be removed. If the particles have close dielectric properties and crossover frequencies, this method cannot be used alone for the sorting. Linear traveling wave

dielectrophoresis (twDEP) may be used along with differential affinity DEP for such type of sorting (Wang et al. 1994; Cui et al. 1994). The twDEP was developed (Wang et al. 1994) and used to study the levitation and motion of microbead as a function of applied potential and frequency, medium conductivity, size of the bead and surface properties. In a microfluidic channel, positive DEP is first created using integrated pair of parallel electrodes. First, particles are collected at the electrodes from the sample, and then their motion is achieved by twDEP using array of electrodes placed behind the DEP electrodes within the microchannel. A modification of twDEP can be achieved by single 3D electrode array for high-throughput continuous sorting of the particles. Here, sorting is based on the differences in particle twDEP mobility on both sides of the crossover frequency (Cheng et al. 2009).

DEP-based sorting that exploits physical properties of the particles has been widely investigated. However, use of this approach is limited to separation of particles that have significantly different dielectrophoretic responses. In some applications, the target and nontarget particles have similar DEP responses; thus, sorting based on intrinsic physical properties may not be possible. To address this issue, in a recent work (Hu et al. 2005), cells were labeled with polymeric beads to achieve significant difference in DEP amplitude response between cells bound to beads and the unlabeled cells. The DEP force was designed to be insufficient in deflecting the unlabeled cells but large enough to selectively deflect the labeled cells. This separation process is analogous to FACS and thus termed as DEP-activated cell sorting (DACS). DACS was applied to affinity-based separation of cells labeled with biotinylated T7tag monoclonal antibody (attaching to streptavidin-coated polystyrene beads) from unlabeled cells. When targeting on more than one particle for sorting, multitarget dielectrophoresis-

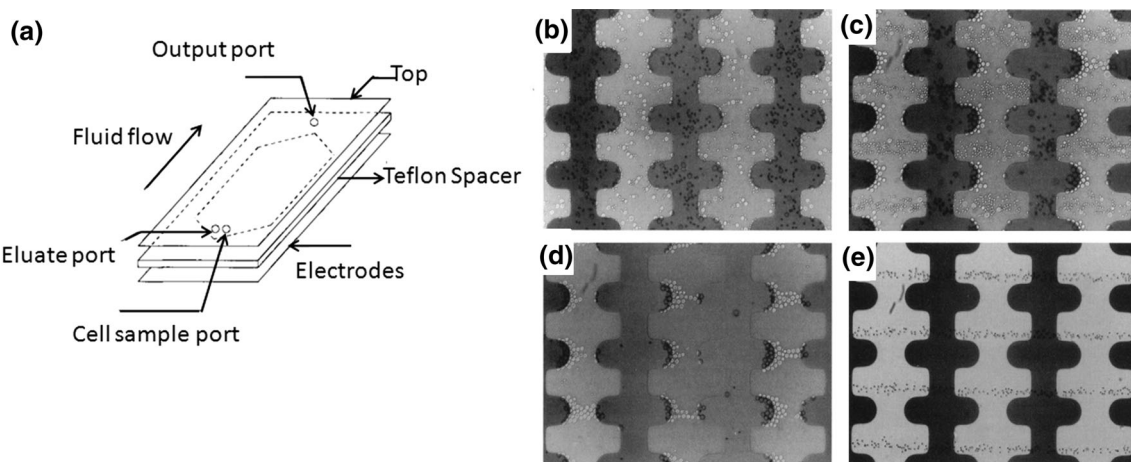
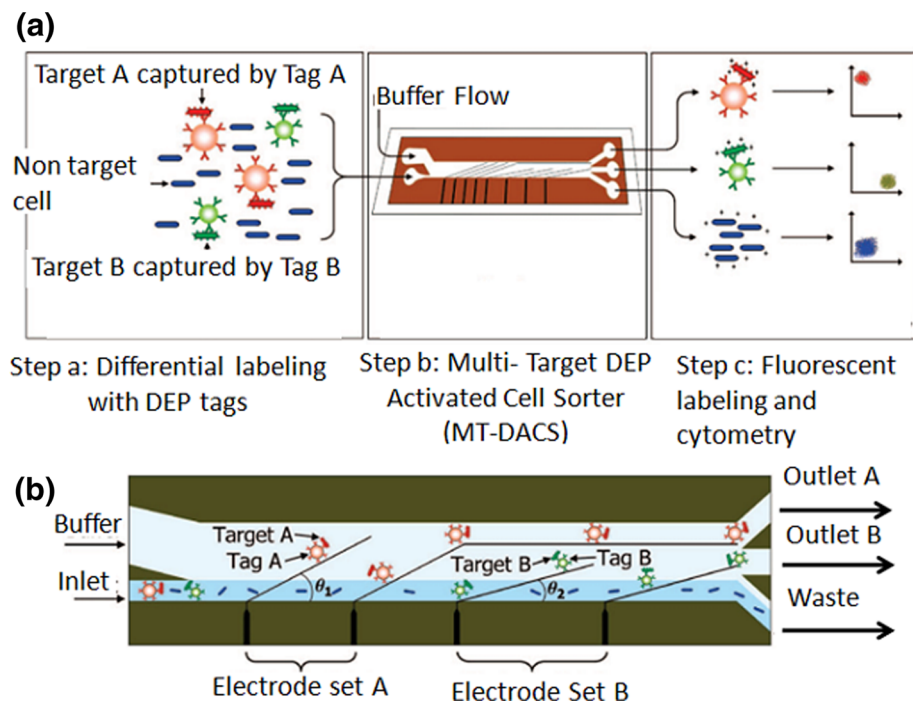


**Fig. 43** a DEP affinity separation chamber; b–e various steps involving in sorting of blood cells and cancer cells using DEP affinity separation method (Gascoyne et al. 1997)

**Fig. 44** Multitarget bacterial cell sorting procedure using the MT-DACS device (Kim et al. 2008)



activated cell sorter (MT-DACS) chip should be used (Kim et al. 2008). As shown in Fig. 44, MT-DACS has a number of stages including tagging and sorting followed by counting using a flow cytometer. The chip has inlets for the buffer solution and the sample. The device is designed such that the electrodes are placed at an angle to the flow. Target A cells labeled with tag A are sorted through the outlet A by electrode set A, and similarly, target B cells are sorted through outlet B by electrode set B. The unlabeled cells are not deflected by any electrode and move into the waste outlet (Kim et al. 2008). To increase the throughput of sorting, DEP force along with hydrodynamic effect inherent in the fluid flow is also used (Wang et al. 2000). In this method, at least one particle is removed from the DEP electrode in each analysis by flushing the untrapped particle from the sorting chamber. When high positive DEP is applied, particle will stick to the electrode and removal of single particle can be done by decreasing the DEP force

and increasing the flow rate of the medium. But, in order to sort two different particles having close crossover frequency, this method of sorting is not suitable. This issue can be solved if the particles are trapped from their levitated position in the moving fluid, and the particles reach a position inside the channel where DEP force is sufficient to overcome the lift force.

One of the earliest microfluidic particle separation methods is the field flow fractionation (FFF), which is a flow-injection-based separation method (Lenshof and Laurell 2010). This method is based upon the difference in the retention time of the particle in the separation chamber. There are three modes of operations in FFF. In the ‘normal mode’ (Giddings 1973), as shown in Fig. 45a, microparticles are fractionated. When an external field is applied, those particles will move toward the wall in the direction of the applied field. The concentration of particle increases on the wall, and the motion is counteracted by the Brownian

**Fig. 45** Different modes of field flow fractionation (FFF): **a** normal mode; **b** steric mode; **c** hyperlayer mode (Lenshof and Laurell 2010)

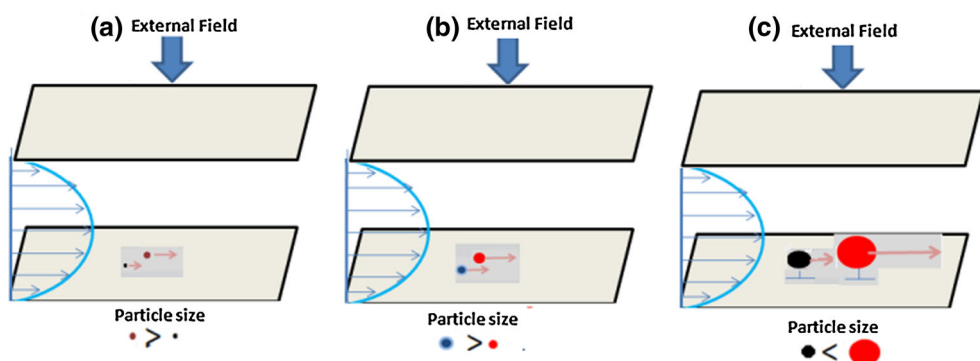
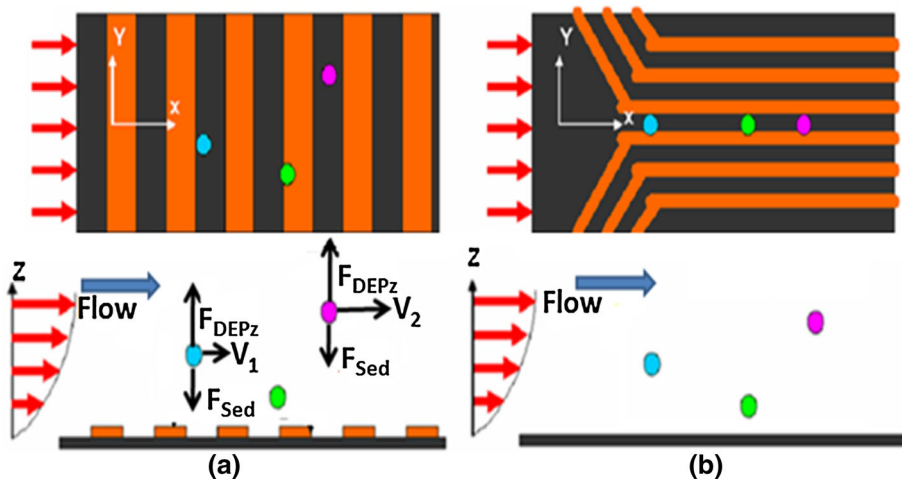


**Fig. 46** **a** Conventional DEP–FFF electrode array; **b** modified DEP–FFF with convergent electrode array (Leu and Weng 2009)



diffusion. Brownian force will be predominant in macromolecule, and they move away from that wall. Due to the parabolic velocity profile, the resident time of the larger particles will be lesser than that of the smaller particles that can be used for segregation. In the ‘steric mode’ (Caldwell et al. 1984), as shown in Fig. 45b, the particles of 0.5–10 mm are separated. In this mode, both particles will be moved to the accumulation wall and form a thin layer on the wall. But, the larger particle projected to the streamline moving faster than the streamline in which the smaller particle lies, which is used to achieve the separation. If the particle size is greater than 10 mm, the lift force acting on the particle tends to move the particle away from the wall at a distance greater than the diameter of particle. This mode of operation is called ‘hyperlayer mode’ (Giddings 1983), as depicted in Fig. 45c, which operates similar to the ‘steric mode.’ Bigger particles will exit from the channel first due to higher speed. This sorting technique is based on the size and shape and deformability of particle.

A combined DEP and FFF method has been reported (Giddings 1983). Both steric and hyperlayer mode FFF can be used along with DEP. The frequency and voltage can be adjusted to control the position of particles in the channel. As the crossover frequency is approached, the DEP levitation force decreases due to which the sorting ability of the hyperlayer FFF–DEP method increases unlike DEP affinity method. The steric and hyperlayer DEP–FFF methods have been used together to sort complex particle mixture (Huang et al. 1998). Particles with lower crossover frequency were trapped by steric FFF–DEP, but particles having higher crossover frequency were separated by the hyperlayer FFF–DEP method. In conventional FFF–DEP sorting system, the electrodes are placed perpendicular to the flow direction. In this case, the particle levitated up has a wavy character, which leads to uncertainty in sorting using FFF. In a recent technique (Leu and Weng 2009), shown in Fig. 46, all the particles are concentrated into a single

stream at the center using a convergent electrode placed on the microchannel. The DEP–FFF electrodes are placed parallel to the flow direction for which particles are levitated to different height without any wave trajectory.

In another design (Becker et al. 2001), the electrodes are placed vertical so that the flow through the chamber is perpendicular to it and the sedimentation force is perpendicular to the lift force. This improved the sorting efficiency, but there exists a metastable equilibrium between the lift force and positive DEP force. In another example of hydrodynamic DEP for cell separation and sorting, three planar electrodes are placed at the bottom of a micro-channel (Doh and Cho 2005), as shown in Fig. 47. The positive DEP cells are moved away from the central streamline, while the negative DEP cells remain in the central streamline. The sorting of dead and live yeast cells was demonstrated. Due to the difference in the direction of the DEP forces acting on the cells, they move to different locations and sorted into different outlets. Iso-dielectric separation (IDS) (Vahey and Voldman 2008) is another label-free method for sorting of particles, which is done in an electrical conductivity gradient environment inside the

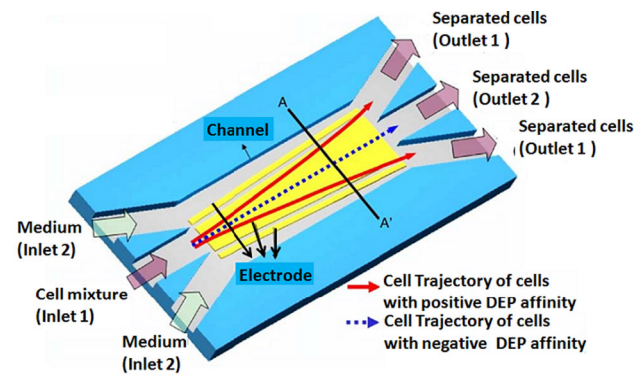


**Fig. 47** Schematic diagram of a hydrodynamic DEP cell sorter (Doh and Cho 2005)

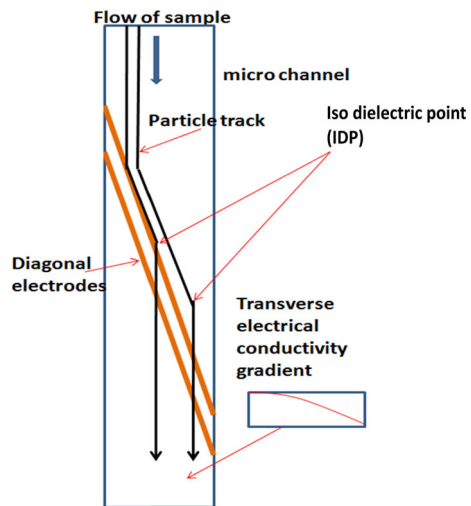


**Fig. 48** Schematic diagram explains the working principle of IDS (Vahey and Voldman 2008)

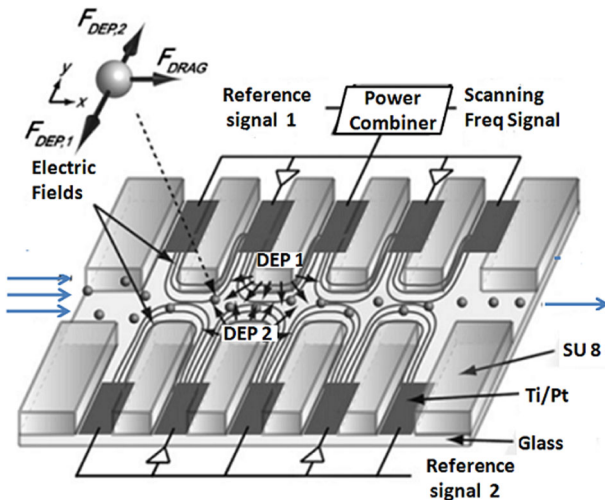


**Fig. 49** Insulator-based ‘electrodeless’ dielectrophoresis (Demierre et al. 2008)

microchannel. The working principle of IDS is depicted in Fig. 48. In IDS, DEP moves the particles to a point in the conductivity gradient where the net polarization charge vanishes. This point is called iso-dielectric point (IDP). By adjusting the operating conditions such as the frequency and voltage of the applied electric field, different particles can be moved to different IDPs. After the particle reaches the IDP, DEP has no effect on the particle that follows the fluid path.

Initially, in DEP, electrodes were placed inside the microchannel device itself. However, due to the problems of electrolysis, fouling of electrodes and complicated lithographic process, electrodes were placed outside the channels. Recently, insulator-based electrodeless dielectrophoresis has been introduced (Demierre et al. 2008). Here, nonuniform electric field is produced by a

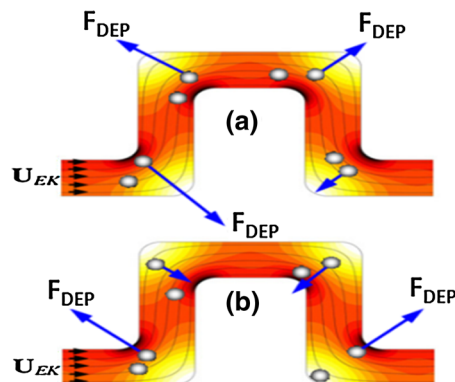
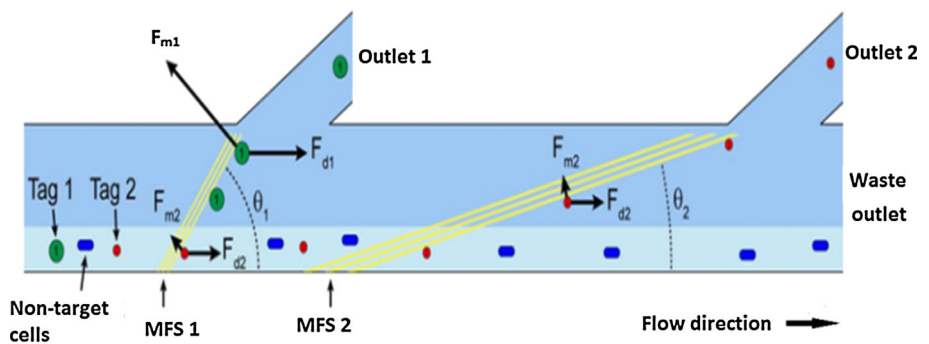


**Fig. 50** **a** Negative DEP and **b** positive DEP forces acting on the particle with different electrical conductivity (Church et al. 2010)

number of posts or ridges placed in the structure. As shown in Fig. 49, the electrodes are placed on the sides of a microchannel that are separated from each other using a patterned insulator. The dark rectangles represent the electrodes, and transparent rectangles represent patterned insulators used to create nonuniform electric field in the channel. Forces acting on the particle are  $F_{DEP,1}$ ,  $F_{DEP,2}$  and  $F_{drag}$ . According to the frequency of applied signal as well as the dielectric properties of the particles and the surrounding medium, an equilibrium position of the particle is reached. This method does not require a pre-focusing step and can be used to separate infected cells from healthy cells.

The use of DC electric field enables finer manipulation of particles by adjusting the magnitudes of electrokinetic flow and DEP (Cummings and Singh 2003). Constant-voltage DEP effect can be produced by uniformly patterned array of insulating posts. The particles show two types of phenomena: (a) electrophoretic streaming in which fluids having high and low concentrations flow through the array and (b) trapping in which particles are immobilized on the insulating posts. Streaming occurs when DEP overrides diffusion but is weaker than electrokinetic flow, and trapping of particle occurs when DEP overrides diffusion, electrokinetic flow and advection. This trapping mode can be used to separate the target particles from a medium (Cummings and Singh 2003). The use of posts as insulators inside microchannels leads to the problem of clogging and joule heating. As a modification of electrodeless DEP, insulating walls of curved microchannel are used to create nonuniform electric field and control the particle motion (Church et al. 2010), as shown in Fig. 50. Using this principle, a serpentine channel was created in which the electric field is more in the inner wall of each turn and lesser on the outer wall as shown by dark and light colors. When particle is less conductive than medium (i.e., particle has higher dielectric constant than the medium), then the CM is negative (according to Eq. 7) and the DEP force is

**Fig. 51** Multitarget magnetic-activated cell sorter (MT-MACS) (Adams et al. 2008)



negative (according to Eq. 6), so particles move to the lower electric field region (i.e., outer wall in each turn of serpentine channel) and vice versa. As per Eq. 6, DEP force is also proportional to the gradient of electric field. So, the particles at the inner wall suffer large DEP as indicated by the length of the force vector. Particles that suffer negative DEP are deflected toward the channel centerline after few turns. Positive DEP force is acting on particles at inner turn, where both electric field strength and gradients are stronger. So, the particles continue to move along the channel wall itself. This method can be used to separate particles of different size and electrical conductivity (in a medium whose electrical conductivity value lies in between that of the particles to be sorted). This principle has also been demonstrated with series of ‘S’-shaped channels using negative DEP (Lil et al. 2012).

### 3.2 Magnetic

Separation techniques based on the intrinsic properties of the cells lead to cell damage due to the shear stress acting on the cells in centrifuging, membrane pressure in filtration and joule heating in electrophoresis. The magnetic separation and sorting technique offers several advantages, including high specificity, less chance of cell damage and only shorter sorting time. The experimental setup required in magnetic separation technique is cheaper (Kersaudy-Kerhoas et al. 2010b) compared with other active techniques. A review of magnetic sorting techniques is reported by Chen et al. (2007) and Pamme et al. (2007).

Fluorescence-activated cell sorting (FACS) is a method of sorting and separation of particle from a mixture, but it has low efficiency with only  $10^7$  particles per hour. By this method, the time consumed for the isolation of rare cells is much large (Miltenyi et al. 1990). As an alternative method of cell separation, high-gradient magnetic (HGM) fields along with fluorescent labeling can be used to make the process more efficient. This is called magnetic cell separation system (MACS) in which fluorescent and magnetic labeling is given to the cells. A multitarget magnetic-activated cell sorter (MT-MACS) has been reported (Adams

et al. 2008), as shown in Fig. 51. In usual MACS, separation was based on the presence and absence of magnetization, and therefore, simultaneous sorting of multiple targets with high purity and throughput was not possible. This device was used to purify two types of target cells. Here, the combination of hydrodynamic force produced from flow and magnetophoretic force produced from ferromagnetic strips (MFS) placed in two regions of channel is used. Different tagging was done on two different target cells. When Tag 1 target cell reaches MFS1 region and magnetic force acting on that cell is more than the drag force ( $f_{m1} > f_{d1}$ ), the cell escapes through outlet 1. Similar phenomena occur in the case of Tag 2 target cell at MFS2 ( $f_{m2} > f_{d2}$ ). Nontagged waste particles will exit without deflection. A micropillar array (MPA) was proposed to trap and separate magnetic beads (MBs) in microfluidic systems (Gooneratne and Kosek 2012). Nickel–iron micropillars were fabricated on a silicon substrate by standard lithographic process. Experimental results showed that the MBs could be trapped on the MPA at the single bead level and separated from other nonmagnetic particles.

A high-gradient magnetic field (HGMF) separation system was developed in which a column is filled with ferromagnetic stainless wool and magnetic field is applied using permanent magnet (Miltenyi et al. 1990). The labeled magnetic particles will stick to the steel wool, and when the magnetic field is removed, these particles can be separated.

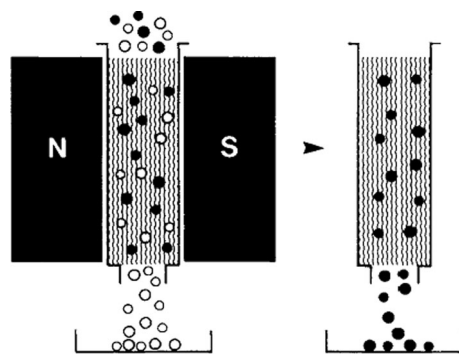


**Fig. 52** Schematic of magnetic cell separation system (MACS) (Miltenyi et al. 1990)

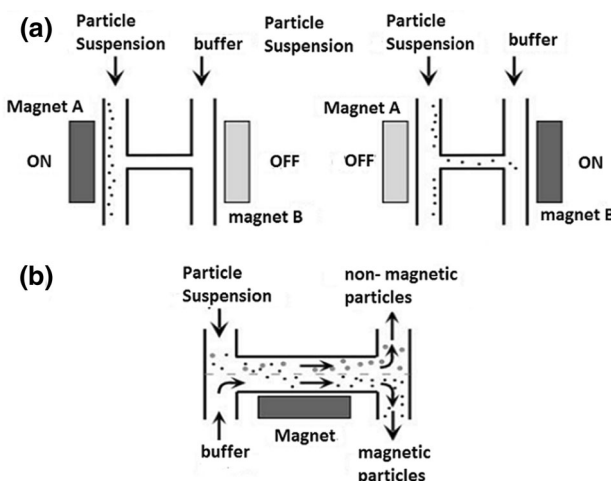


**Fig. 53** Principle of H-shaped separators: **a** particle separation into buffer streams; **b** continuous separation of particles (Chronis et al. 2001)

A schematic diagram of this technique is shown in Fig. 52. As a modification to MACS, H-shaped channel networks can be used for magnetic separation (Ostergaard et al. 1999). For particle isolation into separate streams, two magnets A and B are placed at the end of a horizontal channel connecting parallel channels. A stream with magnetic particles is pumped through the first channel with magnet A switched on which leads to the attachment of particles to this channel. Next, magnet A is switched off and magnet B is switched on at the same time. Then, the particles stuck to the first channel are dragged through the connecting channel to the parallel channel in which magnet B is present (refer Fig. 53a). A throughput of 30 particles per cycle was observed. Another H-shaped device with two inlet channels merging into a wider channel and splitting into two outlet channels for the separation of magnetic particles has been reported (Chronis et al. 2001). A sample stream with particles is introduced through one inlet and buffer solution through the other inlet with a magnet fixed at the connecting channel. In the absence of the magnetic field, both streams will flow like stratified streams to the corresponding outlet channels. When the magnetic field is applied, the magnetic particles are dragged from the original stream into the buffer stream as shown in Fig. 53b.

The magnetophoretic force acting on a spherical particle (Bruus 2009) placed in a nonuniform magnetic field is given by the equation:

$$F_{MAP} = 2\pi\mu_0 f_{CM} a^3 \nabla [H_{ext}(r_0)^2] \quad (8)$$

In Eq. 8,  $\nabla[H_{ext}]$  is the gradient of magnetic field,  $a$  is the diameter of the particle, and  $f_{CM}$  is the Clausius–Mossotti factor of magnetization (CM) similar to the dielectrophoresis. CM can be represented as  $f_{CM}(\mu_0, \mu) = \frac{\mu - \mu_0}{\mu + 2\mu_0}$ . Here,

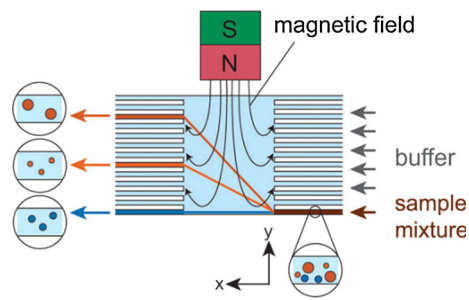


**Fig. 54** Schematic diagram of on-chip free-flow magnetophoresis (Pamme et al. 2006)

$\mu$  is the magnetic permeability of the spherical particle, and  $\mu_0$  is the permeability of vacuum. Thus, from Eq. 8, the magnetophoretic force acting on the particle is proportional to the gradient of magnetic field. If particle is placed in a homogeneous magnetic field where the magnetic gradient is zero, then the force acting on the particle is zero. Thus, sorting based on magnetic force requires nonhomogeneous magnetic field. Permanent magnet is used for the actuation process rather than the coils. A permanent magnet is specified by the magnetic induction  $B_m = 0.5 – 1$  T. Cylindrical permanent magnet of 5 mm diameter induces a magnetic moment of  $m = 2.6 \times 10^{-19}$  T m<sup>3</sup> over a spherical particle of diameter 500 nm and unit susceptibility. The resulting magnetic force of 40 pN is acting on the particle. On the other hand, for a current-carrying coil, the magnetic field created is much smaller. For example, a coil having millimeter size with ten windings and current 0.5–1 A produces a magnetic induction of 1–10 mT on a particle of same diameter. This value of magnetic induction is 100 times lesser than that generated by permanent magnet. Similarly, the gradient of magnetic field is also smaller by two orders of magnitude. So, the force produced by a permanent magnet is higher than that of a coil by a factor of 10<sup>4</sup> (Gijs 2004). On-chip free-flow magnetophoresis is used for the separation of magnetic particles not only from nonmagnetic material but also from different magnetic materials based on their size and magnetic susceptibility (Pamme et al. 2006). A laminar flow was generated in a chamber through a number of inlets and outlets, and magnetic field was applied perpendicular to the flow direction as shown in Fig. 54 (Pamme et al. 2006). Non-magnetic particle left the chamber through the opposite outlet of sample inlet without any deflection. The magnetic particle deflected by the field and the deflection of particles depends on the particle size and susceptibility. The separation of biological cells, such as tumor cells and macrophages, internally labeled with magnetic nanoparticles according to their magnetic loading has been explained (Pamme and Wilhelm 2005). Also, continuous immune magnetic sorter for biological particles has been studied in

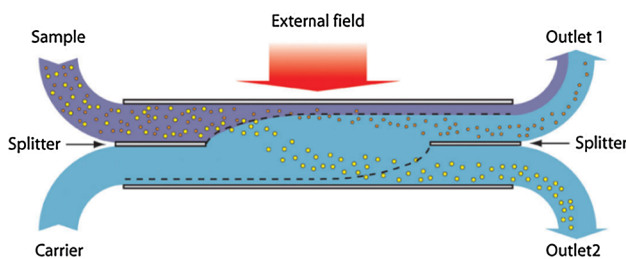


**Fig. 55** Split-flow lateral-transport thin (SPLITT) separation (Lenshof and Laurell 2010)

which particles can be immunologically fixed to magnetic beads by antigen–antibody coupling. Two streams are injected into the sorting chamber separated by a thin separation medium in the upward direction using a peristaltic pump. The nonhomogeneous magnetic field is applied perpendicular to the direction of flow. The particles with magnetic property are deviated and thus separated from the nonmagnetic particles. After passing through the field area, the separation medium is split into several fractions to enable collection of separated particles (Hartig et al. 1995).

A system closely related to FFF is the split-flow lateral-transport thin (SPLITT) separation (Lenshof and Laurell 2010). It has two inlets, one sample stream and the other buffer stream. Both are separated by a splitter, and streams are kept unmixed up to the region where the external field is acting. Effect of the field is large on larger particle than on the smaller one. So, the larger particles (yellow color) present in the sample are separated from the smaller particles (orange color) and move into the carrier fluid as shown in Fig. 55 (Lenshof and Laurell 2010). SPLITT is mainly used for preparative applications, whereas FFF is mainly used for analytical applications.

Magnetic split-flow thin (SPLITT) fractionation has been demonstrated (Tsai et al. 2006), which is used for sorting particles having different induced velocities into two fractions by manipulating the magnetic fields and flow rate at inlet and outlet. The field-induced velocity mainly depends on sample magnetic susceptibility, sample diameter, carrier viscosity and magnetic field intensity. As the size of microchannel decreases, the nonspecific binding of the particles to the channel walls and clogging in the channel increase, and this limits the development of LOC microfluidic devices. A combination of magnetic field along with capillary force and surface tension effects for the separation of magnetic particle from solution has been demonstrated (Zabow et al. 2002). It is an electromagnetic guiding approach that makes use of the natural electrical charge of biological microparticles such as DNA. A PDMS channel, kept as hydrophilic at bottom and hydrophobic at top, was used in the design (Zabow et al. 2002). The aqueous suspension of magnetic particle and air were pumped through the channel, and magnetic field was

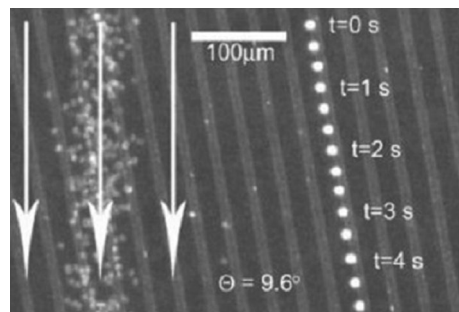
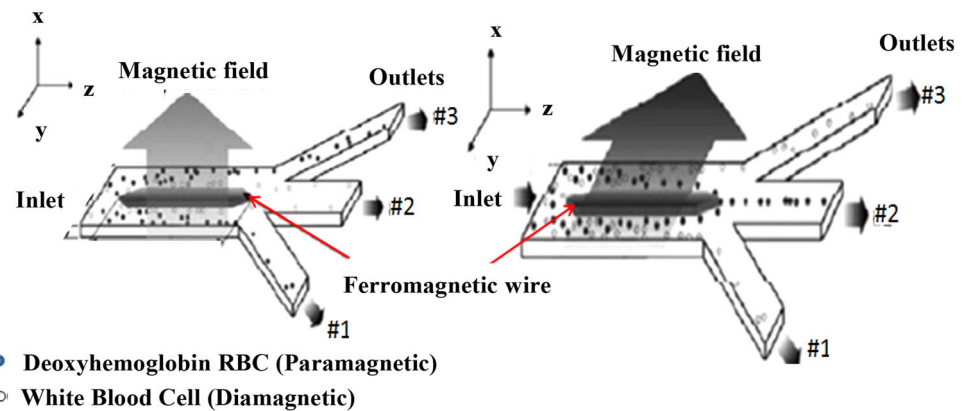


**Fig. 56** Separation of WBC from RBC using ferromagnetic nickel strip (Inglis et al. 2004)

applied from the top. The net force on the particles is the electromagnetic force along with the surface tension inherent to the microfluidic capillary network. Due to this, the particles were pulled to the air–water interface and finally separated.

A device in which ferromagnetic nickel strips were placed at the bottom of separation chamber at an angle of  $10^\circ$  to the direction of the continuous flow was developed (Inglis et al. 2004). When external magnetic field is applied, magnetic flux lines are concentrated on the nickel strips. Magnetically labeled cells are deviated away from the flow direction and move along the direction of strips. The sample flow rate should be kept lower in order to ensure that the magnetic force acting on the particle is of the order of or larger than drag force acting on the particle to have a proper deflection of the particles. This method was used to separate WBCs from human blood as shown in Fig. 56. In another method (Han and Frazier 2005), a uniform magnetic field is applied normal to the ferromagnetic nickel wire, which is incorporated along the length of the microchannel. The magnetic field deforms near the ferromagnetic wire and creates a high gradient of magnetic field. Most of the biological tissues and cells such as WBCs are considered as diamagnetic materials, whereas deoxyhemoglobin RBCs in peripheral blood have paramagnetic nature. Magnetic particle experiences magnetophoretic force when they reach this high-gradient region. Deoxyhemoglobin RBCs and other biological components will move in opposite directions due to this magnetophoretic force. If magnetic field is applied normal to the  $x$ -axis of the microchannel (diamagnetic capture mode), RBCs deflected away from the ferromagnetic wire to the side outlets 1 and 3. In reverse, if the magnetic field is applied normal to the  $y$ -axis of microchannel (paramagnetic capture mode), then the WBCs are deflected away from the ferromagnetic wire and exited through outlets 1 and 3 as shown in Fig. 57. Separation of the breast cancer cells from peripheral blood based on their electrophysiological characteristics without any tagging such as with magnetic probe has been reported (Han et al. 2006). The system was

**Fig. 57** Ferromagnetic wire operated in diamagnetic mode and paramagnetic mode for the separation of WBC and deoxyhemoglobin RBC (Han and Frazier 2005; Han et al. 2006)



fabricated on silicon and glass substrates utilizing micro-fabrication and stereolithography technologies.

Recently, high-gradient magnetic field separators to remove malaria-infected red blood cells (pRBCs) from blood samples of patients with severe malaria in a dialysis-like treatment have been reported (Han and Frazier 2005). In a numerical work (Kim et al. 2012) on the transport of the malaria-infected RBCs (pRBCs), they are treated as paramagnetic particles suspended in a Newtonian fluid. In this work, ODEs governing the movement of particles under periodic magnetic fields due to magnetic wires were solved. Theoretical and experimental method of separation of particles based on the size (even size~nm) using combined hydrodynamic and magnetic forces has been presented (Weddemann et al. 2009). Here, the main channel was split into two outlet channels, and depending on the geometry of the channel (shown in Fig. 58), the flow rate in the upper and lower channels is different. In this device, the nonhomogeneous magnetic field is created by the two end ring-shaped wires. Magnetic forces due to electric currents are always attractive as the particle magnetization aligns with the inhomogeneous field. To produce a force in the Y-direction (as shown in Fig. 58), a homogeneous field stronger than the nonhomogeneous field is applied in the Z-direction. Thus, the

aligned particles are obtained in the two outlets depending on the size and flow velocity in each outlet channel.

Recently, separation of magnetic particles in droplet-based microfluidic device for magnetic-bead-based bioassays has been reported (Lee et al. 2012), which is shown in Fig. 59. The device included a droplet generator module in which aqueous phase I (containing biotin with fluorescence label) and phase II (containing magnetic beads coated with streptavidin) were supplied through the two inlets. Oil phase was the continuous phase supplied through the other inlet. AC voltage was applied through the two aqueous phases, so that coalescence of droplets takes place. At the location where electro-coalescence occurs, minimum pressure is maintained to produce stable droplets. The flow passes through the U-shaped channel to have chemical reaction between the magnetic beads coated with streptavidin and fluorescently labeled biotin inside the droplet after the electro-coalescence. When a magnetic field is applied normal to the direction of flow, the magnetic particle is moved to one side of the droplet. At the droplet breakup junction, the droplet is split into two, one with the magnetic particle inside it and another with no magnetic particle inside it.

Magnetic particles can also be transported by a simple planar coils placed in a uniform magnetostatic field for separation (Rida et al. 2003). The device consists of two permanent magnets placed symmetrically over a metallic sheet to produce a uniform magnetic field over a microfluidic channel placed between them. Magnetic particles in the channel are magnetized. Then, a simple planar coil array placed below the microchannel transports the beads in the channel. Long-range displacement of microbeads is possible by arranging nearest coils in the planar array in a spatial overlap of three-phase actuation scheme. Time-dependent actuation scheme of planar coils arranged in three-phase geometry is shown in Fig. 60. Direction of arrows in the figure shows the sense of magnetic field generated by the planar coil array. The microparticles are only attracted to the position in the planar coil where the sense of magnetic field is same as that of the magnetic field produced by the permanent magnet (i.e.,  $B_0$ ).

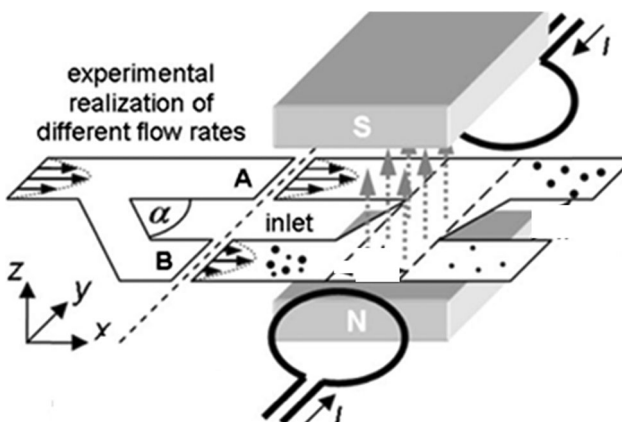


**Fig. 58** Sorting of particles with homogeneous and nonhomogeneous magnetic field (Weddemann et al. 2009)

**Fig. 59** Magnetic particle separation in droplet-based device for magnetic-bead-based bioassays (Lee et al. 2012)

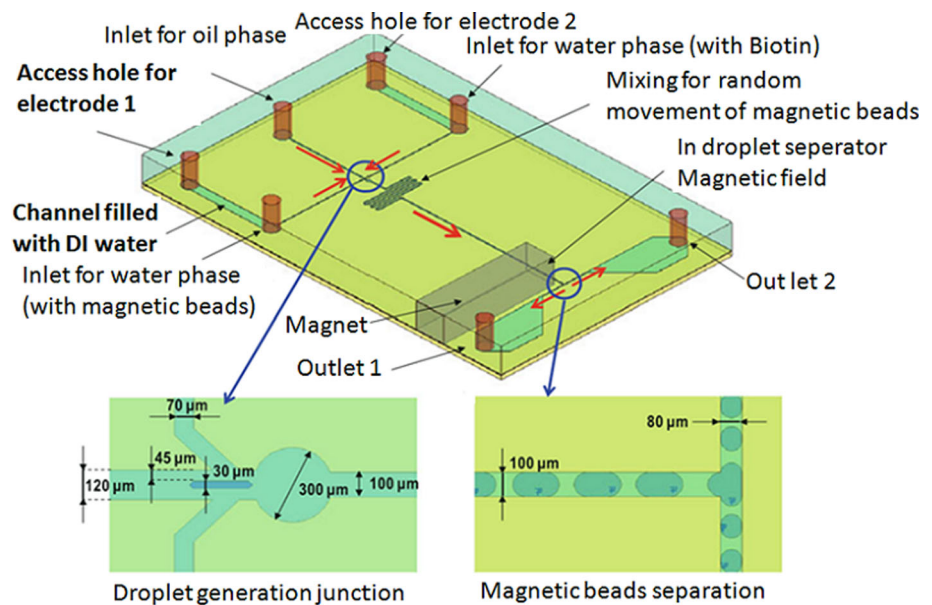
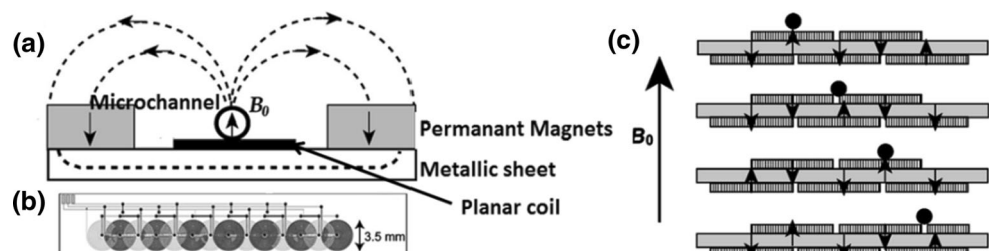


**Fig. 60** **a** Schematic diagram of magnetic microbead transport device; **b** layout of simple planar array; **c** time-dependant actuation scheme of simple planar coil (Rida et al. 2003)



In another method, a microelectromagnet matrix is used for the manipulation of biological cells in a microchannel (Lee et al. 2004). The matrix is created by two layers of straight Au wires aligned perpendicular to each other and covered by an insulating layer. Then, current applied to each independent wire is adjusted to create a magnetic field pattern for the motion and separation of the cells in the channel. In another design, traveling magnetic field created by four-phase conductors on the chip is used for sorting (Liu et al. 2007a). Four conductors are identical in structure and independent in operation. When current is allowed to pass through each conductor, maximum magnetic field is created at the center of that conductor structure and superparamagnetic particles are attracted toward the center. By alternatively passing the current to the adjacent conductors, the movement of the particles can be controlled. In this case, the speed of the particles can be increased with increase in the switching frequency. Different particles possess different magnetophoretic mobilities; thus, at a particular switching frequency, the faster-moving particles can be separated from the slower-moving particles. In all the above methods that are based on traveling magnetic field, the out-of-plane movement of the particles cannot be achieved. However, in a modified method, magnetophoresis

along with dielectrophoresis has been used by generating both traveling magnetic field and AC electric field. Therefore, both in-plane and out-of-plane movement of the magnetic particles can be achieved (Liu et al. 2007b).

### 3.3 Optical

A particle subjected to an incident beam of light scatters light and produces a change in momentum of the photons present in the light beam. The change in the momentum of the photons produces a force. Typically, a light beam has a Gaussian intensity profile which takes a maximum value at the center and decreases as we move outward. When a beam is scattered by the particle and the ratio of refractive index of the particle to that of the medium is less than one, due to imbalance of intensity across the beam, the scattering force tries to attract the particle toward the center as shown in Fig. 61 (McGloin 2006). This phenomenon was explained as a ‘single-beam gradient force trap for dielectric particles,’ which was later named as ‘optical tweezers’ (Ashkin et al. 1986; Ashkin 1997). By adjusting the laser wavelength, power and trap geometry, this technique can be used to separate and sort objects ranging in size from less than 100 nm to near 100 μm. Optical trap

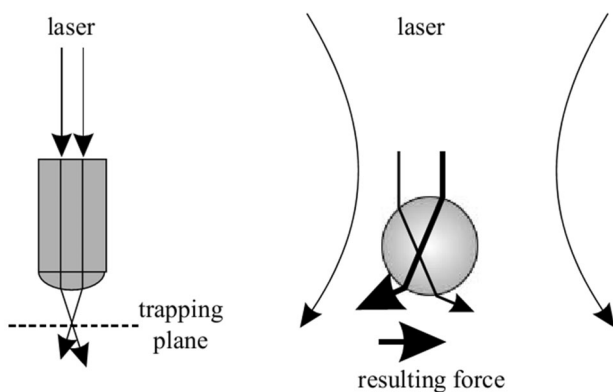


**Fig. 61** Schematic of the optical gradient force and its directions in optical tweezers (McGloin 2006)

produced can be shifted in lateral direction by adjusting the angle of light going into the objective lens with the help of a steering mirror (McGloin 2006).

When a single trap is created by optical tweezer, the trap and thus the particle can be moved by the motion of microscope stage. But for a multiple trap, this type of design requires a complex setup. Instead of using the laser beam splitter and beam steering mirror for the complex multiple trapping, manipulation of optical tweezer is used, which is a diffraction grating called ‘holographic optical tweezer’ (HOT). Optical tweezer is an example of a simple harmonic oscillator in which the particle motion is analogous to that of a spring, creating a restoring force that brings the particle back to the trap center (Dholakia and Cizmar 2011). Holographic optical tweezers (HOTs) create the optical traps for the particle and cells, when these objects are forced by a flowing fluid through a sample chamber in which the laser traps are projected with a microscope objective lens. The array of optical trap in the chamber is created from a single laser beam by diffractive optic with a computer-designed diffractive optical element and is placed inclined to the direction of fluid flow. A camera is used to monitor the particle motion through the traps. The diffractive optic is placed away from trapping plane, and hence, this calculated optics is called ‘computer-generated holograms.’ A structure of simple HOT (Lee and Padgett 2012) is shown in Fig. 62.

As a modification of optical tweezers, liquid crystal display (LCD) is used for the reconstruction of computer-generated holograms, which can be used to generate arbitrary light fields in the Fourier plane of the LCD and to change them dynamically for lateral trapping of independently moving polystyrene particles in water. The main drawback of this technique is the poor overall efficiency that results from the pixilated structure of the LCD (Reicherter et al. 1999). A schematic of the experimental setup is depicted in Fig. 63. An Ar<sup>+</sup> laser illuminates the LCD

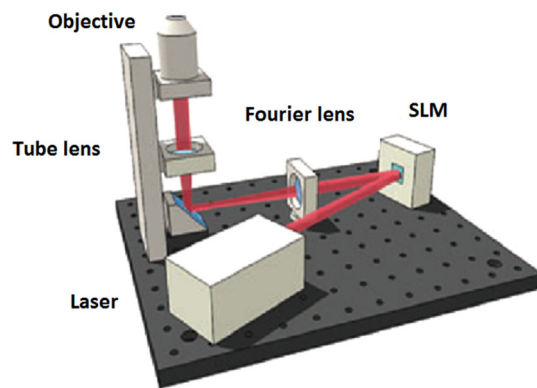


**Fig. 62** Simplified holographic optical tweezers (HOTs) (Lee and Padgett 2012)

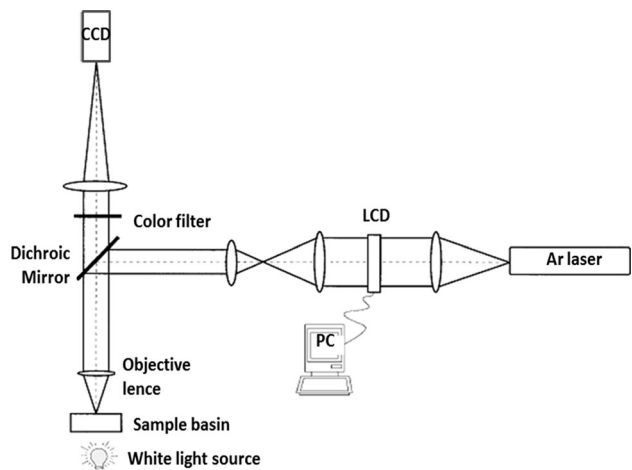
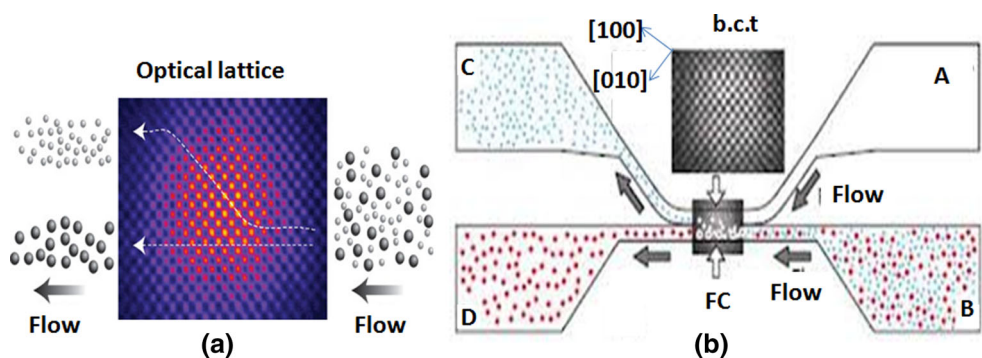


**Fig. 63** Experimental setup for the reconstruction of computer-generated algorithm by LCD (Reicherter et al. 1999)

panel, and the display is placed on a rotary stage. The phase-shifting capability of the LCD display is required for the diffraction efficiency. The display is read out with a collimated beam. A dichroic mirror reflects the beam into the aperture of a microscope objective lens. White light is used to illuminate the sample dish from below, and this light is scattered by polystyrene beads present in the sample fluid. These programmable pixilated LCDs are called ‘spatial light modulators (SLMs)’ in which each pixel can introduce a phase change between 0 and  $2\pi$ . A programmable SLM with a suitable hologram gives 3D control of trap position, which cannot be achieved by a simple mirror. For multiple traps, a number holograms can be used and two or more holograms can be combined into a single design.

As shown in Fig. 64a (Gluckstad 2004), when a 1,070-nm laser beam is passed through a diffractive splitter, it is split into different beams that diverge from the central undiffracted point. Collimation of these beams produces a

**Fig. 64** **a** Working principle of an optical lattice (Gluckstad 2004); **b** schematic of optical fractionators with optical lattice (MacDonald et al. 2003)



three-dimensional optical lattice at which accurate control of amplitude and phase of each beam can be done. When a laminar flow with particles having various intrinsic properties and size reaches the optical lattice, particles that interact less with the optical potential energy landscape are deflected from their path, whereas the more interacting molecule follows the flow streamlines as shown (Gluckstad 2004). In the example (MacDonald et al. 2003) given in Fig. 64b, body-centered tetragonal optical lattice is used. Chamber A supplies the buffer solution into which the target particles are supposed to migrate. If there is no optical actuation, all the particles from chamber B would flow into chamber D. When the optical actuation is given and the sample is moving through the lattice, then the smaller particles migrated to chamber C along with buffer solution and undeflected larger particles migrate to chamber D along with buffer. The optical lattice can be reconfigured for the dynamic updating of selection criterion for sorting.

In another optical fractionation method, sorting of sample into more fractions or more refined fractions can be done using holographic optical tweezers (HOTs) technology (Xiao and Grier 2010a). With optical fractionation, forces exerted by flowing fluid drive the objects of interest through an array of optical traps created by the HOT technology. Depending on the competition between the driving force and the forces exerted by the optical traps, the objects can either continue in their original direction or get deflected into a new direction that is dictated by the asymmetry of the array. A schematic of the optical fraction using HOT (Xiao and Grier 2010a) is presented in Fig. 65. Optical fractionation combined with holographic optical trapping and holographic video microscopy system is used to track each particle in three dimensions and simultaneously measure the dimensions and refractive index of the particles. Thus, optical-fractionation-based sorting is achieved with part-per-thousand resolution on multiple characteristics simultaneously. As shown in Fig. 65 (Xiao and Grier 2010a), the method is demonstrated by the aqueous dispersions of colloidal silica spheres driven using a syringe pump at a constant flow rate through a

rectangular PDMS microfluidic channel. In this method, the optical tweezers array was designed to sort an input distribution of colloidal spheres into two fractions that are kinetically locked into two distinct lattice directions and thus are deflected by the array in opposite directions. Particle that is kinetically locked into the directions shown by circles is deflected toward the apex of the array before flowing downstream. The particles that are locked into the directions shown by rectangles weakly interacted with the traps and deflected away from the apex to the sides of the array as shown in Fig. 65.

The above-said HOT technology can be extended to the multiple fractionations of Brownian particles. With the same setup (refer Fig. 65), particles move through a periodically structured potential energy landscapes entrained by the landscapes symmetries. Direction of particles depends on the variation in its physical properties. Thus, the homogeneously structured force field sorts particles into multiple fractions as the optical prism refracts light into different-wavelength components. Such continuous multichannel sorting is termed as ‘prismatic optical fractionation.’ Experimental and numerical studies of movement of colloidal spheres through periodic arrays of optical

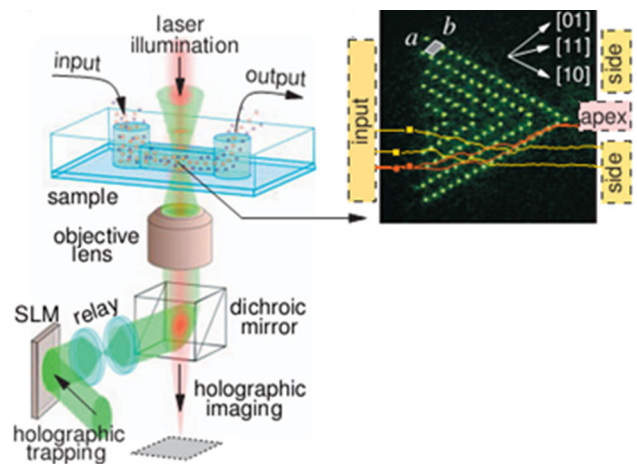


**Fig. 65** Schematic of optical fractionation with HOT (Xiao and Grier 2010a)

tweezers have been carried out using this technique (Xiao and Grier 2010b). Optical fractionation can also be used for continuous sorting of waterborne colloidal particles flowing past a linear array of holographic optical tweezers (Ladavac et al. 2004). Density of colloidal silica spheres is twice as that of water, and thus, the spheres settle in a layer above the lower wall of the channel. When the flow is induced, the larger spheres travel slower compared to the smaller spheres. Twelve discrete optical tweezers were arranged in a line at an angle of 12.5° to the direction of flow. Each trap is powered by laser light. The power of this laser is more than the lock-in threshold of larger spheres. Then, the larger spheres are deflected by the array of traps, while the smaller spheres continue the direction of flow; thus, particle sorting can be achieved.

HOT technology that can be used to create 2D and 3D trap arrays within a sample chamber is more versatile compared with Acousto-Optic Deflector (AOD). AOD is the conventional device used to spatially control the optical beam. However, the formation of HOT is more complicated than traditional optical tweezer. Optical trap produced by HOT is stiff which has large spring constant that produces extension to the biomolecules such as DNA strand which requires the analysis under constant force without any extension. Thus, sorting and separation of particles in such situations requires another method that is known as ‘asymmetric scanning line optical tweezer (LOT)’ (Liesfeld et al. 2003). In LOT, shown in Fig. 66 (Ma et al. 2012), there is an asymmetric beam profile in the back-focal plane of the microscope objective, and this applies a small but approximately constant, lateral radiation pressure forces on a trapped particle over a distance of several microns. In a new approach to sorting, two conventional spot optical traps with different wavelengths and intensity distributions were transformed into two LOTs by

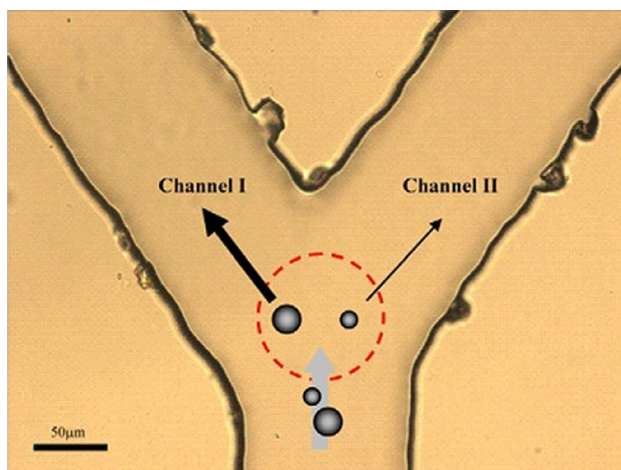


**Fig. 66** Micrograph of the operational area of the microfluidic chip for LOT (Ma et al. 2012)

employing two cylindrical lenses (Ma et al. 2012). These two LOTs are patterned in a ‘Y’ shape. When yeast cells passed through the dashed circle area, where both LOT1 and LOT2 act on the cells, they are optically separated and sorted to channel 1 and channel 2, respectively, based on their size as shown in Fig. 66.

Optically induced flow cytometry was developed to count and sort particles based on optically induced dielectrophoresis (ODEP) (Zheng et al. 2013). As shown in Fig. 67, the device consists of two indium tin oxide (ITO)-coated glass electrodes, and amorphous silicon layer is deposited on the bottom ITO layer. The solution containing particles to be separated is kept in between the electrodes. When an AC voltage is applied, an electric field is produced. If amorphous silicon is not illuminated, the entire voltage drop will happen only in this layer because of its high electrical impedance. When this layer is illuminated, local photoconductivity of the layer is increased and most of the voltage drop shifted to the liquid layer. Light-induced virtual electrodes are created via illumination through a mask to generate nonuniform electric field in the solution layer. When particles reach this area of illumination, they are subjected to DEP force. As shown in Fig. 68, first, the particles are aligned, and the optical fibers are used to determine the number and diameter of particles passing through the channel. These optical fibers are used for dynamic control of the configuration of the virtual electrodes to separate the small and large particles into the upper and lower channels, respectively. In another design (shown in Fig. 68c, d), both of these patterns are composed into two different inclinations placed in the path of the focused particle stream. The first electrode produces a weaker ODEP, and second one produces a stronger one. The larger particles are deflected down, and smaller particles penetrate through it and further deflected upward by the second virtual electrode (Lin and Lee 2009; Lin and Lee 2008). This method can be used for selective lyses of a single cell from a group of cells (Lee et al. 2009).

In another ODEP device, shown in Fig. 69, commercial digital projector coupled to a computer creates a moving

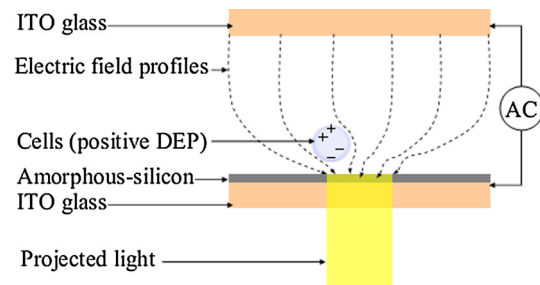


**Fig. 67** Schematic diagram for the optically induced dielectrophoresis (ODEP) (Huang et al. 2012)

light bar generated in a predefined speed (Huang et al. 2012). This light bar is used to activate the photoconductive layer to produce the ODEP force. Different cells

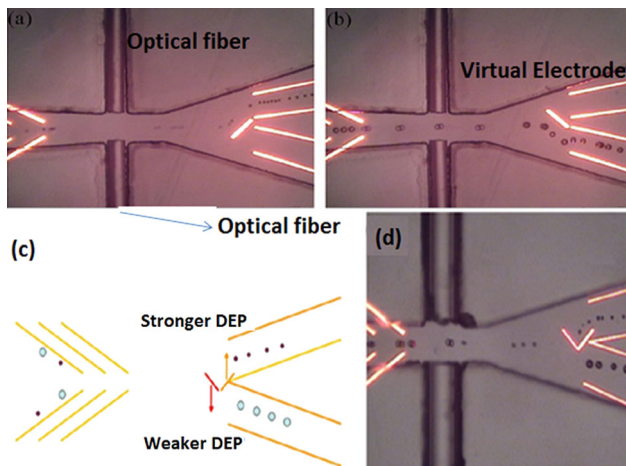


**Fig. 68** When ODEP switch activated, **a** smaller microparticles are switched upward; **b** larger microparticles are switched downward; **c** schematic illustration of the continuous separation of particles; **d** microparticles are continuously separated by combined weaker and stronger virtual electrodes induced by different intensity of illumination (Zheng et al. 2013)

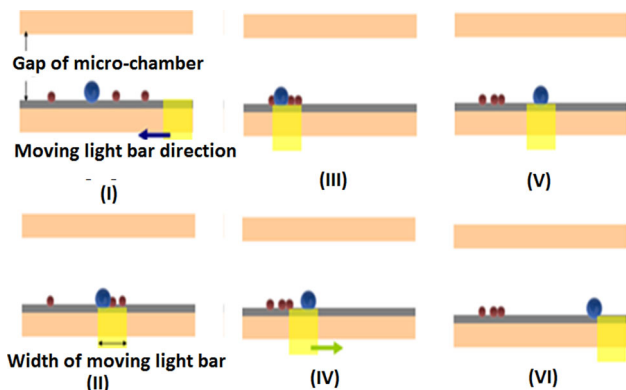
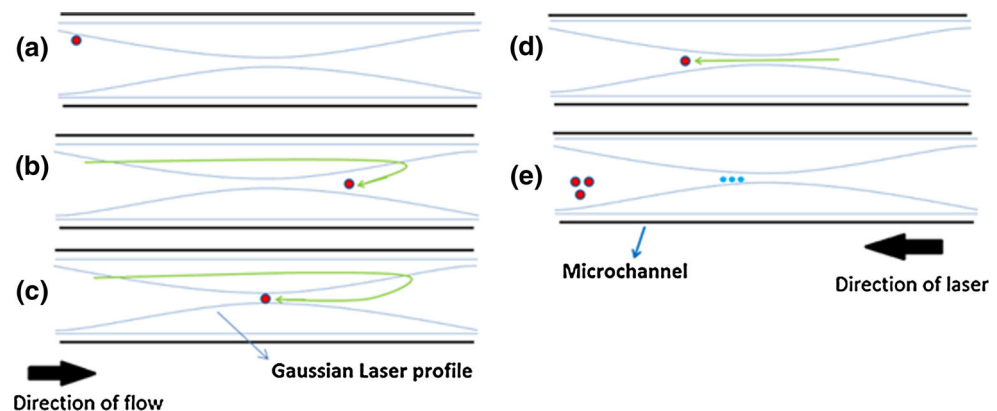


**Fig. 69** Schematic illustration of sorting larger cancer cells from the smaller leukocytes by a moving light bar (Huang et al. 2012)

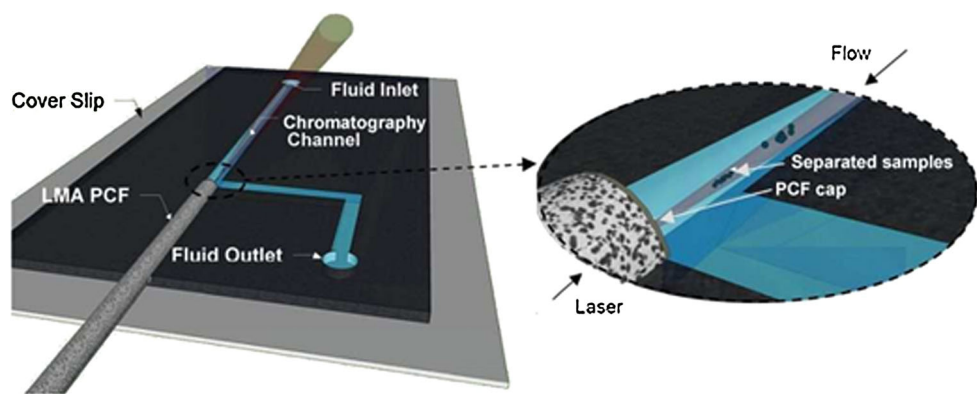
**Fig. 70** Schematic of an optical chromatography: **a** particle introduced into the channel; **b** focusing to the beam center; **c** acceleration of particle; **d** deceleration of particle; **e** different-sized particles in their equilibrium positions (Kaneta et al. 1997a)



undergo different ODEP force and have different velocities, thus can be separated. First, a moving light bar is used to drag all the cells to one side of the microchamber, and another moving light bar in the opposite direction takes only the larger particle along with it. This procedure can be used to separate the prostate cancer cells and leukocytes. There is a complex dependency of optical power and resolution on various electrical parameters such as resistance and applied AC voltage (Neale et al. 2007). Flexible ODEP devices can be bent into concave and convex shapes. This increases the separation and sorting efficiency by ODEP. The separations become rapid with the help of gravity in a concave- and convex-shaped bended ODEP chip than a flat ODEP chip (Lin et al. 2012). In other polymer-based optically induced dielectrophoretic devices, a film of a bulk-heterojunction polymer is used as a photoconductive layer. So, the variation in ODEP force can be created depending upon the color of illuminated light, which is due to the variation of absorption coefficient in the bulk-heterojunction polymer (Wang et al. 2010).

Optical chromatography (OC) is another sorting technique, which works based on the balance between microfluidic drag force and optical radiation force for the spatial separation of particles (Kaneta et al. 1997a). A particle introduced into a microchannel in a direction opposite to a focused laser beam (Fig. 70a) is focused to the center by the gradient forces created due to the Gaussian laser profile (Fig. 70b). At some point, the particle is accelerated and guided in the direction of laser and then gets decelerated when moves away from the beam waist. Finally, the particle comes to an equilibrium position (Fig. 70c–e) inside the channel depending on the balance between the Stokes drag force and optical force. Optical radiation force is highest at the focal point, and it decreases with increasing distance from the focal point (Kaneta et al. 1997b). The distance of this equilibrium point from the focal point of laser beam is called ‘retention distance.’ According to a theoretical model for the OC of dielectric particles based on ray optic approach, this retention distance depends on

**Fig. 71** Optical chromatography chip integrated with LMA-PCF (Knight et al. 1998)



the size (proportional to the square of the particle size when the particle diameter is smaller than beam diameter) (Kaneta et al. 1997b), refractive index and shape of the particle (Imasaka et al. 1995). As the size and refractive index of the particle increase, the retention distance also increases. Depending on the difference in the physical and chemical properties of different particles, sorting of particles can be achieved (Hart et al. 2008). Further, retention distance can be manipulated by the fluid flow rate and laser power. When an OC beam is completely focused to a fluid channel, this method can be used as a tunable filter for the separation of inorganic polymeric, colloidal, metallic and biological samples from a mixture (Hart and Terray 2003).

In a cascaded OC device (Terray et al. 2009), three lasers are accommodated simultaneously for the complete sample fractionation of two three-component colloidal mixtures. This microfluidic chip has three OC regions separated by certain distance. In order to orient the laser beams in a direction perpendicular to the previous chromatographic region, a prism is glued to the surface of the microfluidic chip. In each chromatography region, the mixture is pushed into a region of lower microfluidic flow, where they can be retained and fractionated. OC device is usually mounted on the five-axis positioner for accurately coupling the laser beam into the fluid channel by free space alignment method which requires a specialist hand for every single run of experiment. The separation efficiency depends on the exact beam focusing conditions and the stabilities of the laser and liquid-flow parameters. In a recent method, photonic crystal fiber (PCF) is integrated with the OC chip for the on-chip delivery of optical beam without any aberration (Knight et al. 1998; Napierala et al. 2011). In this modified device (refer Fig. 71), the PCF selected is large mode area photonic crystal fiber (LMA-PCF). This PCF ensures the guiding of single-mode laser that is required for the OC process irrespective of the fiber diameter (Knight et al. 1998; Napierala et al. 2011). The flow is maintained in the channel by a syringe pump. In this method, LMA-PCF can also be used for the launching of beams having multiple wavelengths; one beam is used for

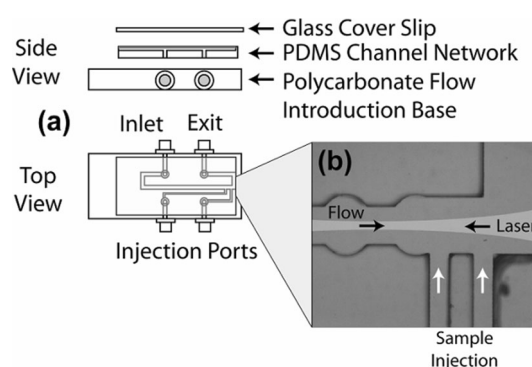


**Fig. 72** Schematic diagram of modified OC device setup with ripple channel structure (Arnold and Hart 2005)

the spatial separation, and other beam is used for the fluorescence excitation of separated samples in the chip. By this method, the mobility and functionality of the chip are increased (Ashok et al. 2010).

In another modified OC device made in PDMS by soft lithography (shown in Fig. 72), ripple structure is provided on the channel (Arnold and Hart 2005). This ripple structure in the channel produces a change in linear velocity of flow, which can be utilized for specific separation processes. This separation process is efficient than OC devices having constant linear flow velocity. In this device, the sample injection ports are placed near and below the focal point of the laser as shown in Fig. 72 to prevent optical disruption of the beam. Particles can be positioned either on a wide or on a narrow side of the ripple channel structure by adjusting the focal point with the movement of focus lens that focuses the beam. Due to this tailored velocity environment, linear velocity of particle increases or decreases in the narrow and wide channel sections, respectively. This augments the retention distance of the particles to be separated. Additionally, if the size difference between the particles is high, then nontailored devices cannot be used to trap both types of particles in the chip. In that case, particles of one size are trapped, whereas particles of other size are allowed to flow along with the fluid.

But, by this modified ripple structure, both of these particle types can be separated and retained in the channel. Theoretical model for cross-type OC is also developed where laser beam would be aligned orthogonal to the flow direction (Kim et al. 2006). Here, the separation is based on the parabolic velocity profile inside the channel. OC can also be used to selectively separate an antibody-coated beads and specific cell types from a mixture (Dholakia et al. 2007). This selective tagging of cells changes the refractive index between healthy and diseased cells; thus, the diseased cell can be separated from the healthy cells.

As discussed earlier, particles exposed to a light beam tightly focused with the help of a lens with high numerical aperture drift toward the center of the beam because of the optical gradient force. This is the principle of ‘optical tweezers.’ Similarly, if the beam is not focused, the particles will move by the scattering force of radiation, which is called ‘photophoresis’ (Monjushiro et al. 2000). When light is scattered and absorbed by particle in a fluid, it produces an uneven heat flux over the entire volume of the particle. Due to this heat distribution, the particle can suffer a force, which is the reason for ‘photophoresis.’ If the particle has high light absorptivity, it will move away from the light source, which is called positive photophoresis, and if the particle has low absorptivity, then it will move toward the light source, which is called negative photophoresis (Xin et al. 2011). This photophoretic force is much higher than the optical gradient force. Photophoretic efficiency of laser technology for the separation process decreases with decrease in the size of the particles in the suspension (Monjushiro et al. 2000). When light is introduced into the fiber arranged perpendicular to the flow direction, particles from the stationary fluid are aggregated around the fiber by negative photophoretic force. These assembled particles can be separated into two different positions downstream according to their size where the negative photophoretic force is balanced by drag force due to the fluid (Lei et al. 2012; Zhang et al. 2012).

Using the same method, the separation efficiency can be improved by two optical fibers placed in the channel (Xin et al. 2013). Photophoretic efficiency of carbon particles having light-absorbing property and the metal particles having light-reflecting property is much larger than that of the transparent particles. Various types of particles in the decreasing order of photophoretic efficiency are carbon, stainless steel, gold and plated nickel and polystyrene (Tamagawa et al. 2003). If the surface of the particle is hydrophobic and has high fluid slippage at the particle–fluid interface, the photophoretic velocity of particle in the suspension increases. As the thermal conductivity of the particles or size of liquid molecules increases, the

photophoretic velocity of particles deceases (Soong et al. 2010).

If a temperature gradient is also established in the bulk medium, particles have isotropic diffusion along a temperature gradient (from hot to cold), which is called ‘thermophoresis.’ Combined photophoresis and thermophoresis have been utilized for the separation of particles from water in water purification process (Xin et al. 2011). In this method, a racket-shaped fiber ring is introduced into the water to be purified. Using a light beam transmitted through an optical fiber, the foreign particles present in water move toward the ring by a negative photophoresis force ( $F_p$ ). Temperature gradient is also established inside the bulk of water due to strong absorption of light, which induces thermophoretic force ( $F_T$ ), which is larger than  $F_p$ . Both of these forces act in the opposite direction, and finally, particles slow down and accumulated and trapped at the center of the ring.

Thermophoretic action has also been used for the separation of droplets (Monjushiro et al. 2002). During the light irradiation, uneven heat generation is established in the front- and backside of a droplet, which produces the temperature gradient leading to thermophoresis. Thermophoretic velocity of droplet decreases with increase in absorptivity. Droplets with high photoabsorptivity migrate in a direction opposite to that of the laser irradiation. This is because of less heat being generated on the irradiated side than on the opposite side due to the lens effect of the droplet. Effect of photophoresis on water droplet is less because of the less optical density for water. However, the above-said photophoresis is mainly due to the uneven heat generation inside the droplet. Since the temperature gradient is larger for smaller droplet, the thermophoretic force is significant in smaller droplet.

### 3.4 Acoustic

When a particle is placed in an acoustic field, the one-dimensional primary acoustic radiation force acting on a particle is given by the following equation (Lenshof et al. 2012):

$$F_{ax} = 4\pi a^3 E_{ac} k \sin(2kz)\phi \quad (9)$$

In Eq. 9,  $E_{ac}$  is the acoustic energy density,  $a$  is the particle radius,  $k$  is the wave number that is equal to  $\frac{2\pi f}{c_0}$ , where  $f$  is the frequency of wave, and  $z$  is the distance from pressure antinode in the wave propagation axis.  $\Phi$  is called acoustic contrast factor (CF) given by:

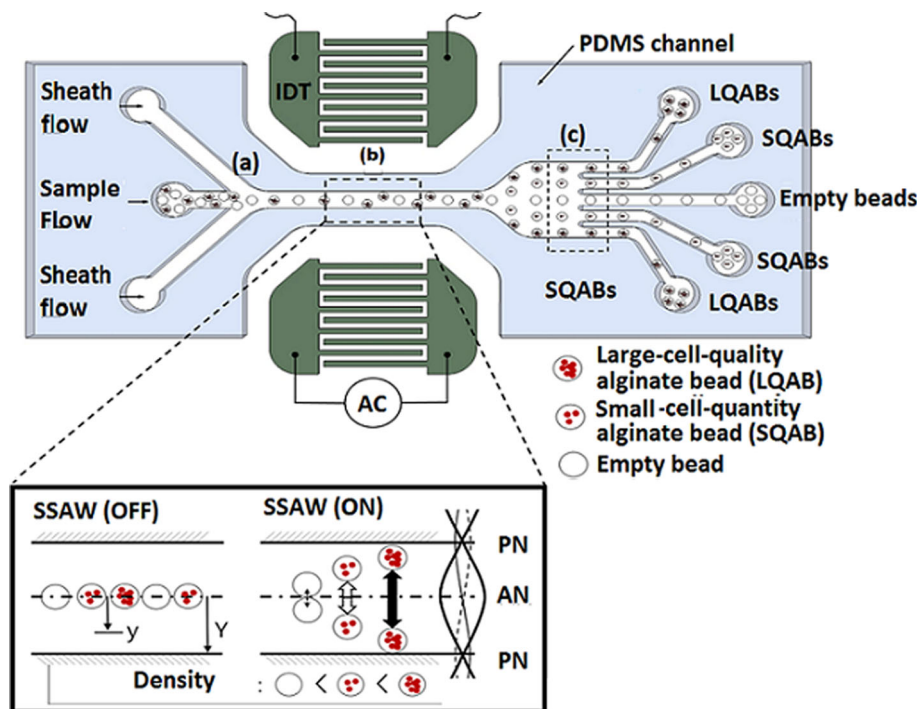
$$\phi = \frac{\rho_p + \frac{2}{3}(\rho_p - \rho_0)}{2\rho_p + \rho_0} - \frac{1}{3} \frac{\rho_0 c_0^2}{\rho_0 c_p^2} \quad (10)$$

In Eq. 10,  $\rho_p$  and  $\rho_0$  are the density of particle and medium and  $c_0$  and  $c_p$  are the speed of sound in medium and particle material, respectively. The sign of the radiation force is determined by the sign of the contrast factor (CF). If CF is positive, it means that movement of particle is toward the pressure node, while negative CF denotes movement of particle to the antinode. Usually, interdigitated transducer (IDT) electrodes are placed in the sides of the channel. Two standing acoustic waves (SAW) are created from the IDT. Commonly, the standing waves are formed between two parallel walls of the channel with one wall as an ultrasonic transmitter and the other wall as a reflector. These two SAW superimpose to form a pressure fluctuation in the channel. Usually, for half-wavelength resonators, the pressure node (minimum pressure amplitude) is located at the center of the flow channel, while antinode (maximum pressure amplitude) is located on the channel wall itself (Lenshof et al. 2012). From Eq. 9, it can be observed that the acoustic radiation force acting on the particle is proportional to the third power of the radius of the particle. So, the force acting on a larger particle should be more than that on a smaller particle. The process of deflection of particle from its fluid path by the application of acoustic standing wave is called ‘acoustophoresis,’ a property that can be exploited for the sorting of particles based on size. Similarly, the particle having different signs of CF in a mixture can be sorted by this method. Cells or particles with positive acoustic contrast factors are moved to the pressure node and with negative contrast factor moved to

the antinode. So, they can be separated continuously toward the center and a side outlet for a half-wavelength resonator.

Recently, use of acoustophoresis for the sorting of beads (cell encapsulated) of same size but different density has been reported (Nam et al. 2012). The radiation force depends on the density and compressibility of the particle and medium. The density of the beads is changed based on the number and density of cells encapsulated. The beads are focused to the center by a side sheath flow, and then by the radiation force, beads undergone a lateral shift based on the density. Bead with large density (large number of cells encapsulated) deflected maximum and bead with no cell has no deflection from the center as shown in Fig. 73. An acoustic continuous fractionation method has been demonstrated for sorting of particles having same density and size but different compressibility (Gupta et al. 1995). The manipulation of pressure nodes (Liu and Lim 2011) can be achieved by switching of acoustic field, as shown in Fig. 74. There are two operational modes. In the first mode, frequency  $f_1$  is applied and one pressure node is created in the channel. In second mode, frequency is tripled and three nodes are generated in the channel, and then cells are aligned along wall node A. When this stage is repeated, the larger particles move to node C passing through the position indicated by antinode B. Smaller particles are again moved to node A, and larger particles remain in central node when frequency  $f_3$  is applied again. The procedure is explained in Fig. 74.

**Fig. 73** Schematic diagram of the working principle of the SAW for the separation of bead based on density (Nam et al. 2012)



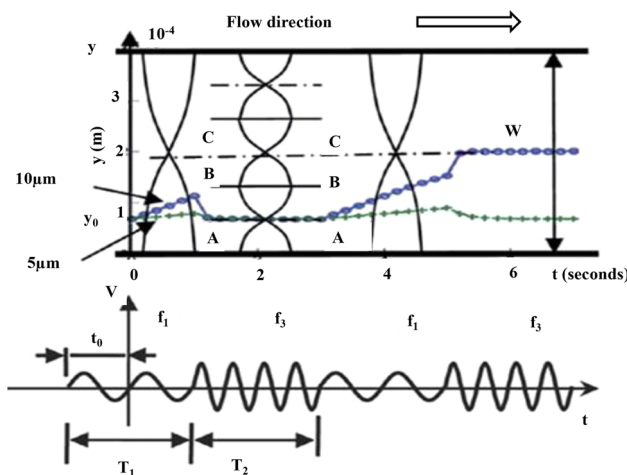


**Fig. 74** Manipulation of frequency of the acoustic wave for the sorting of particles (Liu and Lim 2011)

If the concentration of the particles is more, the particles experience a secondary acoustic force apart from the primary force due to the waves scattered by other particles. This force determines whether the force between the particles is attractive or repulsive. This secondary force will come into picture when acoustic wavelength is much greater than the particle radius or the distance between the particles is less. So, this becomes important in aggregation and sedimentation applications (Laurell et al. 2006). As a simple approach, the ultrasonic transducer can be placed parallel to the direction of the force field, and standing wave is induced parallel to the wave propagation (Nilsson et al. 2004), as shown in Fig. 75a. Lateral resonance perpendicular to the force field is also possible by placing the transducer as shown in Fig. 75b, where standing wave induced perpendicular to the primary wave propagation (Nilsson et al. 2004). Figure 75c produces a shear wave (Wiklund et al. 2006) using a wedge transducer to couple the waves. Here, the ultrasonic standing waves (USWs) and dielectrophoresis (DEP) are combined in a microfluidic chip. DEP is manipulated by the electric field between two coplanar electrodes placed on the surface of fluid. Particles will occupy a position inside the chip based on the balance between long-range ultrasonic forces, short-range dielectrophoretic forces and viscous drag forces from the fluid flow.

**Fig. 75** Different methods of actuation of USW (Nilsson et al. 2004; Wiklund et al. 2006)

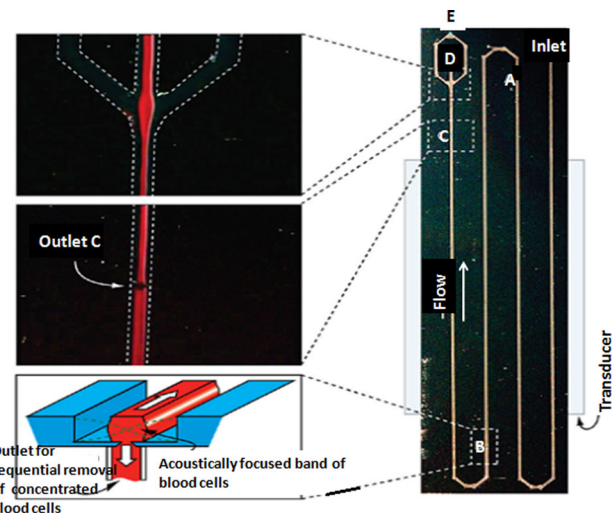
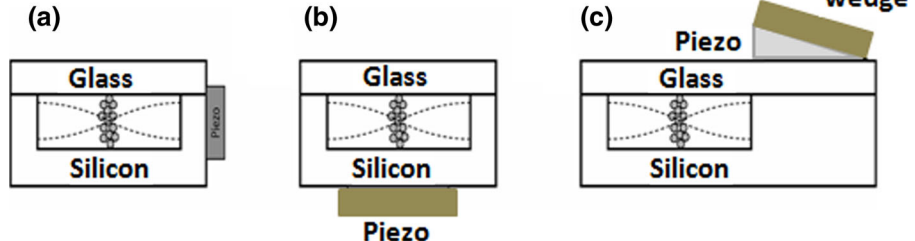


**Fig. 76** Schematic of plasmaphoresis chip (Lenshof et al. 2009)

Free-flow acoustophoresis is a method that combines the laminar flow with axial primary radiation force to sort mixed particles into multiple outlets (Petersson et al. 2007; Guldiken et al. 2012). The primary acoustic force moves the different-sized particles into different positions in the channel, and they are sorted out through different outlets. This method has been used to separate acoustically inseparable particles by manipulating the density of the medium for the fractionation of RBC, platelets and leukocytes. This method can also be used to remove lipid emboli from shed blood recovered during cardiac surgery (Petersson et al. 2004). The device enables sorting of erythrocytes to the central outlet and lipid particles to the two side outlets of the channel. Plasmaphoresis is a continuous separation technique that is widely used for the separation of cells from blood to produce pure plasma. Clogging is one of the major problems in the operation of such devices due to the presence of hematocrit. Using appropriate design, the concentration of hematocrit can be reduced before reaching the exit and thus preventing clogging. As shown in Fig. 76, the blood cells focused at the center by acoustophoresis are removed at three different outlets (A–C) placed in the flow path (Lenshof et al. 2009). The remaining blood cells are

taken through outlet D and pure plasma through E. In this study, the chip is connected to a porous silicon sandwich antibody microarray chip for prostate-specific antigen (PSA) detection test (Lenshof et al. 2009).

As an early stage of separation and sorting, acoustophoresis is usually performed in a single medium (Hammarstrom et al. 2010). Sometimes, these separated particles or cells are required to be diluted in another fluid for flow cytometry. The system is designed to keep the pressure node at the destination fluid, so that the particles with positive CF move to the pressure node in the destination fluid from the source fluid. Similarly, the source and destination fluids are interchanged to particles with negative CF, where particles are concentrated on the pressure antinode. In these cases, two fluid systems are used where particles from one fluid are transmitted to the other fluid. This principle is widely used for the washing of cells and removal of contaminated plasma with clean plasma in blood. Acoustophoresis was demonstrated for switching five different micron-sized polyamide spherical particles from contaminated water to distilled water (Petersson et al. 2005). In medical applications, it is required to wash out the blood plasma from RBC, when the plasma contains high levels of inflammatory, coagulation and complement activation factors or drugs. These contaminants are then washed out before RBC is again returned to the patient. Usually, centrifuging is used for the washing purpose, but in this process, high shear causes damage to the cells and also the process is not continuous. An example of a device used for switching cells from one medium to another using acoustic force is demonstrated in Fig. 77 (Laurell et al. 2007). Contaminated plasma is supplied as sheath fluid through the side inlets, and pure plasma is supplied through the central inlet. When these blood cells pass through the acoustic field, radiation pressure pushes the cells to the

clean plasma, which is taken through the central outlet, while the contaminated medium exits through the side outlets (Laurell et al. 2007). To increase the throughput of this device, an arbitrary number of channels can be used in parallel. When the contaminated medium comes in contact with the clean medium, there is chance of diffusion of contaminants into the clear buffer across the laminar flow borders in microchannel. To reduce this contamination, the time period at which two media come in contact should be reduced. It would be possible by applying high flow rate through the central inlet and side outlets relative to side inlet and central outlet.

A new design for the exchange of buffer using acoustophoresis and hydrodynamic principles has been reported (Harris et al. 2003), which is shown in Fig. 78. Here, a piezoceramic crystal is placed in the initial stage of the main channel, which will prefocus the particles in the buffer by the pressure node created at the center of the channel. Eight outlet channels are provided on the sides to remove the existing waste buffer. Similarly, eight side channels are provided on the main channel to supply the new buffer using syringe pump. After each junction, the concentration of existing buffer is reduced, and the new buffer is introduced but the particles remain at the center of the channel due to the acoustic standing wave. At the exit of the main channel, suspension of particle in a new buffer is collected. In another acoustophoresis method, the separation of WBCs from platelets was demonstrated (Dykes et al. 2011). Usually, lateral resonance acoustophoresis chips are fabricated in silicon by anisotropic wet etching or deep reactive ion etching (DRIE). But, silicon is expensive and the manufacturing process is complicated. Recently, acoustophoresis chips have been fabricated in glass by isotropic etching. At its fundamental resonance mode, both glass and silicon chips show same resonance characteristics, but at higher-order resonance modes, glass chip shows resonance at lower frequency than silicon chip. This chip has been used for the separation of particles, washing of blood sample as well as exchange of medium (Evander et al. 2008). In another method, microchannel having width with one-quarter of wavelength was used (Kapishnikov et al. 2006). Ultrasonic transducers having same frequency of vibration were placed on both sides of the channel. The phase difference between the transducers was adjusted to create pressure node at one wall and pressure antinode at the other wall. Source fluid is supplied near the antinode wall and destination fluid on the other wall. Due to acoustic force, positive CF particles shifted to the destination fluid with pressure node. The method is complicated since it is difficult to control the phase difference between the two transducers and design the thickness of the channel wall and coupling layers. The acoustophoresis method can be extended to two miscible fluid streams (Liu et al. 2012) in

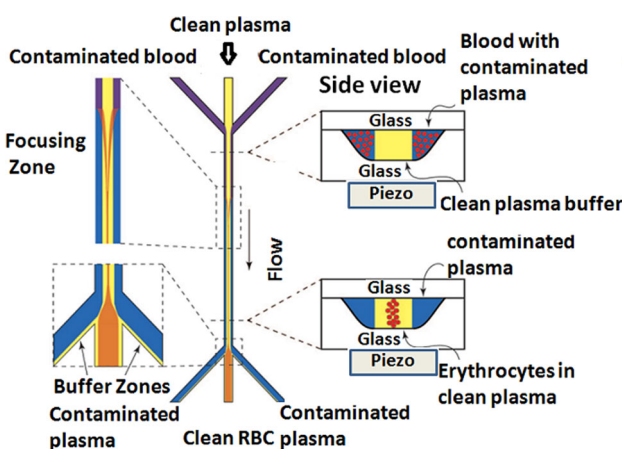
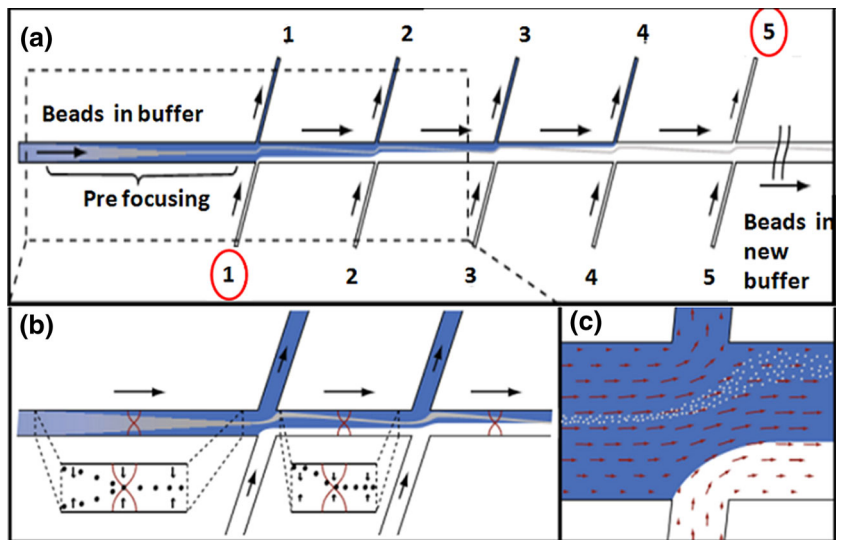


**Fig. 77** Purification of plasma by buffer exchange (Laurell et al. 2007)

**Fig. 78** **a** Buffer exchange chip configured with side channels; **b** magnified view of the pressure node between each junction; **c** flow of two different buffers and particle at the junction (Harris et al. 2003)



which the pressure nodal line is shifted from center because of the difference in compressibility and density of two fluids. A schematic of the arrangement is depicted in Fig. 79. Position of pressure nodal line can be manipulated by adjusting the relative flow rate of the two streams. It was also observed that the diffusion occurring between two miscible fluids has no effect on sorting and separation process.

In order to create dynamic acoustic field, slanted-finger interdigital transducers (SFIT) have been used (Ding et al. 2012), as shown in Fig. 80. SSA waves of different wavelengths are created between a pair of SFIT. When frequency of RF signal is half the tunable range, SAW of maximum amplitude (solid black line) and narrow bandwidth is excited at the center of the SFIT. Excitation of SAW beam can be manipulated to high (dotted red line) and low frequency (dashed blue line) by tuning the RF signal frequency. So, SFIT can be used to control the position of maximum SAW amplitude and its wavelength. Thus, patterned SSA wave can be created. PDMS channel

is placed in between a pair of SFIT deposited on a piezoelectric substrate. SFIT create identical SAW in the y-direction, which are in opposite direction and interface each other to form a superimposed wave. This creates acoustic pressure distribution inside the channel. Pressure nodes are arranged in multiple lines, resulting in a one-dimensional dynamic patterning of particles along these lines. Using this method, different particles can be aligned in different regions by dynamic control of the frequency of input signal by a SFIT arrangement.

Acoustic band-pass particle sorter (ABPS) is another acoustic tunable device for sorting cells and particles based on the size of particles (Adams and Soh 2010), which is shown in Fig. 81. The ABPS consists of three inlets and three outlets arranged into two separation stages. At each stage, relatively smaller particles are rejected out from the main channel, and larger particles are introduced into the next stage which subjected to another set of acoustophoretic zone. The flow rate, voltage and frequency of input can be adjusted to sort particles of any size into the band-pass outlet. In order to increase the throughput of sorting, integrated acoustic-magnetic separation (IAMS) device has been reported (Adams et al. 2009), which is shown in Fig. 82. Here, acoustic and magnetic separators are serially arranged in a single chip. A sample containing acoustic target, magnetic target and nontarget particles is injected into the inlet and is kept close to the wall by buffer solution at the other inlet. Nontarget particles escaped through the waste outlet stream. When the acoustic target and magnetic target particles reach the magnetic zone, magnetic target particles are laterally shifted by the ferromagnetic structure placed in the channel and sorted out through different outlets.  $F_{ac}$ ,  $F_{mag}$  and  $F_{hyd}$ , shown in Fig. 80, represent acoustic force, magnetic force and hydrodynamic force, respectively.

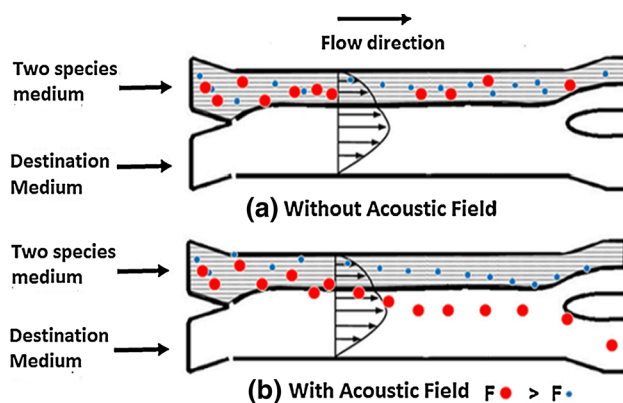


**Fig. 79** Cell separation and transportation between two miscible fluid streams (Liu et al. 2012)

**Fig. 80** Dynamically controlled acoustophoretic field using SFIT (Ding et al. 2012)

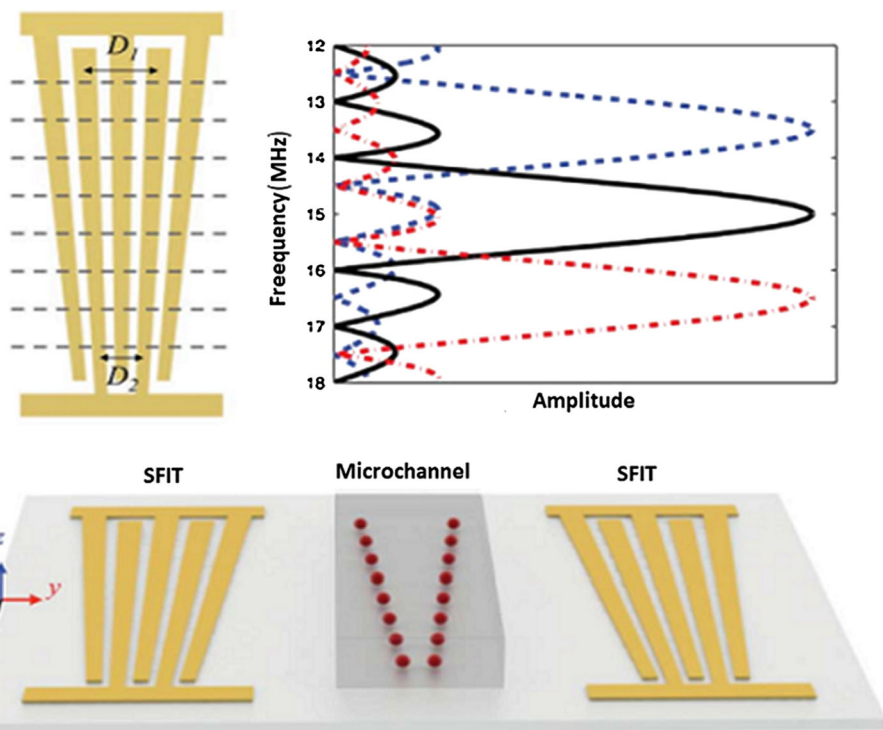


**Fig. 81** Tunable acoustophoretic band-pass filter (Adams and Soh 2010)

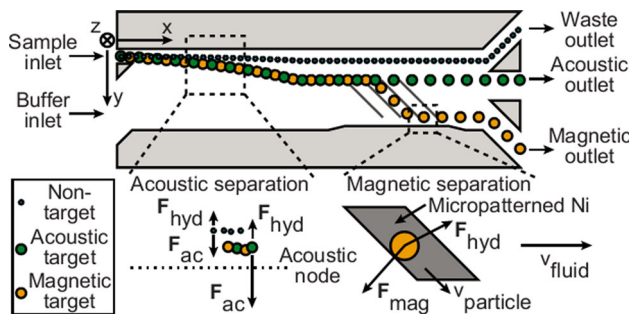
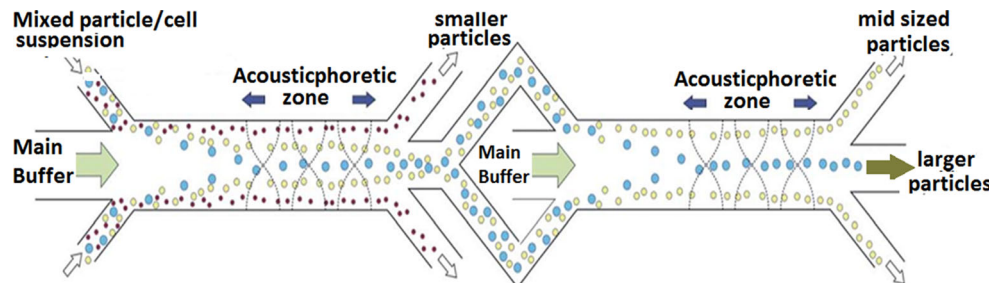


**Fig. 82** Schematic of an integrated acoustic-magnetic separation chip (Adams et al. 2009)

#### 4 Combined techniques

Here, passive separation and sorting techniques that also employ external fields are discussed. In tunable pinched flow fractionation (PFF), shown in Fig. 83, stabilized pressure-driven flow is combined with tunable electro-

osmotic flow (EOF) for tuning the size separation of particles. When the mechanical pressure that is used to drive the sample is equivalent to the electro-osmotically induced pressure, the EOF tuning on the pressure-driven flow becomes significant. In this method, the same pressure is applied on both carrier flow and sample flow, and the voltage applied to the carrier flow is controlled for the tuning of hydrodynamic spreading of different-sized particles. Separation of *E. coli* and yeast cells was achieved using tunable PFF (Wu et al. 2007). In another method, fluid flow is maintained in the channel by electro-osmotic phenomena, and the voltage applied to the electrodes inserted in each inlet (positive electrode) and outlet (negative electrode) can be controlled. Thus, tuning of PFF can be done by adjusting the flow rate in all outlets (Kawamata et al. 2008).

As another modification to PFF, optically enhanced pinched flow fractionation (OEPFF) (Lee et al. 2010) has been reported. After pinching of particles at the sidewall

**Fig. 83** **a** The principle of particle/cell separation using tunable PFF; **b** cell separation demonstrated between yeast cells (larger and brighter ones) and *E. coli* cells (smaller and darker ones), voltage 131 V (Wu et al. 2007)

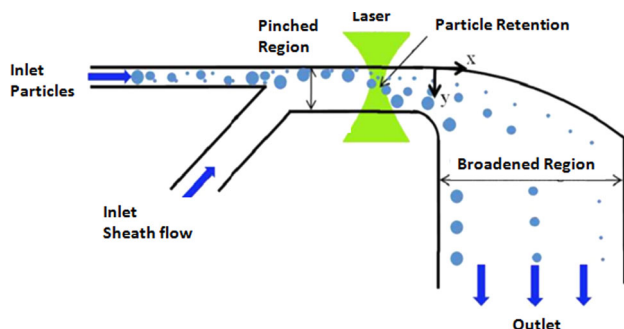
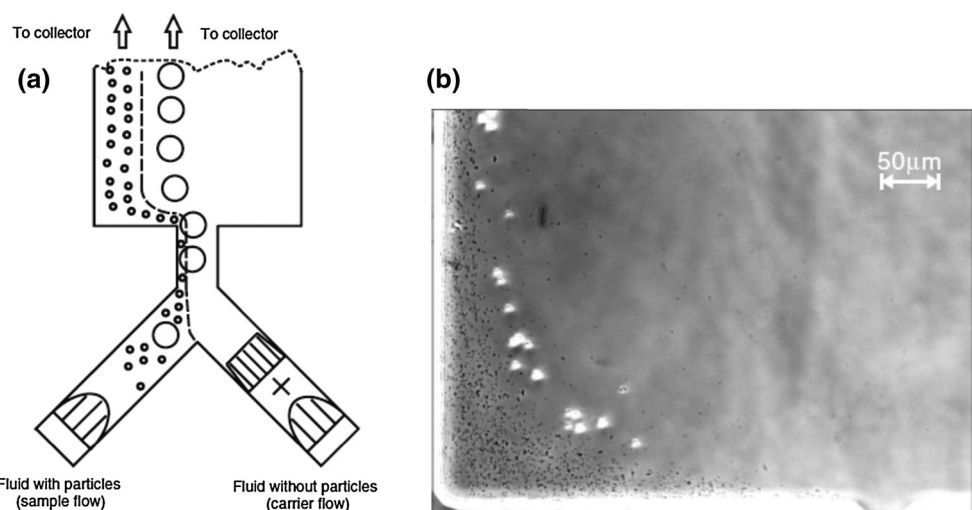


**Fig. 84** Schematic diagram of optically enhanced PFF (Lee et al. 2010)

by the sheath fluid, these particles pass through the region of laser beam exposure. The scattering force pushes the particle in a direction perpendicular to the flow direction of sample as shown in Fig. 84. This displacement is known as the retention distance, which relates to the size of the particle and laser beam parameters. Due to this difference in their retention distance, the effluent position of different size particles at the pinched segment will be amplified. So, at the outlet of the pinched segment, particles follow streamlines that are separated by larger distance. Thus, particles can be easily sorted with improved efficiency. DLD can also be used along with DEP to improve sorting efficiency (Beech et al. 2009), as shown in Fig. 85. Here, electrodes are placed outside the DLD structure, and posts are kept as insulators to produce a nonuniform electric field in the structure. DEP force acting on the larger particles is more than that on the smaller particles. The DEP force and steric force together move the larger particles to the next stream along the displacement mode. This method can be used to separate particles having diameter close to the critical diameter of the structure.

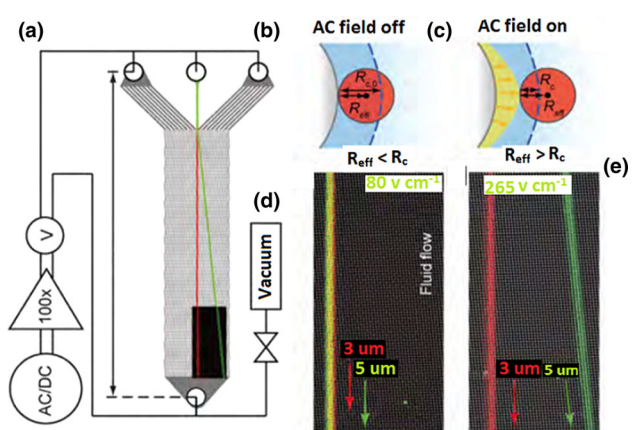


**Fig. 85** **a** Schematic diagram of DLD with DEP; **b** interaction of large particles when no DEP force; **c** additional lateral shift of particle due to DEP force; **d** inefficient separation at low DEP field; **e** improved sorting at high DEP field for sorting 3- and 5-μm particles (Beech et al. 2009)

## 5 Comparison of separation and sorting techniques

The major advantage of pinched flow fractionation (PFF) technique is the simplicity of the device, but it requires an additional particle-free sheath fluid for focusing of the sample containing particles to be sorted. This method is suitable for low  $Re$  flows ( $Re \leq 1$ ) and may not be applicable to high  $Re$  flows ( $Re \gg 1$ ) where there may be formation of vortices after the pinched segment. Particles with diameters of the order of the sidewall roughness or less cannot be separated using pinched flow fractionation method (Jain and Posner 2008). The inertial and dean flow technique is applicable to higher  $Re$  flow and relies on balance between the inertial shear-gradient-induced lift force and wall-effect-induced lift force. In this method, the dean number ( $De$ ) should be maintained less than 20 to avoid entrainment of the particles in the dean vortices

(Chatterjee 2011). To achieve the equilibrium position stability that is required for the separation of particles, the channel Reynolds number ( $R_c$ ) in the range 10–270 (Pamme 2007; Carlo et al. 2009; Gossett and Carlo 2009a), particle Reynolds number in the range 0.05–5.0 (Russom et al. 2009; Wu et al. 2009) and the Stokes number ( $S_t$ ) in the range 9–64 (Wu et al. 2009) have been used. The inertial and dean flow method requires curved channels or flow structure that facilitates movement of particles following a curved path. Deterministic lateral displacement (DLD) is a steric method of continuous separation that makes use of asymmetric bifurcation of laminar flow around obstacles (Huang et al. 2004). The advantage of the DLD method is that it is applicable to sorting of both rigid and deformable particles, circular and noncircular particles. DLD is also capable of sorting of cells based on biological contents present inside. However, this technique employs an array of posts in a microchannel for which the fabrication may be challenging. According to ‘Zweifach–Fung effect,’ particle at a bifurcation point has a tendency to follow the high flow rate channel (Yang et al. 2006). This method is applicable to deformable particles, and sorting based on size and deformability is possible. The structure of the device is simple and thus easy to fabricate. Microfiltration method requires complicated fabrication procedure to assemble the device with filters or to include embedded filter structures within the device. The size-based separation requires the appropriate pore size so a device with a fixed filter pore size is only applicable to sorting of specific sizes of particles. Hydrodynamic filtration is similar to cross-flow filtration, but they are based on different principles. In cross-flow filtration, only carrier fluid is collected through the side channels, but in hydrodynamic filtration, the particles are also collected through the side channels. Hydrodynamic filtration cannot be used for the separation of a mixture of particles having size smaller than the virtual channel width. The micro-hydrocyclone device can be applied to the separation of particles at high flow rates (~mL/min), but fabrication of the device is very challenging.

As opposed to the passive separation and sorting techniques, the active techniques employ an external field and many times require more involved fabrication procedures (e.g., to integrate electrodes on chip). However, the active separation and sorting methods offer higher separation efficiency and throughput. The DEP method is applicable to charge neutral dielectric particles having different dielectric constants than that of the medium present in a nonuniform external electric field. Particles having same dielectric constants and/or sizes cannot be sorted using DEP method. The magnetic separation and sorting method is applicable to particles that are magnetizable and employs

a nonuniform magnetic field. Also, the magnetic permeability of the particles should be different from the permeability of vacuum. The magnetic separation and sorting technique offers several advantages, including high specificity, less chance of cell damage and only shorter sorting time. The particle separation and sorting based on optical methods utilizes scattering of light that produces a change in momentum of the photons present in the light beam. The light beam has Gaussian intensity profile with maximum value at the center, and if the refractive index of the particle is less than that of the medium, the particle is attracted toward the center. The force exerted on the particles in optical separation technique is smaller compared to that in case of DEP and magnetic methods. Additionally, the optical separation method requires a complicated experimental setup. The acoustic separation method exploits the difference in the density of the particle and medium and speed of sound in the particle and the medium. The acoustophoretic force depends on the particle size; thus, size-based separation is possible using this method. Also, particles having different signs of contrast factor (CF) can be separated due to their movement toward pressure nodes and antinodes.

## 6 Conclusions

In this paper, an extensive review of various passive and active separation techniques is discussed. Both passive and active techniques have their distinctive advantages. Passive separation and sorting devices have simpler structure and do not employ external fields for the operation. However, the footprint of the devices is relatively large, requiring long and complicated microchannel structures. The flow rate involved in passive separation devices is relatively lower for which the process becomes relatively more time-consuming. The active separation techniques use various forms of external fields to generate external force to manipulate and separate particles with relatively better performance compared to passive techniques. Selection of an appropriate separation and sorting technique would depend on the particular application. The devices reported in this review paper have been used for the separation of a wide range of microparticles including cells and pathogens for various applications. The performance of these devices was characterized in terms of throughput and sorting efficiency. Future microfluidics applications would necessitate development of suitable separation and sorting devices that would require simple and low-cost fabrication techniques, provide ease of operation and handling and offer high throughput and separation efficiency with lower energy input.

## References

- Abkarian M, Viallat A (2005) Dynamics of vesicles in a wall-bounded shear flow. *Biophys J* 89:1055–1066
- Adams JD, Soh HT (2010) Tunable acoustophoretic band-pass particle sorter. *Appl Phys Lett* 97:064103
- Adams JD, Kim U, Soh HT (2008) Multi target magnetic activated cell sorter. *Natl Acad Sci PNAS* 105(47):18165–18170
- Adams JD, Thevoz P, Bruus H, Soh HT (2009) Integrated acoustic and magnetic separation in microfluidic channels. *Appl Phys Lett* 95:254103
- Alshareef M, Metrakos N, Perez EJ, Azer F, Yang F, Yang X, Wang G (2011) Separation of tumor cells with dielectrophoresis-based microfluidic chip, Southeast biomedical engineering career conference-Herndon, October 28, 2011
- Aran K, Fok A, Sasso LA, Kamdar N, Gua Y, Su Q, Undar A, Zahn JD (2011) Microfiltration platform for continuous blood plasma protein extraction from whole blood during cardiac surgery. *Lab Chip* 11:2858–2868
- Arnold TJ, Hart SJ (2005) Enhanced optical chromatography in a PDMS microfluidic system. *Opt Express* 13(25):10406–104016
- Ashkin A (1997) Optical trapping and manipulation of neutral particles using lasers. *Proc Natl Acad Sci USA* 94:4853–4860
- Ashkin A, Dziedzic JM, Bjorkholm JE, Chu S (1986) Observation of a single-beam gradient force optical trap for dielectric particles. *Opt Lett* 11:288–290
- Ashok PC, Marchington RF, Mthunzi P, Krauss TF, Dholakia K (2010) Optical chromatography using a photonic crystal fiber with on-chip fluorescence excitation. *Opt Express* 18(6): 6396–6408
- Asmolov ES (1999) The inertial lift on a spherical particle in a plane Poiseuille flow at large channel Reynolds number. *J Fluid Mech* 381:63–87
- Balvin M, Sohn E, Iracki T, Drazer G, Frechette J (2009) Directional locking and the role of irreversible interactions in deterministic hydrodynamics separations in microfluidic devices. *Phys Rev Lett* 103:078301
- Becker FF, Wang XB, Huang Y, Pethigt R, Vykoukal J, Gascoyne PRC (1995) Separation of human breast cancer cells from blood by differential dielectric affinity. *Proc Natl Acad Sci* 92:860–864
- Becker FF, Gascoyne PRC, Huang Y, Wang XB, Yang J (2001) Method and apparatus for fractionation using conventional dielectrophoresis and field flow fractionation, WO 01/1487
- Beech JP (2011) Micro fluidics separation and analysis of biological particles. PhD thesis, Lund University
- Beech JP, Tegenfeldt JO (2008) Tunable separation in elastomeric micro fluidics devices. *Lab Chip* 8:657–659
- Beech JP, Jonsson P, Tegenfeldt JO (2009) Tipping the balance of deterministic lateral displacement devices using dielectrophoresis. *Lab Chip* 9(18):2698–2706
- Beech JB, Holm SH, Adolfsson K, Tegenfeldt JO (2012) Sorting cells by size, shape and deformability. *Lab Chip* 12(6): 1048–1051
- Bhagat AAS, Kuntaegowdanahalli SS, Papautsky I (2008a) Enhanced particle filtration in straight microchannels using shear-modulated inertial migration. *Phys Fluids* 20(101702):1–4
- Bhagat AAS, Kuntaegowdanahalli SS, Papautsky I (2008b) Continuous particle separation in spiral microchannels using dean flows and differential migration. *Lab Chip* 8(11):1906–1914
- Bhagat AAS, Bow H, Hou HW, Tan SJ, Han J, Lim CT (2010) Microfluidics for cell separation. *Med Biol Eng Compu* 48:999–1014
- Bhardwaj P, Bagdi P, Sen AK (2011) Microfluidic device based on a micro-hydrocyclone for particle-liquid separation. *Lab Chip* 11(23):4012–4021
- Bowman T, Frechette J, Drazer G (2012) Force driven separation of drops by deterministic lateral displacement. *Lab Chip* 12:2903–2908
- Brody JP, Osborn TD, Forster FK, Yager P (1996) A planar microfabricated fluid filter. *Sens Actuators A* 54:704–708
- Brunet E, Degre G, Okkels F, Tabeling P (2005) Aggregation of paramagnetic particles in the presence of a hydrodynamic shear. *J Colloid Interface Sci* 282:58–68
- Bruus H (2009) Theoretical microfluidics. Oxford University Press, ISBN 9780199235094
- Caldwell KD, Cheng ZQ, Hradecky P, Giddings JC (1984) Separation of human and animal cells by steric field-flow fractionation. *Cell Biochem Biophys* 6:233–251
- Carlo DD, Irimia D, Tompkins RG, Toner M (2007) Continuous inertial focusing, ordering, and separation of particles in microchannels. *Proc Natl Acad Sci* 104(48):18892–18897
- Carlo DD, Edd JF, Irimia D, Tompkins RG, Toner M (2008) Equilibrium separation and filtration of particles, using differential inertial focusing. *Anal Chem* 80:2204–2211
- Carlo DD, Edd JF, Humphry KJ, Stone HA, Toner M (2009) Particle segregation and dynamics in confined flows. *Phys Rev Lett* 102(9):094503–094504
- Chan P, Leal L (1979) The motion of a deformable drop in a second-order fluid. *J Fluid Mech* 92:131–170
- Chatterjee A (2011) Size-dependant separation of multiple particles in spiral microchannels, Phd thesis, University of Cincinnati
- Chen X, Cui D, Liu C, Li H, Chen J (2007) Continuous Flow Microfluidic Device for Cell Separation, Cell Lysis and DNA Purification. *Anal Chim Acta* 84:2
- Chen X, Cui DF, Liu CC, Li H (2008) Microfluidic chip for blood cell separation and collection based on crossflow filtration. *Sens Actuators B Chem* 130(1):216–221
- Cheng I-F, Froude VE, Zhu Y, Chang H-C (2009) A continuous high-throughput bio particle sorter based on 3D traveling-wave dielectrophoresis. *Lab Chip* 9:3193–3201
- Chronis N, Lam W, Lee L (2001) In: Ramsey JM, van den Berg A (eds) Micro total analysis system. Kluwer Academic, Monterey, p 497
- Church C, Zhu J, Nieto J, Keten G, Ibarra E, Xuan X (2010) Continuous particle separation in a serpentine microchannel via negative and positive dielectrophoretic focusing. *J Micromech Microeng* 20:065011–065017
- Cranston HA, Boylan CW, Caroll GL, Sutera SP, Williamson JR, Gluzman IY, Krogstad DJ (1984) Plasmodium falciparum maturation abolishes physiologic red cell deformability. *Science* 223(4634):400–403
- Crowley TA, Pizziconi V (2005) Isolation of plasma from whole blood using planar microfilters for lab-on-a-chip applications. *Lab Chip* 5:922–929
- Cui L, Holmes D, Morgan H (1994) The dielectrophoretic levitation and separation of latex beads in microchips, 22(18), pp. 3893–3901, October 2001, *J Phys D Appl Phys*, 27, 1571–1574
- Cummings EB, Singh AK (2003) Dielectrophoresis in microchips containing arrays of insulating posts: theoretical and experimental. *Anal Chem* 75:4724–4731
- Davis JA (2008) Micro fluidic separation of blood components through deterministic lateral displacement. PhD thesis, Princeton University
- Davis JA, Inglis DW, Morton KJ, Lawrence DA, Huang LR, Chou SY, Stur JC, Austin RH (2006) Deterministic hydrodynamics: taking blood apart. *PNAS* 103(40):14779–14784
- Demierre N, Braschler T, Muller R, Renaud P (2008) Focusing and continuous separation of cells in an micro fluidic device using lateral dielectrophoresis. *Sens Actuators B* 132:388–396

- Devendra R, Drazer G (2012) Gravity driven deterministic lateral displacement for particle separation in micro fluidic devices. *Anal Chem* 84:10621–10627
- Dholakia K, Cizmar T (2011) Shaping the future of manipulation. *Nat Photonics* 5:335–342
- Dholakia K, Lee WM, Paterson L, MacDonald MP, McDonald R, Andreev I, Mthunzi P, Brown CTA, Marchington RF, Riches AC (2007) Optical separation of cells on potential energy landscapes: enhancement with dielectric tagging. *IEEE J Sel Top Quantum Electron* 13(6):1646–1654
- Ding X, Shi J, Lin S-CS, Yazdi S, Kiraly B, Huang TJ (2012) Tunable patterning of microparticles and cells using standing surface acoustic waves, The Royal Society of Chemistry, Lab chip
- Doddabasavanna GB, PadmaPriya K, Nagabhushana K (2012) A review of recent advances in separation and detection of whole blood components. *World J Sci Technol* 2(5):05–09
- Doddi SK, Bagchi P (2008) Lateral migration of a capsule in a plane Poiseuille flow in a channel. *Int J Multiph Flow* 34:966–986
- Doh II, Cho Y-H (2005) A continuous cell separation chip using hydrodynamic dielectrophoresis (DEP) process. *Sens Actuators A* 121:59–65
- Dong Y, Skelley AM, Merdek KD, Sprott KM, Jiang C, Pierceall WE, Lin J, Stocum M, Carney WP, Smirnov DA (2013) Microfluidics and circulating tumor cells-review article. *J Mol Diagn* 15(2):149–157
- Dykes J, Lenshof A, Astrand-Grundstrom I-B, Laurell T, Scheding S (2011) Progenitor cell products using a novel micro-chip based acoustophoretic platform. *PLoS ONE* 6:8
- Evander M, Lenshof A, Laurell T, Nilsson J (2008) Acoustophoresis in wet-etched glass chips. *Anal Chem* 80:5178–5185
- Fahraeus R (1929) The suspension stability of the blood. *Physiol Rev* 2:241–274
- Faivre M, Abkarian M, Bickraj K, Stone HA (2005) Geometrical focusing of cells in a microfluidic device: an approach to separate blood plasma. *Lab Chip* 5(7):778–784
- Faivre M, Abkarian M, Bickraj K, Stone HA (2006) Geometrical focusing of cells in a microfluidic device: an approach to separate blood plasma. *J Biorheol* 43(2):147–159
- Frechette J, Drazer G (2009) Directional locking and deterministic separation in periodic arrays. *J Fluid Mech* 627:379–401
- Gagnon ZR (2011) Cellular dielectrophoresis: applications to the characterization, manipulation, separation and patterning of cell. *Electrophoresis* 32(18):2466–2487
- Gascoyne PRC, Vykovkal J (2002) Particle separation by dielectrophoresis. *Electrophoresis* 23(13):1973–1983
- Gascoyne PRC, Wang XB, Huang Y, Becker FF (1997) Dielectrophoretic separation of cancer cells from blood. *IEEE Trans Ind Appl* 33(3):670–678
- Geng Z, Zhang L, Ju Y, Wang W, Li Z (2011) A plasma separation device based on centrifugal effect and Zweifach-Fung effect. In: 15th international conference on miniaturized systems for chemistry and life sciences, Seattle, Washington, USA
- Ghasemi M, Holm SH, Beech JP, Bjornmalm M, Tegenfeldt JO (2012) Separation of deformable hydrogel micro particles in deterministic lateral displacement devices. In: 16th International conference on miniaturized systems for chemistry and life sciences, Okinawa, Japan
- Giddings JC (1973) The conceptual basis of field-flow fractionation. *J Chem Educ* 50:667–669
- Giddings JC (1983) Hyperlayer field-flow fractionation. *Sep Sci Technol* 18:765–773
- Gijs MAM (2004) Magnetic bead handling on-chip: new opportunities for analytical applications. *Microfluid Nanofluid* 1(1):22–40
- Gluckstad J (2004) Microfluidics: sorting particles with light. *Nat Mater* 3:9–10
- Gooneratne CP, Kosel J (2012) A micro-pillar array to trap magnetic beads in microfluidic systems. In: Sixth international conference on sensing technology (ICST)
- Gossett DR, Carlo DD (2009a) Particle focusing mechanisms in curving confined flows. *Anal Chem* 81:8459–8465
- Gossett DR, Carlo DD (2009b) Particle focusing mechanisms in curving confined flows. *Anal Chem* 81(20):8459–8465
- Gossett DR, Weaver WM, Mach AJ, Hur SC, Tse HTK, Lee W, Amini H, Carlo DD (2010a) Label-free cell separation and sorting in microfluidic systems. *Anal Bioanal Chem* 397:3249–3267
- Gossett DR, Weaver WM, Mach AJ, Hur SC, Tse HTK, Lee W, Amini H, Carlo DD (2010b) Label-free cell separation and sorting in microfluidic systems. *Anal Bioanal Chem* 397(8):3249–3267
- Guldiken R, Jo MC, Gallant ND, Demirci U, Zhe J (2012) Sheathless size-based acoustic particle separation. *Sensors* 12:905–922
- Gupta S, Feke DL, Manas-Zloczower I (1995) Fractionation of mixed particulate solids according to compressibility using ultrasonic standing wave fields. *Chem Eng Sci* 50:3275–3284
- Hammarstrom B, Evander M, Barbeau H, Bruzelius M, Larsson J, Laurell T, Nilsson J (2010) Non-contact acoustic cell trapping in disposable glass capillaries. *Lab Chip* 10:2251–2257
- Han K, Frazier A (2005) Microfluidic system for continuous magnetophoresis separation of suspended cells using their native magnetic properties. *Proc Nanotech* pp 187–190
- Han K-H, Han A, Frazier AB (2006) Microsystems for isolation and electrophysiological analysis of breast cancer cells from blood. *Biosens Bioelectron* 21:1907–1914
- Harris NR, Hill M, Beeby S, Shen Y, White NM, Hawkes JJ, Coakley WT (2003) A silicon micro fluidic ultrasonic separator. *Sens Actuators B* 95:425–434
- Hart SJ, Terray A (2003) Refractive-index-driven separation of colloidal polymer particles using optical chromatography. *Appl Phys Lett* 83:25
- Hart SJ, Terray A, Arnold J, Leski TA (2008) Preparative optical chromatography with external collection and analysis. *Optical Express* 16(23):18782–18789
- Hartig R, Hausmann M, Cremer C (1995) In continuous focusing of biological particles by continuous immuno magnetic sorter: technique and applications. *Electrophoresis* 16:789–792
- Heller C (2001) Principles of DNA separation with capillary electrophoresis. *Electrophoresis* 22(4):629–643
- Herrmann J, Karweit M, Drazer G (2009) Separation of suspended particles in microfluidic systems by directional locking in periodic fields. *Phys Rev E Stat Nonlin Soft Matter Phys* 79(6):061404
- Holm S, Beech JP, Barrett MP, Tegenfeldt JO (2011) Separation of parasites from human blood using deterministic lateral displacement. *Lab Chip* 11:1326–1332
- Holmes D, Morgan H (2002) Cell positioning and sorting using dielectrophoresis. *Eur Cells Mater* 4(2):120–122
- Hou HW, Gan HY, Bhagat AAS, Li LD, Lim CT, Han J (2012) A microfluidics approach towards high-throughput pathogen removal from blood using margination. *Biomicrofluidics* 6:024115
- Hsu C-H, Carlo DD, Chen C, Irimia D, Toner M (2008) Microvortex for focusing, guiding and sorting of particles. *Lab Chip* 8:2128–2134
- Hu X, Bessette PH, Qian J, Meinhart CD, Daugherty PS, Soh HT (2005) Marker-specific sorting of rare cells using dielectrophoresis. *Proc Natl Acad Sci* 102(44):15757–15761
- Huang Y, Wang XB, Becker FF, Gascoyne PRC (1998) Separation of polystyrene microbeads using dielectrophoretic gravitational field-flow-fractionation. *Biophys J* 74:2689–2701

- Huang LR, Cox EC, Austin RH, Sturm JC (2004) Continuous particle separation through deterministic lateral displacement. *Science* 304(5673):987–990
- Huang S-B, Chen J, Wang J, Yang C-L, Wu M-H (2012) A new optically-induced dielectrophoretic (ODEP) force-based scheme for effective cell sorting. *Int J Electrochem Sci* 7:12656–12667
- Hur SC, Henderson-MacLennan NK, McCabe ERB, Carlo DD (2011) Deformability-based cell classification and enrichment using inertial microfluidics. *Lab Chip* 11:912
- Hyun K-A, Kim S-I, Kim Y-S, Han H, Jung H-I (2012) Continuous separation of circulating tumor cells from blood samples using a newly developed multi orifice flow fractionation (MOFF) chip. In: 6th international conference on miniaturized systems for chemistry and life sciences, Okinawa, Japan
- Imasaka T, Kawabata Y, Kaneta T, Ishidzu Y (1995) Optical chromatography. *Anal Chem* 67:1763–1765
- Inglis DW, Riehn R, Austin RH, Sturm JC (2004) Continuous micro fluidic immunomagnetic cell separation. *Appl Phys Lett* 85(21):5093–5095
- Inglis DW, Davis JA, Austin RH, Sturm JC (2006) Critical particle size for fractionation by deterministic lateral displacement. *Lab Chip* 6:655–658
- Inglis DW, Herman N, Vesey G (2010) Highly accurate deterministic lateral displacement device and its application to purification of fungal spores. *Biomicrofluidics* 4:024109
- Inglis DW, Lord M, Nordon RE (2011) Scaling deterministic lateral displacement arrays for high throughput and dilution-free enrichment of leukocytes. *J Micromech Microeng* 21(054024): 1–8
- Jain A, Posner JD (2008) Particle dispersion and separation resolution of pinched flow fractionation. *Anal Chem* 80(5):1641–1648
- Ji HM, Samper V, Chen Y, Heng CK, Lim TM, Yobas L (2008) Silicon-based microfilters for whole blood cell separation. *Biomed Microdevices* 10(2):251–257
- Joensson HN, Uhlen M, Svahn HA (2010) Deterministic lateral displacement device for droplet separation by size: towards rapid clonal selection based on droplet shrinking. In: 14th International conference on miniaturized systems for chemistry and life sciences, Groningen, The Netherlands
- Joensson HN, Uhlen M, Svahn HA (2011) Droplet size based separation by deterministic lateral displacement: separating droplets by cell-induced shrinking. *Lab Chip* 11:1305–1310
- Kaneta T, Ishidzu Y, Mishima N, Imasaka T (1997a) Theory of optical chromatography. *Anal Chem* 69(14):2701–2710
- Kaneta T, Ishidzu Y, Mishima N, Imasaka T (1997b) Theory of optical chromatography. *Anal Chem* 69:2701–2710
- Kapishnikov S, Kantsler V, Steinberg V (2006) Continuous particle size separation and size sorting using ultrasound in a micro channel. *J Stat Mech: Theory Exp* P01012
- Kawamata T, Yamada M, Yasuda M, Seki M (2008) Continuous and precise particle separation by electro-osmotic flow control in microfluidic device. *Electrophoresis* 29:1423–1430
- Kersaudy-Kerhoas M, Dhariwal R, Desmulliez MPY (2008) Recent advances in microparticle continuous separation. *IET Nanobiotechnol* 2(1):1–13
- Kersaudy-Kerhoas M, Kavanagh DM, Dhariwal RS, Campbell CJ, Desmulliez MPY (2010a) Validation of a blood plasma separation system by biomarker detection, lab on chip, pp 1587–1595
- Kersaudy-Kerhoas M, Dhariwal R, Desmulliez MPY, Jouvet L (2010b) Hydrodynamic blood plasma separation in microfluidic channels. *J Microfluid Nanofluid* 8(1):105–114
- Kim SB, Kim JH, Kim SS (2006) Theoretical development of in situ optical particle separator: cross-type optical chromatography. *Appl Opt* 45(27):6919–6924
- Kim U, Qian J, Kenrick SK, Daugherty PS, Soh HT (2008) Multi target dielectrophoresis activated cell sorter. *Anal Chem* 80:8656–8661
- Kim J, Massoudi M, Antaki JF, Gandini A (2012) Removal of malaria-infected red blood cells using magnetic cell separators: a computational study. *Appl Math Comput* 218:6841–6850
- Knight JC, Birks TA, Cregan RF, St P, Russell J, De Sandro J-P (1998) Large mode area photonic crystal fibre. *Electron Lett* 34(13):1347–1348
- Kuberka V, Czekaj P, Davis R (1998) Flux enhancement for membrane filtration of bacterial suspensions using high-frequency backpulsing. *Biotechnol Bioeng* 60(1):77–87
- Kuntaegowdanahalli SS, Bhagat AAS, Kumar G, Papautsky I (2009) Inertial microfluidics for continuous particle separation in spiral microchannels. *Lab Chip* 9:2973–2980
- Kwon K, Sim T, Moon H-S, Lee J-G, Park JC, Jung H-I (2010) A novel particle separation method using multi-stage multi-orifice flow fractionation (MS-MOFF). In: 14th International conference on miniaturized systems for chemistry and life sciences, Groningen, The Netherland
- Ladavac K, Kasza K, Grier DG (2004) Sorting mesoscopic objects with periodic potential landscapes: optical fractionation. *Phys Rev E* 70:010901(R)
- Laurell T, Petersson F, Nilsson A (2006) Chip integrated strategies for acoustic separation and manipulation of cells and particles. *Chem Soc Rev* 36:492–506
- Laurell T, Petersson F, Nilsson A (2007) Chip integrated strategies for acoustic separation and manipulation of cells and particles. *Annual Chem Soc Rev* 36:492–506
- Leal L (1980) Particle motions in a viscous fluid. *Annu Rev Fluid Mech* 12:435–476
- Lee MP, Padgett MJ (2012) Optical tweezers: a light touch. *J Microsc* 248:219–222
- Lee H, Purdon AM, Westervelt RM (2004) Manipulation of biological cells using a microelectromagnet matrix. *Appl Phys Lett* 85(6):1063–1065
- Lee G-B, Lin Y-H, Lin W-Y, Wang W, Guo T-F (2009) Optically-induced dielectrophoresis using polymer materials for biomedical applications, *Transducers 2009*, Denver, CO
- Lee KH, Kim SB, Lee KS, Sung HJ (2010) Adjustable particle separation in pinched flow fractionation with optical force, ISFV14–14th international symposium on flow visualization, Daegu, Korea
- Lee WC, Bhagat AAS, Huang S, Vliet KJV, Han J, Lim CT (2011a) High-throughput cell cycle synchronization using inertial forces in spiral microchannels. *Lab Chip* 11:1359
- Lee MG, Choi S, Park JK (2011b) Inertial separation in a contraction-expansion array micro channel. *J Chromatogr A* 1218(27): 4138–4143
- Lee MG, Choi S, Kim H-J, Lim HK, Kim J-H, Huh N, Park J-K (2011c) High-yield blood plasma separation by modulating inertial migration in a contraction-expansion array microchannel. *Transducers'11*, Beijing, China
- Lee MG, Choi S, Kim H-J, Lim HK, Kim J-H, Huh N, Park J-K (2011d) Inertial blood plasma separation in a contraction-expansion array microchannel. *Appl Phys Lett* 98:253702
- Lee H, Xu L, Ahn B, Lee K, Oh KW (2012) Continuous-flow in-droplet magnetic particle separation in a droplet-based microfluidic platform. *J Microfluid Nanofluid* 13:613–623
- Lei H, Zhang Y, Li B (2012) Particle separation in fluidic flow by optical fiber. *Opt Express* 20(2):1292–1300
- Lenshof A, Laurell T (2010) Continuous separation of cells and particles in microfluidic systems. *Chem Soc Rev* 39:1203–1217
- Lenshof A, Ahmad-Tajudin A, Jaras K, Sward-Nilsson A-M, Aberg L, Marko-Varga G, Malm J, Lilja H, Laurell T (2009) Acoustic

- whole blood plasmapheresis chip for prostate specific antigen microarray diagnostics. *Anal Chem* 81:6030–6037
- Lenshof A, Magnusson C, Laurell T (2012) Acoustofluidics 8: applications of acoustophoresis in continuous flow microsystems. *Lab Chip* 12:1210
- Leu TS, Weng CY (2009) Dynamics of dielectrophoretic field-flow fractionation(Dep-FFF) based micro sorter for cell separation. *Mod Phys Lett B* 23(3):389–392
- Liesfeld B, Nambiar R, Meiners JC (2003) Particle transport in asymmetric scanning-line optical tweezers. *Phys Rev E* 68:051907
- Lil M, Li S, Cao W, Li W, Wen W, Alici G (2012) Continuous particle focusing in a waved microchannel using negative dc dielectrophoresis. *J Micromech Microeng* 22:095001–095009
- Lin Y-H, Lee G-B (2008) Optically induced flow cytometry for continuous microparticle counting and sorting. *Biosens Bioelectron* 24:572–578
- Lin Y-H, Lee G-B (2009) Optically-induced flow cytometry for continuous microparticle counting and sorting. *Res Exp* 11(4):1–3
- Lin S-J, Hung S-H, Jeng J-Y, Guo T-F, Lee G-B (2012) Manipulation of micro-particles by flexible polymer-based optically-induced dielectrophoretic devices. *Opt Express* 20(1):583–592
- Link DR, Grasland-Mongrain E, Duri A, Sarrazin F, Cheng Z, Cristobal G, Marquez M, Witz DA (2006) Electric control of droplets in microfluidic devices. *Angew Chem* 118(16): 2618–2622
- Liu Y, Lim KM (2011) Particle separation in microfluidics using a switching ultrasonic field. *Lab Chip* 11:3167–3173
- Liu C, Lagae L, Wirix-Speetjens R, Borghs G (2007a) On-chip separation of magnetic particles with different magnetophoretic mobilities. *J Appl Phys* 101(024913):1–4
- Liu C, Lagae L, Borghs G (2007b) Manipulation of magnetic particles on chip by magnetophoretic actuation and dielectrophoretic levitation. *Appl Phys Lett* 90:184109
- Liu Y, Hartono D, Lim K-M (2012) Cell separation and transportation between two miscible fluid streams using ultrasound. *Biomicrofluidics* 6:012802
- Lo M, Zahn JD (2012) Development of a multi-compartment microfiltration device for particle fractionation, 16th international conference on miniaturized systems for chemistry and life sciences, Okinawa, Japan
- Long BR, Heller M, Beech JP, Link H, Bruus H, Tegenfeldt JO (2008) Multi-directional sorting modes in deterministic lateral displacement devices. *Physical Review E: Statistical, Nonlinear and Soft Matter Physics* 78, 4, 2, 046304
- Loutherback K, Chou KS, Newman J, Puchall J, Austin RH, Sturm JC (2010) Improved performance of deterministic lateral displacement arrays with triangular posts. *Microfluid Nanofluid* 9:1143–1149
- Loutherback K, D'Silva J, Liu L, Wu A, Austin RH (2012) Deterministic separation of cancer cells from blood at 10 mL/min. *Am Inst Phys Adv* 2:042107
- Lubbersen YS, Schuttyse MAI, Boom RM (2012) Suspension separation with deterministic ratchets at moderate Reynolds numbers. *Chem Eng Sci* 73:314–320
- Lubbersen YS, Dijkshoorn JP, Schuttyser MAI, Boom RM (2013) Visualization of inertial flow in deterministic ratchets. *Sep Purif Technol* 109:33–39
- Ma B, Yao B, Peng F, Yan S, Lei M, Rupp R (2012) Optical sorting of particles by dual-channel line optical tweezers. *J Opt* 14:105702–105707
- MacDonald MP, Spalding GC, Dholakia K (2003) Microfluidic sorting in an optical lattice. *Lett Nat* 426(27):421–424
- Maenaka H, Yamada M, Yasuda M, Seki M (2008) Continuous and size-dependent sorting of emulsion droplets using hydrodynamics in pinched microchannels. *Langmuir* 24:4405–4410
- Magnaudet J, Takagi S, Legendre D (2003) Drag, deformation and lateral migration of a buoyant drop moving near a wall. *J Fluid Mech* 476:115–157
- Manz A, Harrison D, Verpoorte EMJ, Fettinger JC, Paulus A, Ludi H, Widmer HM (1992) Planar chips technology for miniaturization and integration of separation techniques into monitoring systems - capillary electrophoresis on a chip. *J Chromatogr* 593:253–258
- McGloin D (2006) Optical tweezers: 20 years on. *Philos Trans R Soc A* 364:3521–3537
- Mielnik MM, Ekpatpure RP, Saetran LR, Schonfeld F (2005) Sinusoidal cross flow microfiltration device- experimental and computational flow field analysis. *Lab Chip* 5(8):897–903
- Miltenyi S, Muller W, Weichel W, Radbruch A (1990) High gradient magnetic cell separation with MACS. *Cytometry* 11:231–238
- Monjushiro H, Hirai A, Watarai H (2000) Size dependence of laser-photophoretic efficiency of polystyrene microparticles in water. *Langmuir* 16(22):8539–8542
- Monjushiro H, Takeuchi K, Watarai H (2002) Anomalous laser photophoretic behavior of photo-absorbing organic droplets in water. *Chem Lett* 31:788–789
- Moorthy J, Beebe DJ (2003) In situ fabricated porous filters for Microsystems. *Lab Chip* 3:62–66
- Morgan H, Hughes MP, Green NG (1999) Separation of submicron bioparticles by dielectrophoresis. *J Biophys* 77(1):516–525
- Morijiri T, Sunahiro S, Senaha M, Yamada M, Seki M (2011) Sedimentation pinched-flow fractionation for size- and density-based particle sorting in microchannels. *Microfluid Nanofluid* 11:105–110
- Murthy SK, Sethu P, Vunjak-Novakovic G, Toner M, Radisic M (2006) Size-based microfluidic enrichment of neonatal rat cardiac cell populations. *Biomed Microdevices* 8(3):231–237
- Nam J, Lim H, Kim C, Kang JY, Shin S (2012) Density dependent separation of encapsulated cells in a microfluidic channel by using a standing surface acoustic wave. *Biomicrofluidics* 6:024120
- Napierala M, Nasilowski T, Beres-Pawlak E, Mergo P, Berghmans F, Thienpo H (2011) Large-mode-area photonic crystal fiber with double lattice constant structure and low bending loss. *Opt Express* 19(23):22628–226236
- Nascimento EM, Nogueira N, Silva T, Braschler T, Demierre N, Renaud P, Oliva AG (2008) Dielectrophoretic sorting on a microfabricated flow cytometer: label free separation of Babesia bovis infected erythrocytes. *Bioelectrochemistry* 73(2):123–128
- Neale SL, Mazilu M, Wilson JIB, Dholakia K, Krauss TF (2007) The resolution of optical traps created by Light Induced Dielectrophoresis (LIDEP). *Opt Express* 15(20):12619–12626
- Nilsson A, Petersson F, Jonsson H, Laurell T (2004) Acoustic control of suspended particles in micro fluidic chips. *Lab Chip* 4:131–135
- Oakey J, Allely J, Marr DWM (2002) Laminar-flow-based separations at the microscale. *Biotechnol Prog* 18(6):1439–1442
- Ostergaard S, Blankenstein G, Dirac H, Leistikow O (1999) A novel approach to the automation of clinical chemistry by controlled manipulation of magnetic particles. *J Magn Magn Mater* 194:156–162
- Pamme N (2007) Continuous flow separations in microfluidic devices. *Lab Chip* 7:1644–1659
- Pamme N, Wilhelm C (2005) Micro total analysis systems 2005 In: K. Jensen (ed) Kluwer Academic Publishers, Boston, pp 1389
- Pamme N, Eijkel JCT, Manz A (2006) On-chip free-flow magnetophoresis: separation and detection of mixtures of magnetic particles in continuous flow. *J Magn Magn Mater* 307:237–244
- Park JS, Jung H (2009) Multiorifice flow fractionation: continuous size-based separation of microspheres using a series of contraction expansion microchannels. *Anal Chem* 81:8280–8288

- Petersson F, Nilsson A, Holm C, Jonsson H, Laurell T (2004) Separation of lipids from blood utilizing ultrasonic standing waves in micro fluidic channels. *Analyst* 129:938–943
- Petersson F, Nilsson A, Jonsson H, Laurell T (2005) Carrier medium exchange through ultrasonic particle switching in microfluidic channels. *Anal Chem* 77:1216–1221
- Petersson F, Berg LA, Sward-Nilsson A, Laurell T (2007) Free flow acoustophoresis: micro fluidic-based mode of particle and cell separation. *Anal Chem* 79:5117–5123
- Pohl HA (1977) Dielectrophoresis: applications to the characterization and separation of cell. *Methods Cell Sep Biol Sep* 1:67–169
- Pries AR, Secomb TW, Gaehtgens P (1996) Biophysical aspects of blood flow in the microvasculature. *Cardiovasc Res* 32:654–667
- Quck R, Le DV, Chiam K-H (2011) Separation of deformable particles in deterministic lateral displacement devices. *Phys Rev E* 83:056301
- Rainer D, Sandoz R, Effenhauser CS (2007) Microfluidic depletion of red blood cells from whole blood in high-aspect-ratio microchannels. *Microfluid Nanofluid* 3:47–53
- Redkar SG, Davis RH (1995) Cross-flow microfiltration with high-frequency reverse filtration. *Am Inst Chem Eng J* 41(3):501–508
- Reicherter M, Haist T, Wagemann EU, Tiziani HJ (1999) Optical particle trapping with computer-generated holograms written on a liquid-crystal display. *Opt Lett* 24:9
- Reyes DR, Lossifidis D, Auroux PA, Manz A (2002) Micro total analysis systems: introduction, theory, and technology. *Anal Chem* 74:2623–2636
- Rida A, Fernandez V, Gijs MAM (2003) Long-range transport of magnetic microbeads using simple planar coils placed in a uniform magnetostatic field. *Appl Phys Lett* 83(12):2396–2398
- Ripperger S, Altmann J (2002) Crossflow microfiltration: state of the art. *Sep Purif Technol* 26(1):19–31
- Rivet C, Lee H, Hirsch A, Hamilton S, Lu H (2011) Microfluidics for medical diagnostics and biosensors. *Chem Eng Sci* 66(7):1490–1507
- Russom A, Gupta AK, Nagrath S, Carlo DD, Edd JF, Toner M (2009) Differential inertial focusing of particles in curved low-aspect-ratio microchannels. *New J Phys* 11:075025–075034
- Sai Y, Yamada M, Yasuda M, Seki M (2006) Continuous separation of particles using a microfluidic device equipped with flow rate control valves. *J Chromatogr A* 1127:214–220
- Segre G, Silberberg A (1961) Radial particle displacements in Poiseuille flow of suspensions. *Nature* 189:209–210
- Seo J, Lean MH, Kole A (2007) Membrane-free microfiltration by asymmetric inertial migration. *Appl Phys Lett* 91:033901
- Sethu P, Sin A, Toner M (2006) Microfluidic diffusive filter for apheresis (leukapheresis). *Lab Chip* 6:83–89
- Sim TS, Kwon K, Park JC, Lee J-G, Jung H-I (2011) Multistage-multiorifice flow fractionation (MS-MOFF): continuous size-based separation of microspheres using multiple series of contraction expansion microchannels. *Lab Chip* 11:93
- Situma C, Hashimoto M, Soper SA (2006) Merging microfluidics with microarray-based bioassays: review article. *Biomol Eng* 23(5):213–231
- Sollier E, Cubizolles M, Faivre M, Fouillet Y, Achard JL (2009) A passive microfluidic device for plasma extraction from whole human blood, 31st Annual International Conference of the IEEE EMBS Minneapolis, Minnesota, USA
- Soong CY, Li WK, Liu CH, Tzeng PY (2010) Theoretical analysis for photophoresis of a microscale hydrophobic particle in liquids. *Opt Express* 18(3):2168–2182
- Sunahiro S, Senaha M, Yamada M, Seki M (2008) Pinched flow fractionation device for size- and density-dependent separation of particles utilizing centrifugal pumping, Twelfth international conference on miniaturized systems for chemistry and life sciences, San Diego, California, USA
- Suresh S (2007) Biomechanics and biophysics of cancer cells. *Acta Mater* 55(12):3989–4014
- Suresh S, Spatz J, Mills JP, Micoulet A, Dao M, Lim CT, Beil M, Seufferlein T (2005) Connections between single-cell biomechanics and human disease states: gastrointestinal cancer and malaria. *Acta Biomater* 1(1):15–30
- Takagi J, Yamada M, Yasuda M, Seki M (2005) Continuous particle separation in a microchannel having asymmetrically arranged multiple branches. *Lab Chip* 5:778–784
- Tam CKW, Hyman W (1973) Transverse motion of an elastic sphere in a shear field. *J Fluid Mech* 59:177–185
- Tamagawa M, Monjushiro H, Watarai H (2003) Microgravity laser-photophoresis of high density microparticles in water. *Colloids Surf A Physicochem Eng Asp* 220:279–284
- Terray A, Taylor JD, Hart SJ (2009) Cascade optical chromatography for sample fractionation. *Biomicrofluidics* 3(044106):1–6
- Toner M, Irimia D (2005) Blood on a chip. *Annu Rev Biomed Eng* 7:77–103
- Tripathi S, Prabhakar A, Kumar N, Singh SG, Agrawal A (2013) Blood plasma separation in elevated dimension T-shaped microchannel. *Biomed Microdevices* 15:415–425
- Tsai H, Fang YS, Fuh CB (2006) Analytical and preparative applications of magnetic split-flow thin fractionation on several ion-labeled red blood cells. *Biomagn Res Technol* 4:6
- Vahey MD, Voldman J (2008) An equilibrium method for continuous-flow cell sorting using dielectrophoresis. *Anal Chem* 80:3135–3143
- VanDelinder V, Groisman A (2006) Separation of plasma from whole human blood in a continuous cross-flow in a molded microfluidic device. *Anal Chem* 78:3765–3771
- VanDelinder V, Groisman A (2007) Perfusion in microfluidic cross-flow: separation of white blood cells from whole blood and exchange of medium in a continuous flow. *Anal Chem* 79(5):2023–2030
- Vaziri A, Gopinath A (2008) Cell and biomolecular mechanics in silico. *Nat Mater* 2007(7):15–23
- Vig AL, Kristensen A (2008) Separation enhancement in pinched flow fractionation. *Appl Phys Lett* 93(203507):1–3
- Wang XB, Huang Y, Becker FF, Gascoyne PRC (1994) A unified theory of dielectrophoresis and travelling wave dielectrophoresis. *J Phys D Appl Phys* 27:1571–1574
- Wang X-B, Yang J, Huang Y, Vykovakal J, Becker FF, Gascoyne PRC (2000) Cell separation by dielectrophoretic field-flow-fractionation. *Anal Chem* 72(4):832–839
- Wang W, Lin Y-H, Wen T-C, Guo T-F, Lee G-B (2010) Selective manipulation of microparticles using polymer-based optically induced dielectrophoretic devices. *Appl Phys Lett* 96(113302):1–3
- Wedemann A, Wittbracht F, Auge A, Hütten A (2009) A hydrodynamic switch: microfluidic separation system for magnetic beads. *Appl Phys Lett* 94(17):3051–3052
- Whitesides GM (2006) The origins and the future of microfluidics. *Nature* 442:368–373
- Wiklund M, Gunther C, Lemor R, Jager M, Fuhr G, Hertz HM (2006) Ultrasonic standing wave manipulation technology integrated into a dielectrophoretic chip. *Lab Chip* 6:1537–1544
- Wu Z, Liu AQ, Hjort K (2007) Microfluidic continuous particle/cell separation via electroosmotic-flow-tuned hydrodynamic spreading. *J Micromech Microeng* 17:1992–1999
- Wu Z, Willing B, Bjerketorp J, Janssonbc JK, Hjort K (2009) Soft inertial microfluidics for high throughput separation of bacteria from human blood cells. *Lab Chip* 9:1193–1199
- Xiao K, Grier DG (2010a) Multidimensional optical fractionation of colloidal particles with holographic verification. *Phys Rev Lett* 104:028302

- Xiao K, Grier DG (2010b) Sorting colloidal particles into multiple channels with optical forces: prismatic optical fractionation. *Phys Rev E* 82:051407
- Xin H, Lei H, Zhang Y, Li X, Li B (2011) Photothermal trapping of dielectric particles by optical fiber-ring. *Opt Express* 19(3):2711–2719
- Xin H, Bao D, Zhong F, Li B (2013) Photophoretic separation of particles using two tapered optical fibers. *Laser Phys Lett*
- Xing C, Fu CD, Lulu Z (2009) Isolation of plasma from whole blood using a microfluidic chip in a continuous cross-flow. *Chin Sci Bull* 54(2):324–327
- Xue X, Patel MK, Kersaudy-Kerhoas M, Desmulliez MPY, Bailey C, Topham D (2012) Analysis of fluid separation in microfluidic T-channels. *Appl Math Model* 36:743–755
- Yamada M, Seki M (2006) Microfluidic particle sorter employing flow splitting and recombining. *Anal Chem* 78:1357–1362
- Yamada M, Nakashima M, Seki M (2004) Pinched flow fractionation: continuous size separation of particles utilizing a laminar flow profile in a pinched microchannel. *Anal Chem* 76:5465–5471
- Yamadaa M, Seki M (2005) Hydrodynamic filtration for on-chip particle concentration and classification utilizing microfluidics. *Lab Chip* 5:1233–1239
- Yang S, Undar A, Zahn JD (2006) A microfluidic device for continuous, real time blood plasma separation. *Lab Chip* 6:871–880
- Yoon DH, Ha JB, Bahk YK, Arakawa T, Shoji S, Go JS (2009) Size-selective separation of micro beads by utilizing secondary flow in a curved rectangular microchannel. *Lab Chip* 9(1):87–90
- Zabow G, Assi F, Jenks R, Prentiss M (2002) Guided microfluidics by electromagnetic capillary focusing. *Appl Phys Lett* 80(8): 1483–1485
- Zeng L, Balachandar S, Fischer A (2005) Wall-induced forces on a rigid sphere at finite Reynolds number. *J Fluid Mech* 536:1–25
- Zhang Y, Lei H, Li Y, Li B (2012) Microbe removal using a micrometre-sized optical fiber. *Lab Chip* 12(7):1302–1308
- Zheng MJ, Qu YL, Zhang YZ, Dong ZL (2013) Optically induced dielectrophoresis based automatic assembly of micro/nano-devices. *Integr Ferroelectr* 145:24–31